

https://dspace.org/

A study of failure in the rock surrounding underground excavations

Cook, Neville G.W.

1962
https://hdl.handle.net/10539/24233

Downloaded from a DSpace repository. https://dspace.org/

A STUDY OF FAILURE IN THE ROCK SURROUNDING UNDERGROUND EXCAVATIONS

A Thesis presented to the Department of Geophysics
of the University of the Witwatersrand,
Johannesburg

For the Degree of Doctor of Philosophy

N.G.W. COOK

JUNE, 1962

UNIVERSITY OF THE WITWATERSRAND LIBRARY
Thesis
G 24736

SUMMARY

Violent failure of the rock surrounding underground excavations forms a major hazard and obstacle in deep-level mining.

It was felt that information concerning the position of these failures in relation to the excavation and the energy released by them could be obtained from a detailed seismic study. Such information would form a useful addition to the knowledge and understanding necessary to devise means of alleviating this problem.

Equipment for an underground seismic network was designed and built. This equipment was installed on F Shaft of East Rand Proprietary Mines, Ltd., at a depth between 8,000 feet and 9,000 feet below surface, where it was operated continuously over a period of six months. The foci of all the releases of seismic energy in excess of 10^3 ft.-lbs. (10^{10} ergs) which occurred over 1,000 feet of longwall face were located to within 20 feet. The foci of the releases of seismic energy greater than 10^4 ft.-lbs. (10^{11} ergs) which occurred within a projected area of 8×10^6 square feet were located to within 200 feet.

The foci of 458 bursts were located. Nearly all of these occurred close to faces which were being worked. The data indicate that the occurrence of bursts both in position and time is closely related to the advance of the working faces. The workings were damaged by 7 rock-bursts during the seismic study. These bursts radiated seismic energy greater than 5×10^4 ft.-lbs. However, 187 bursts radiating energy in excess of 5×10^4 ft.-lbs. were detected seismically. There appear to be no differences in energy or location between major bursts which damage the workings and those which do not. It is suggested that the stability of the hanging and footwall may determine the extent of the damage caused by a burst.

Tests on specimens of quartzite, taken from the mine, under multi-axial stresses indicate that a failure criterion for quartzite can be represented by:

/p_1....

$$p_1 = Q + qp_3$$

where Q = the uniaxial compressive strength (about 30,000 p.s.i)

q = a factor between 6 and 8 and

p_1 and p_3 are the maximum and minimum principal stresses at failure.

Stress measurements made 8,000 feet below the surface on the Witwatersrand indicate that the undisturbed vertical rock stress is equal to the weight of the superincumbent rock and that the horizontal stress is about one-third of the vertical stress.

Discing of a solid diamond-drilled core in quartzite is shown to occur at a minimum stress of about 17,500 p.s.i.

Considerable stress concentration was observed between 10 feet and 80 feet ahead of an advancing longwall face.

A vertical strike section through a longwall stope shows the excavation as a narrow horizontal slit. The magnitudes and directions of the principal stresses in plane strain around such a slit in an elastic body subject to gravity are calculated. The energy release caused by making such an opening, and the strain energy ahead of the slit, are calculated.

The failure criterion for quartzite indicates that failure must occur at the edges of the slit - that is, near the face. Most of the failure foci were located in this region.

Failures must occur in the rock around deep-level excavations as mining proceeds. It is suggested that the most fruitful method of reducing the incidence of rockbursts is to devise mining techniques which will ensure the continuous development of the failures in a series of small events during blasting. Detailed seismic investigation during blasting may enable the effect of different techniques to be measured.

CONTENTS

SUMMARY

INTRODUCTION 1

PART 1 THE SEISMIC LOCATION OF FAILURE FOCI

1.1 Equipment 5

1.2 The Seismic Network on F Shaft East Rand Proprietary Mines Ltd.

a) The Seismometer Network 19

b) The Determination of the Velocities of Propagation 25

c) Location 29

1.3 The Results Obtained from the Seismic Network on F Shaft

a) General 33

b) The Location of Failure Foci and the Seismic Energy Radiated from the Failures 34

c) A Discussion of the Burst Location 40

1.4 Summary 53

PART 2 SOME MECHANICAL PROPERTIES OF QUARTZITE AND ROCK STRESS

2.1 The Failure of Quartzite

a) A Failure Criterion for Quartzite 56

b) Fractures in Quartzite 67

2.2 Information about Rock Stresses Obtained from Diamond Drilling 73

2.3 Absolute Stress in the Rock

a) Stress Measurements using Stress Relief and Restoration 78

b) Rock Stress and the Formation of Discs During Diamond Drilling 93

PART 3 CONCLUSION

3.1 The Theoretical Model 99

3.2 A Comparison Between the Theory and the Experimental Results 110

3.3 Questions Arising from the Results 111

APPENDICES

A.1	Seismic Wave Attenuation	115
A.2	Replay Amplifiers Recording Amplifiers Trigger Circuits	118
A.3	Strain Gauges	127

NOTATION

ACKNOWLEDGEMENTS

REFERENCES

FIGURES

Figure 1.1	Block Diagram of Recording System	7
Figure 1.2	Seismometer Frequency Response	8
Figure 1.3	Overall System Response	12
Figure 1.4	The Underground Recorder	14
Figure 1.5	Tape Transport and Heads of the Replay Deck	16
Figure 1.6	Replay Arrangements	18
Figure 1.7	E.R.P.M. Plan of Underground Workings	20
Figure 1.8	E.R.P.M. Transverse Section	21
Figure 1.9	Mechanism for Installing the Seismometer in the Back of Long Holes	23
Figure 1.10	The Locator	32
Figure 1.11	Plan of Portion Between F and G Shafts showing the Burst Locations	37
Figure 1.12	Section through F East Longwall showing the Burst Locations	38
Figure 1.13	Hourly Distribution of the Occurrence of Medium and Larger Bursts	44
Figure 1.14	Hourly Distribution of the Occurrence of Small and Larger Bursts	45
Figure 1.15	Hourly Distribution of the Total Seismic Energy Radiated by the Bursts	46
Figure 1.16	Total Seismic Energy Radiated by Different Sized Bursts	48
Figure 1.17	Seismic Burst Records	50
Figure 1.18	Seismic Burst Records	51
Figure 2.1	Hysteresis Curves for Quartzite and Steel	64
Figure 2.2	Hysteresis Curves for Constrained Pebbly Quartzite	65
Figure 2.3	Hysteresis Curves for Partially Constrained Pebbly Quartzite	70
Figure 2.4	Hysteresis Curves for Partially Constrained Shaly Quartzite	71
Figure 2.5	Failed Quartzite Specimens	72
Figure 2.6	Diamond Drilling Log	75
Figure 2.7	Diamond Drilling Log	76
Figure 2.8	Diamond Drilling Log	77
Figure 2.9	Centre-Cell and Annular Jacks	81
Figure 2.10	De-Stressing of 6 inch Centre-Cells	84
Figure 2.11	Disced 4 inch Annular Cores	85
Figure 2.12	Annular Quartzite Core showing Tensile Cracks	87
Figure 2.13	De-Stressing of 3 inch Centre-Cells	88

Figure 2.14	Calibration of Stress Cells in a Quartzite Core	90
Figure 2.15	Restoration of Centre-Cell Pressure by Annular Jacks	92
Figure 2.16	Split Steel Block and 4 inch Quartzite Core with the end of the $1\frac{1}{2}$ inch Hole	95
Figure 2.17	The 1 inch Diameter Quartzite Core which broke from the Bottom of the Hole in the 4 inch Core	96
Figure 3.1	Principal Stresses in Plane Strain around a Horizontal Slit in an Elastic Body Subject to Gravity	101
Figure 3.2	Movement Caused by a Horizontal Slit in an Elastic Body Subject to Gravity	105
Figure 3.3	Energy Released when a Horizontal Slit is made in an Elastic Body Subject to Gravity	107
Figure 3.4	Strain Energy ahead of a Horizontal Slit in an Elastic Body Subject to Gravity	109
Figure A.1	Compressional Wave Attenuation in Rock	116
Figure A.2	Shear Wave Attenuation in Rock	117
Figure A.3	Replay Amplifier Circuit Diagram	119
Figure A.4	Recording Amplifier Circuit Diagram	121
Figure A.5	Recording Amplifier Frequency Response	124
Figure A.6	Trigger Circuit Diagram	125

TABLES

Table 1.1	Velocity Calibrations	27
Table 1.2	Classified Rockbursts and Seismic Information	41
Table 1.3	The Number of Bursts of Different Sizes Located Seismically	49
Table 1.4	Galvanometer Traces, Seismometers and their Sensitivities	52
Table 1.5	Phase Distribution of Burst Energy	54
Table 2.1	Strength of Pebbly Quartzite	61
Table 2.2	Strength of Shaly Quartzite	61
Table 2.3	Piano Wire and Hydralic Rig Tests on Shaly Quartzite	63

A STUDY OF FAILURE IN THE ROCK SURROUNDING UNDERGROUND EXCAVATIONS

INTRODUCTION

Rock below the surface of the earth is subject to stress. In some mining procedures, excavations are made underground, and the rock is disturbed. Displacements of the rock occur which tend to close the excavation. These displacements may damage adjacent workings and surface structures. Stress concentrations arise in the rock surrounding excavations, and at depth these concentrations may be sufficient to cause failure of the rock. Such failures are often violent in nature, and sometimes cause loss of life and damage to the workings.

To devise mining techniques which alleviate these problems, it is necessary to have some knowledge of the properties and behaviour of the rock around the excavations. Many persons and organizations have been, and are, engaged in research which illuminates these problems. The directions of this research, and some references, are indicated below:-

1. Practical observations made underground in the course of mining have been recorded and analyzed (Leeman, 1958; Pretorius, 1958).

2. Rock movement and surface subsidence around excavations have been measured and analyzed (Brown, 1959; Barcza, von Willich, 1958).

3. Stress and strain measurements have been made in boreholes, drilled from the excavation, to determine the stress changes caused by the excavation and the original stress existing in the rock (Cumpsty, 1954; Hast, 1958; Leeman, 1960; Mohr, 1956; Potts, 1955).

4. Some of the mechanical properties of rock have been determined in laboratory tests (Denkhaus, Roux, Grobbelaar, 1958; Jaeger, 1959; Robertson, 1955).

5. The stress distributions and failures around excavations of various shapes have been analyzed mathematically, and with the aid of models (Berry, 1960; Berry, Sales, 1960; 1961; Denkhaus, 1958; Hoek, 1961).

/6. ....

6. The propagation of sonic and ultra sonic waves in the rock around an excavation has been studied in attempts to determine the extent of fracturing and the stresses existing in the rock (Lutch, Szendrei, 1958; Lutch, 1959; Szendrei, Lochner, 1958).

7. Seismic waves radiating from failures in the rock have been studied in attempts to relate the rate of seismic activity to major failures (Kundorf, Rotter, 1961; F.K.O. Memorandum No. 30, 1959).

This research has confirmed a general picture in which considerable stress concentrations arise in the solid rock surrounding an excavation. The analysis of rock displacement, and support in the excavation, seems in many instances sufficiently well understood to be used in the design of mine workings and techniques. If the stress concentrations are sufficient, the rock immediately around an excavation is fractured. The positions of the failures produced by an excavation, and hence the limits of the fracture zone, are not well established. The region in which failures are likely to occur can, to some extent, be estimated from the stresses and properties of the rock, but the data are insufficient to understand these failure mechanisms, and to suggest means of alleviating the problems created by violent rock failure.

The rocks of the Witwatersrand System consist, broadly, of alternating groups of argillaceous and arenaceous sediments. The gold-bearing reefs in the vicinity of Johannesburg dip southwards at angles of about 40° and are mined to depths extending to 11,000 feet below the surface (Hamilton and Cooke, 1954, pp. 180-190). Most of the excavations are surrounded by quartzite which is relatively rigid and the problems arising from rock displacement and surface subsidence caused by deep excavations have not been acute. However, as the depth below the surface increases so do the stresses, and the problem of violent rock failure is serious. On the Witwatersrand these failures are sometimes felt on the surface as "earth tremors", and sometimes noticed in the underground workings as "rockbursts".

/In....

In 1939, a network of mechanical seismometers was used by the Bernard Price Institute of Geophysical Research to locate the origins of the earth tremors on the Witwatersrand. All the origins were found to be close to mining excavations. The average seismic energy radiated by the 25 largest tremors was found to be between 10^{17} ergs and 10^{18} ergs (Gane, Hales, Oliver, 1946).

The Bernard Price Institute uses a network of surface seismometers on the Witwatersrand, linked by 40 Mc/s radio transmitters and receivers to a tape delay unit and high speed photographic recorder at the Institute, to locate the origin of tremors. This location is accurate to 2,000 feet, and is used for studies of crustal structure in which the seismic waves radiating from the tremors are detected at points remote from their origin.

This location equipment was used on the surface at one mine to improve the location accuracy to 200 feet. The larger releases of energy which occurred in one month on that mine were located and found to be close to the mine workings (Gane, Seligman, Stephen, 1952).

It was felt that a more accurate study of the position of failures in relation to the excavation, and of the energy released by them might lead to a better understanding of the mechanism of rock failure. Such additional understanding of the actual failures seemed necessary to evaluate and devise different methods of reducing the hazards of rock-bursts in mining.

The accuracy of seismic location is limited by the precision with which the times of arrival at the seismometers of the seismic waves radiating from the failure can be determined and by the accuracy with which the velocities of propagation are known. High frequency attenuation of seismic waves in rock increases the rise-time of the initial seismic pulse radiating from a failure, reducing the accuracy with which the times of arrival can be determined. High frequency attenuation can be considerably reduced by decreasing the lengths of the seismic paths between the failure and the seismometers (See Appendix

/A.1....

A.1). The velocities of propagation are not everywhere the same, and reducing the lengths of the seismic paths reduces the uncertainty in the knowledge of the velocities of propagation. Therefore it was decided that the accuracy of location could be improved by installing many seismometers underground closely around the region in which the failures were to be located. So as to obtain other information about the failures, particularly the energy radiated from them, it was decided that a graphical record of the output of each seismometer must ultimately be available so that a full analysis could be made.

To interpret the results of the seismic location it was necessary to have some knowledge of the properties of the rock and of the stress distribution around the excavation. The information available was not sufficient to establish a failure criterion for quartzite. Therefore some experiments under different multi-axial stress conditions were performed to establish some of the failure characteristics of the quartzite around the excavation. Stress measurements were made underground, to determine the stress in the rock, and further information about the stresses around an excavation was obtained from diamond drilling.

A theoretical model, based on the mathematical theory of elasticity and the concept of the support of the fractured rock immediately around the excavation, has been developed to describe the failure and stability of rock around the excavation. In many respects this model is consistent with the experimental results obtained. It appears that the occurrence of rockbursts is closely related to face advance and that the technique of face advance offers the most promising tool with which to reduce the hazard of rockbursts. Detailed seismic analysis during blasting is suggested as a means of measuring the effectiveness of different mining techniques. It is suggested that the behaviour of the fractured rock around the excavation should be studied in greater detail, to assess its effect on the damage caused to the workings by a rockburst.

/PART....

PART I THE SEISMIC LOCATION OF FAILURE FOCI

1. 1 Equipment

It was anticipated that the seismometer network would embrace a region a few thousand feet in dimensions around an excavation. As it is not possible to predict when a failure will occur, it is necessary to record the seismometer outputs continuously. It was envisaged that such continuous recording would have to be of a few months' duration, so as to obtain a comprehensive picture of the development of the failures.

Some preliminary seismic records were obtained from 64 level pre-developed drive, East Rand Proprietary Mines, Ltd. The output of a single 7.5 c.p.s. seismometer was recorded at three different sensitivities and slow speed on a Bernard Price Institute field oscillograph. These records indicated that there were up to a hundred detectable seismic events per day and the ratio between the energy radiated by the largest and smallest events exceeded 10^6. A large proportion of the energy was radiated between 10 c.p.s. and 50 c.p.s.

Continuous recording of the seismometer outputs on long lengths of magnetic tape was selected as being most suitable. It is relatively easy to handle magnetic tape, and to operate a tape recorder, underground. The seismometers could therefore be connected direct to a multi-channel tape recorder operating underground. By using a number of tapes, it is possible to store the complete records for a few weeks, so that they can be referred to for any further information.

Direct recording of the seismometer outputs on to photographic paper has been suggested as a suitable system for a detailed examination of the failures which occur during a short period of time at and immediately after blasting. A magnetic tape delay unit, operating in

/conjunction....

conjunction with a high-speed photographic recorder, is probably the most suitable system with which to obtain seismic records of major failures soon after they have occurred.

Figure 1.1 is a block diagram of the recording system adopted for a continuous seismic examination of a region around an excavation.

Small electro-magnetic seismometers suitable for use underground were obtained commercially. These seismometers are sensitive to motion along one axis, which may be either vertical or horizontal. The natural frequency of the vertical seismometers is 14 c.p.s., and that of the horizontal seismometers is 7 c.p.s. The output and frequency response of the seismometers were checked. Two seismometers were clamped together and mounted on a low frequency suspension, free to move along the axis of the seismometers. One seismometer was driven by a low frequency signal generator, and the output of the other seismometer was measured on an oscilloscope. The amplitude of vibration of the seismometers was measured with an optical lever. Within the limits of this calibration, $\pm$ 10%, the manufacturers' sensitivity was found to be correct. Figure 1.2 shows the response of the seismometers as they were used underground.

A sixteen-channel oscillograph which could record at a paper speed of 20 inches/second was available. The natural frequency of the recording galvanometers is 70 c.p.s. and their D.C. sensitivity is .5 mm/ micro-amp.

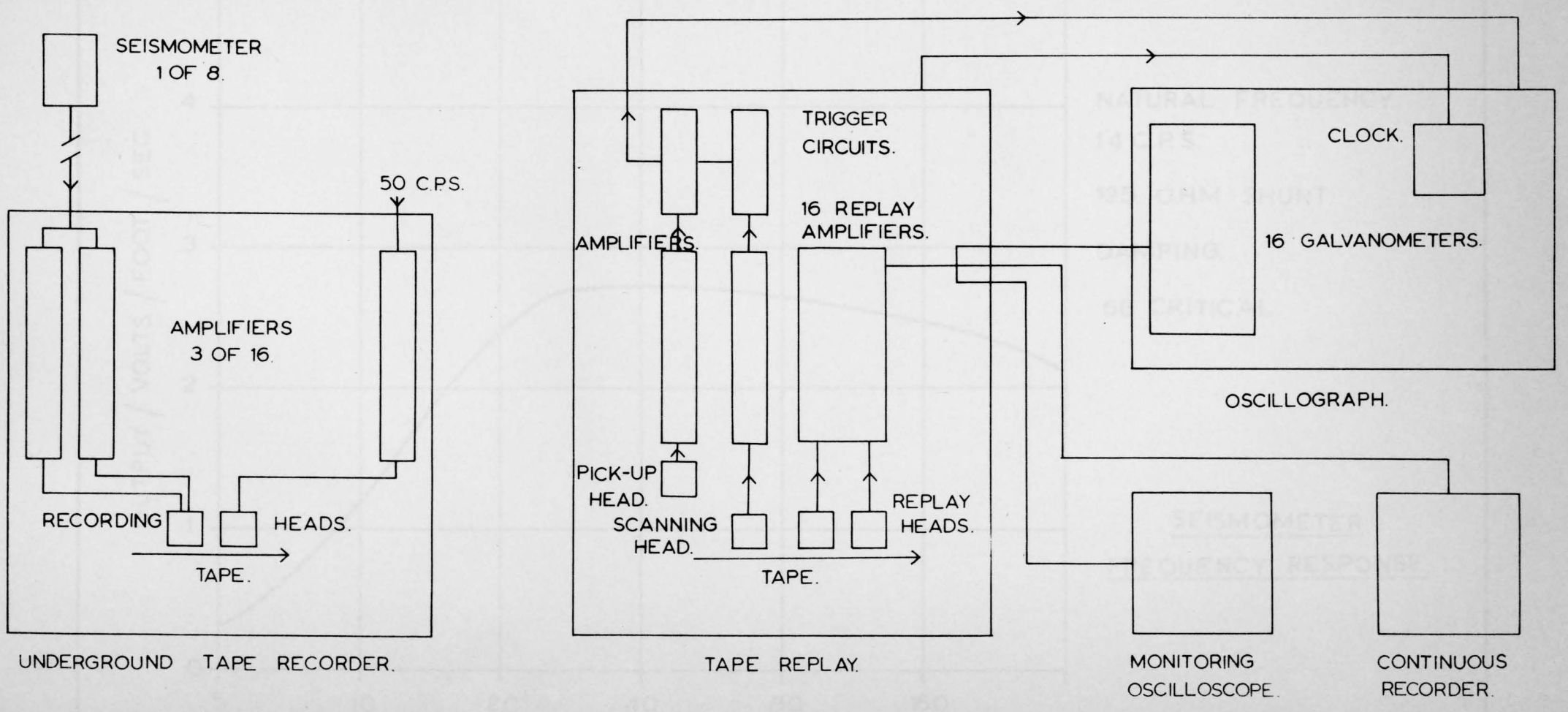
The tape recorder had to fulfil the following requirements:-

a) It must record continuously the outputs of at least six seismometers.

b) It must record a dynamic range of 10^3 corresponding to an energy ratio of 10^6, for each seismometer.

c) Times of 1 millisecond must be resolved to obtain the desired location accuracy.

/d)....



BLOCK DIAGRAM OF RECORDING SYSTEM.

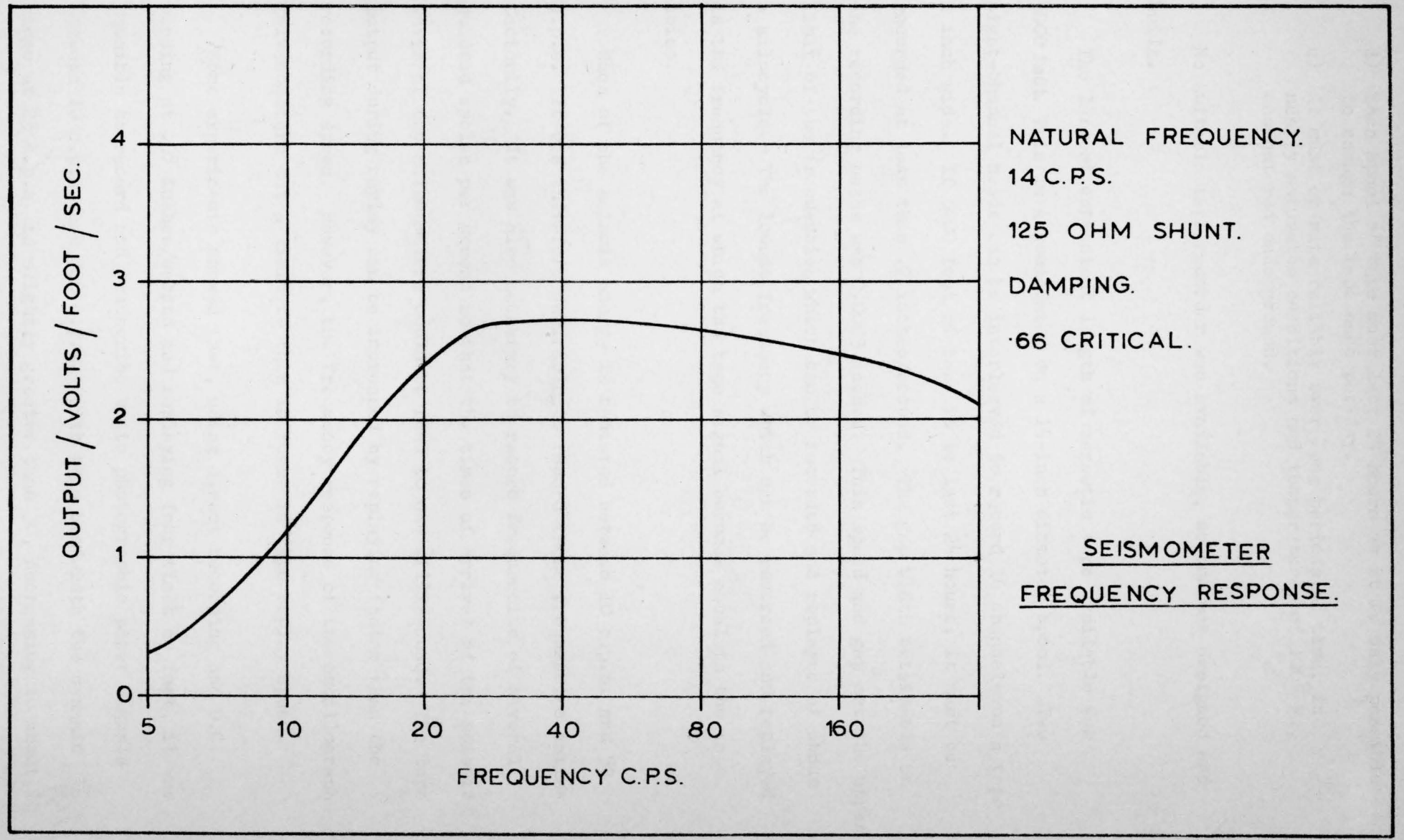

OUTPUT / VOLTS / FOOT / SEC.
0
1
2
3
4
5
10
20
40
80
160
FREQUENCY C.P.S.
NATURAL FREQUENCY.
14 C.P.S.
125 OHM SHUNT.
DAMPING.
·66 CRITICAL.
SEISMOMETER
FREQUENCY RESPONSE.

Figure 1.2

d) Each spool of tape must last 24 hours as it is only possible to change the tape once per day.

e) It must operate reliably over long periods of time, in nearly saturated conditions and temperatures of 100° F., encountered underground.

No suitable tape recorder was available, so one was designed and built.

The largest convenient length of magnetic tape available was 5000 feet. This is accommodated on a 14-inch diameter spool. Two eight-channel heads can be interleaved to record 16 channels on a tape 1 inch wide. If 5000 feet of tape is to last 24 hours, it must be recorded at less than .7 inches/second. The gap width obtainable on the recording heads was 0.0003 inches. This speed and gap set the upper limit of the frequencies which can be recorded and replayed at about a kilocycle. The lowest frequency which can be recorded and replayed is the frequency at which the tape signal becomes equal to the tape noise.

Much of the seismic energy is radiated between 10 c.p.s. and 50 c.p.s. It was therefore desirable to record these frequencies satisfactorily. It was also necessary to record frequencies of several hundred cycles per second so that the times of arrival of the seismic waves at the seismometers could be read to one millisecond. The tape output during replay can be increased by replaying faster than the recording speed. However, the frequency response of the oscillograph galvanometers set a limit to this increase in tape replay speed.

Some experiments showed that, using direct recording and D.C. biasing at .65 inches/second and replaying four times as fast, it was possible to record and transcribe on to photographic paper signals between 10 c.p.s. and 300 c.p.s. With this bandwidth the dynamic range at 25 c.p.s. is slightly greater than 30, decreasing to about 10

/at....

at 10 c.p.s. To accomplish this, careful attention was paid to reducing the noise of the replay amplifiers below the tape noise. (Sacks, 1957, and Appendix A 2 for circuit diagram).

By using two channels of different sensitivities, it is possible to record a dynamic range of 10^3 under these conditions.

A.C. biasing reduces the unrecorded tape noise, but was not used because of the additional electronic complication. Apart from this, the above system makes use of most of the dynamic range and frequency response available on the tape. No system can be better than one which uses the full dynamic range and frequency response direct. Tape transport stability at low recording speed is unlikely to be better than 2%. This is the stability of the centre frequency in a frequency-modulated system, and limits the dynamic range of such a system to 50. In addition, the equation of a frequency-modulated sine wave can be expressed as a series of Bessel functions (Terman, 1943, p. 578), and the frequencies present are ω, $\omega \pm b$, $\omega \pm 2b$, etc., where ω is the centre frequency and b is the modulating frequency. Side bands of the order of the modulation index are important. A larger frequency range is necessary to accommodate a frequency-modulated signal than is necessary to accommodate an amplitude-modulated signal, and in each case the modulated signal occupies a larger frequency range than the original signal. Frequency modulation with a centre frequency of 700 c.p.s., excursions of $\pm$ 700 c.p.s. and a modulation index between 70 at 10 c.p.s. and 1.4 at 500 c.p.s. would give a result comparable with that obtained with direct recording limited at the high frequency end by the galvanometer response. Amplitude modulation of a high frequency can be used in conjunction with the direct recording amplifiers to record frequencies below 10 c.p.s.

The....

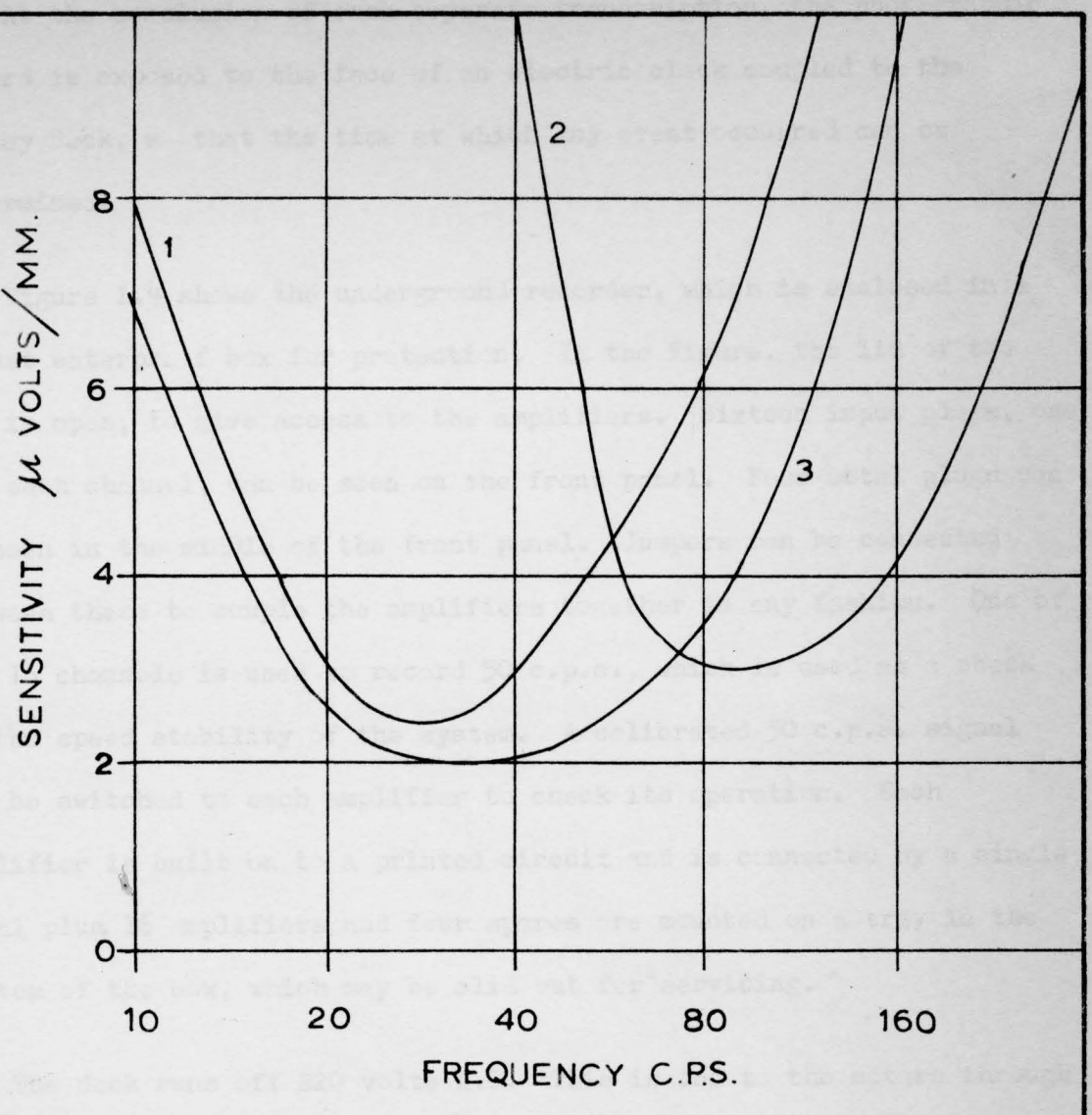
The seismometer output at frequencies above its natural frequency is proportional to the seismic particle velocity. This is used to compute the radiated seismic energy. The frequency response of some of the recording amplifiers was arranged to be flat over those frequencies in which most of the seismic energy is radiated. This facilitates record reading, as it is only necessary to read the amplitude in order to calculate the radiated energy. Most of the background noise and electrical pick up in the mine occurs at and below 50 c.p.s. Some of the recording amplifiers were designed to emphasize frequencies higher than this, so as to reduce the noise and increase the accuracy with which the arrivals of the seismic waves at the seismometers could be determined. The circuit diagram and frequency response curves of the recording amplifiers are shown in Appendix A2.

Each seismometer is connected to two amplifiers, the sensitivities of which differ by 30. The most sensitive amplifier emphasizes the high frequencies. Each of these channels forms one trace on the oscillograph record and the limited dynamic range of each trace facilitates reading the records.

The whole system is calibrated from time to time by applying a signal of constant amplitude and varying frequency to the recorder input, and measuring the amplitude of this signal after is has been transcribed on to photographic paper. Figure 1. 3 shows the over-all frequency response of the recording system.

During replay, the recorded tape is scanned by trigger circuits (See Appendix A 2 for circuit diagram), before it passes the replay heads. Signals exceeding selected levels cause this circuit to switch on the oscillograph and transcribe on to photographic paper the seismic signals from that portion of the record.

/At....



CURVE 1 IS FOR THE STANDARD RECORDING AMPLIFIER.

CURVE 2 IS FOR THE AMPLIFIER WITH HIGH FREQUENCY EMPHASIS.

CURVE 3 IS FOR AN AMPLIFIER WITH A WIDER FREQUENCY RESPONSE.

THE SENSITIVITY IS THE AMPLITUDE OF THE RECORDED SIGNAL IN MICRO-VOLTS, AT THE INPUT TO THE RECORDING AMPLIFIER ON FULL GAIN, TO PRODUCE 1MM. DEFLECTION ON THE OSCILLOGRAPH RECORD.

OVERALL SYSTEM RESPONSE.

Figure 1.3

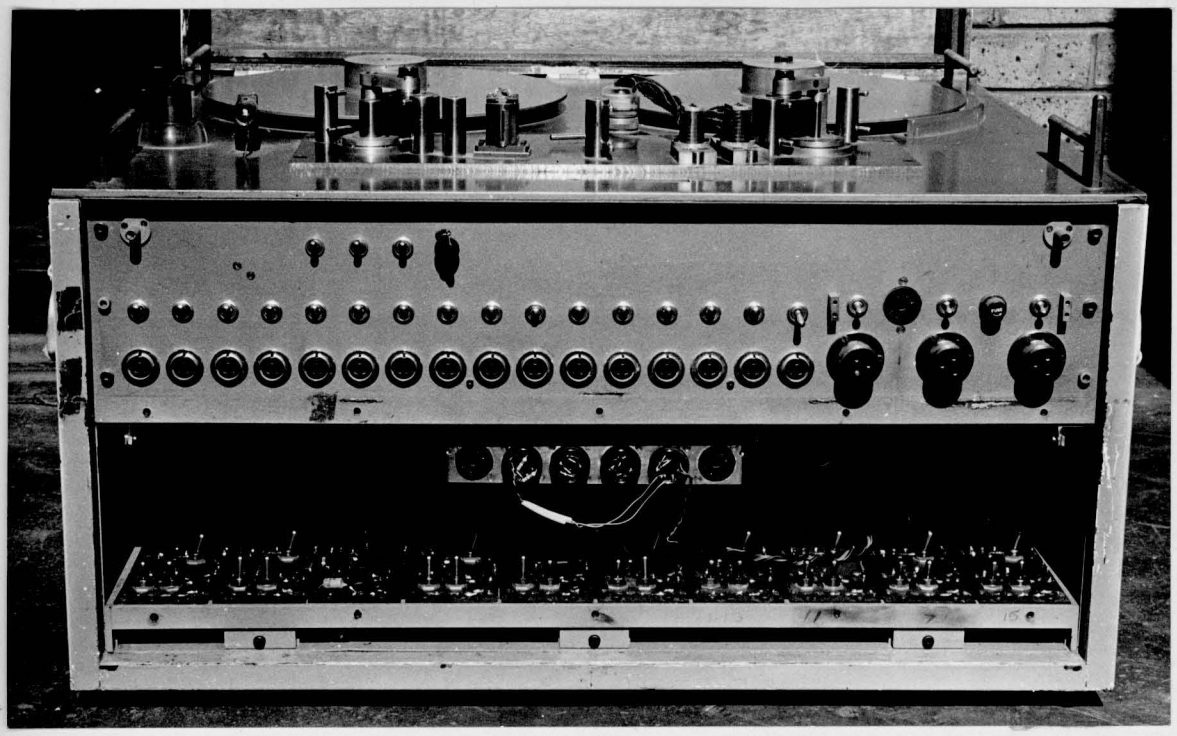
At the conclusion of each separate transcription, the photographic record is exposed to the face of an electric clock coupled to the replay deck, so that the time at which any event occurred can be determined.

Figure 1.4 shows the underground recorder, which is enclosed in a robust waterproof box for protection. In the Figure, the lid of the box is open, to give access to the amplifiers. Sixteen input plugs, one for each channel, can be seen on the front panel. Four octal plugs can be seen in the middle of the front panel. Jumpers can be connected between these to couple the amplifiers together in any fashion. One of the 16 channels is used to record 50 c.p.s., which is used as a check on the speed stability of the system. A calibrated 50 c.p.s. signal can be switched to each amplifier to check its operation. Each amplifier is built on to a printed circuit and is connected by a single octal plug. 16 amplifiers and four spares are mounted on a tray in the bottom of the box, which may be slid out for servicing.

The deck runs off 220 volts A.C. This is fed to the motors through a transformer, and to a trickle charger to charge an accumulator used to supply high tension for the transistorized electronics. The power consumption of the whole deck is only 40 watts. However, as it is designed to run at ambient temperatures up to 120° F., copper tubes, through which cooling water may be circulated, are built into the box. A photo-electric cut-out is arranged to switch the recorder off when the tape is finished.

Figure 1.5 shows the tape transport and heads of the replay deck, which is very similar to the recording deck. The tape moves from left to right across the deck.

/1 ....



THE UNDERGROUND RECORDER

FIGURE 1.4

1 is a guide roller, used to align accurately the height of the tape as it comes off the tape spool. The tape is pressed against this roller by a spring-loaded felt pad. All the other guides are stationary stainless-steel pillars.

2 is a drag roller on to which the tape is pinched by the rubber roller immediately behind it. This drag roller has a torque applied in a reverse direction to the transport of the tape by a high-starting torque induction motor. The drag rollers apply a uniform tension to the tape throughout the periods of recording and replaying.

7 is the drive spindle on to which the tape is pinched by a rubber roller. The drive spindle is attached to a 15 lb. flywheel which is driven by a flat belt from a 750 r.p.m. synchronous induction motor.

Torque is applied to the take-up reel by a high-starting torque induction motor. The torque on the take-up reel is virtually constant, therefore the stacking tension is higher on the inside of the stacked spool than on the outside. This assists in uniform stacking of the tape.

4 is a lever which switches off the tape motors and opens the pinch rollers.

5 is a scanning head which feeds the signals on the tape to a trigger circuit before they cross the replay heads.

3 is a head which is not in contact with the tape and is used to cancel any triggering which might occur, due to stray pick-up in the trigger head.

6 are the two eight-channel interleaved replay heads.

/The....



TAPE TRANSPORT AND HEADS OF THE REPLAY DECK

FIGURE 1. 5

1 is a guide roller

2 is a drag roller

3 is a cancellation head

4 is a lever which switches off the tape motors and opens the pinch rollers

5 is a scanning head

6 are two eight-channel interleaved replay heads

7 is the drive spindle

The drive spindle, the drag roller and heads are all accurately mounted on a heavy gunmetal casting so as to ensure stable and accurate alignment. Each head is separately mounted on a base plate which can be moved by an eccentric, so as to change the position of the head by small amounts along the length of the tape. The distance between the heads on the record and replay decks is adjusted with these eccentrics so that a signal recorded simultaneously on all the channels comes off all the channels simultaneously when transcribed. In practice, the alignment of the gaps in each head is not sufficiently accurate for this to be done, and a small correction has to be applied when reading the records.

Many of the components are made from stainless steel, and most of those which are not are cadmium-plated. All the rotating components are mounted on ball-bearings.

The transport system is somewhat elaborate, but this is necessary to ensure accurate and stable tracking of a wide tape at low recording speeds.

The maximum peak-to-peak variation is 2% in the speed of a tape recorded on one deck and played back four times as fast on the other deck. This speed stability is expressed as the ratio of maxiumm peak fluctuation of the instantaneous tape speed to the average speed. The instantaneous speed was measured as the mean speed over an interval of 2.5 milliseconds during replay.

Figure 1. 6 shows the replay arrangements.

1 is the replay deck.

2 is the 16-channel recording oscillograph.

3 is a dual-trace oscilloscope used to monitor the outputs of the replay amplifiers.

4 is a three-channel, slow-speed oscillograph, which was sometimes used to make continuous records of portions of magnetic tape records.

/5 ....



REPLAY ARRANGEMENTS

FIGURE 1.6

1 is the replay deck

2 is the 16-channel recording oscillograph

3 is a dual-trace oscilloscope

4 is a three-channel oscillograph for continuous recording

5 is a fast-wind deck.

5 is a fast-wind deck, designed to handle long lengths of magnetic tape. Tape can be wound in either direction on this deck and it takes three minutes to transfer 5,000 feet of tape from one spool of tape to the other. The accelerating and braking forces are supplied entirely by electric motors, which are connected to each spool.

1. 2 The Seismic Network on F Shaft East Rand Proprietary Mines, Ltd.

a) The Seismometer Network

Figure 1. 7 is a Plan of the underground workings of East Rand Proprietary Mines, Ltd., and Figure 1. 8 is an Elevation of the same mine.

It was decided that it would be most useful to investigate a region embracing about a 1,000 feet of longwall face in which rockbursts were known to occur frequently.

In consultation with the Management of East Rand Proprietary Mines, Ltd., it was decided that the top portion of the East longwall of F Shaft was the most suitable site for this investigation. This area has a consistent history of rockbursts.

It is known that the rock immediately surrounding a mining excavation is fractured. The velocities of propagation of the seismic waves in this rock are different from those in the solid rock. To avoid the uncertainties of the propagation of seismic waves through the fractured rock, it was hoped that the seismometers could be installed in the solid rock ahead of the excavation. Originally, it was planned to instal seismometers in pre-developed drives ahead of the excavation. These pre-developed drives are very susceptible to failure, and no site with pre-developed drives was available. It was therefore decided that the seismometers should

/be....

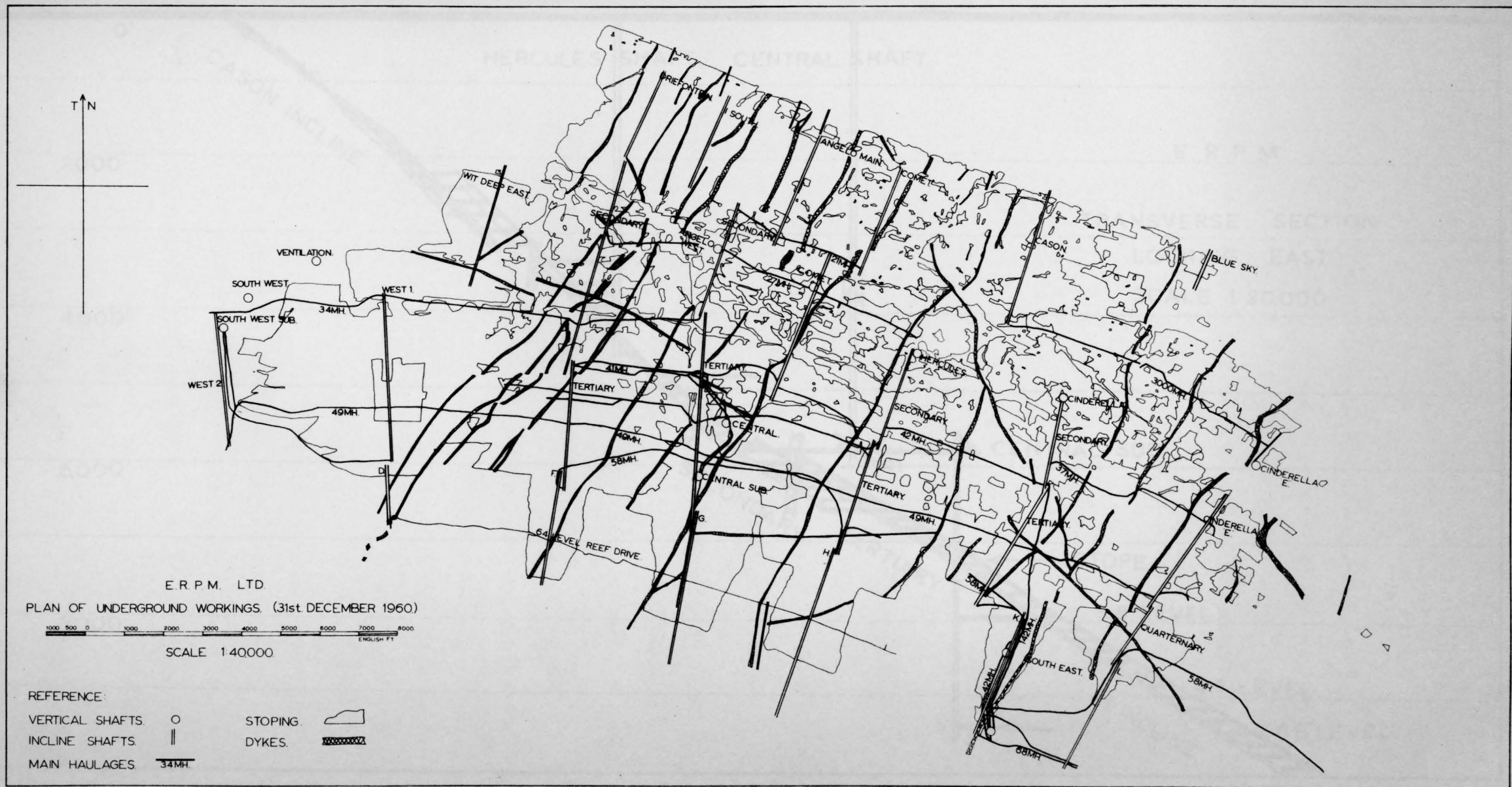
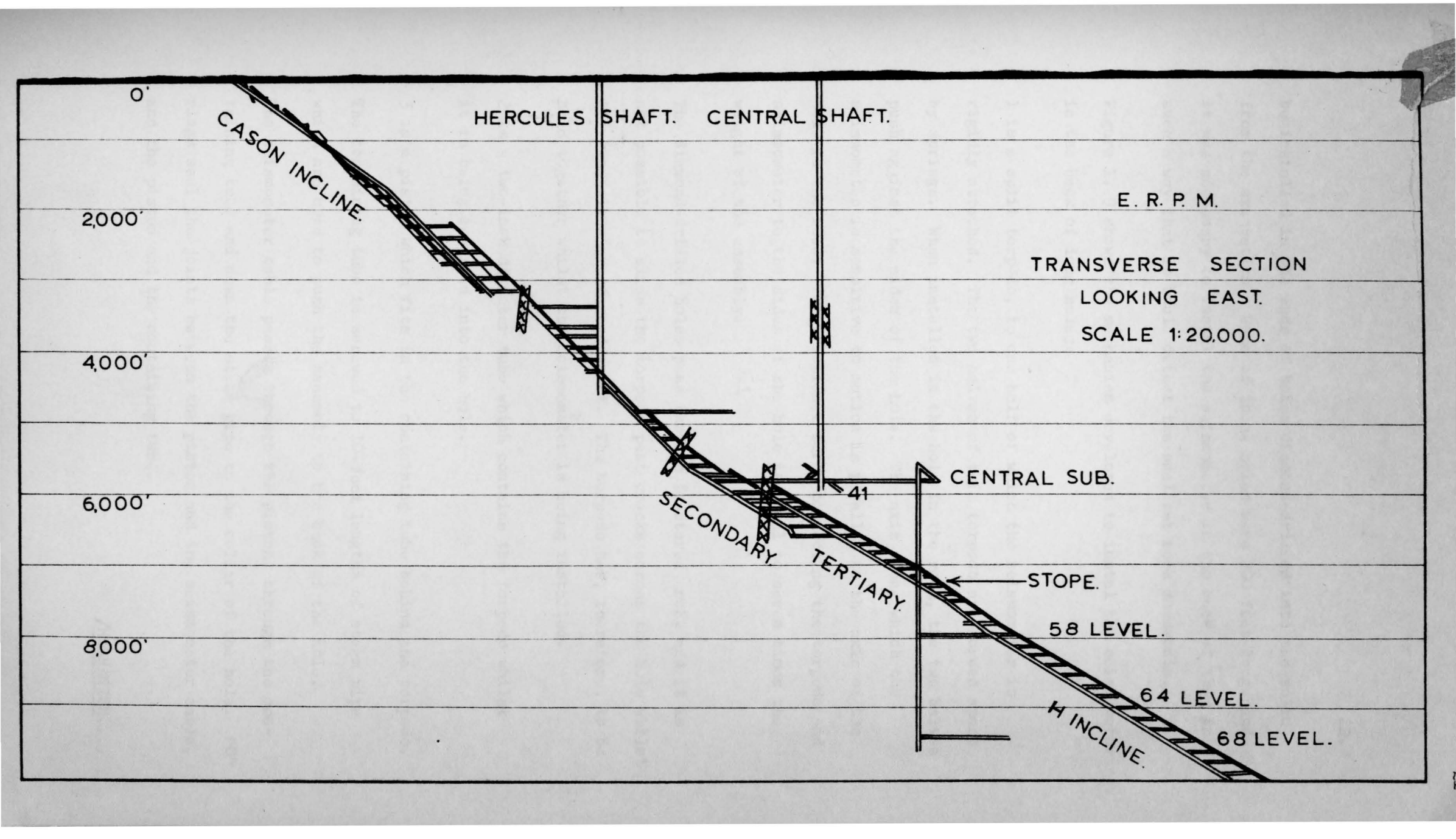

T N
WIT DEEP EAST
VENTILATION.
SOUTH WEST.
SOUTH WEST SUB.
WEST 1.
34MH.
WEST 2.
49MH.
41MH.
TERTIARY
TERTIARY
CENTRAL.
49MH.
58MH.
CENTRAL SUB.
64 LEVEL REEF DRIVE.
SECONDARY
SECONDARY
SECONDARY
27MH.
COMET
ANGELO MAIN
COMET
HERCULES
SECONDARY
42MH.
CASON
BLUE SKY
CINDERELLA
SECONDARY
300MH.
CINDERELLA E.
37MH.
TERTIARY
49MH.
TERTIARY
CINDERELLA E.
58MH.
42MH.
SOUTH EAST.
QUARTERNARY
58MH.
68MH.
E.R.P.M. LTD.
PLAN OF UNDERGROUND WORKINGS. (31st. DECEMBER 1960)
1000 500 0 1000 2000 3000 4000 5000 6000 7000 8000
ENGLISH FT
SCALE 1:40,000
REFERENCE:
VERTICAL SHAFTS.
INCLINE SHAFTS.
MAIN HAULAGES. 34MH.
STOPING.
DYKES.

Figure 1.7


0'
2,000'
4,000'
6,000'
8,000'
CASON INCLINE.
HERCULES SHAFT.
CENTRAL SHAFT.
E. R. P. M.
TRANSVERSE SECTION
LOOKING EAST.
SCALE 1:20,000.
CENTRAL SUB.
41
SECONDARY.
TERTIARY.
STOPE.
58 LEVEL.
64 LEVEL.
68 LEVEL.
H INCLINE.

be installed in the ends of holes diamond-drilled into the solid from the excavation. Some of these holes were 200 feet long, and it was necessary to instal the seismometer in the back of them in such a way that it would detect the smallest rock movements.

Figure 1. 9 shows the mechanism developed to instal the seismometer in the back of long holes.

1 is a split torpedo, to one half of which the seismometer is rigidly attached. The two halves of this torpedo are forced apart by springs. When installed in the hole in the rock, the two halves push against the sides of the hole. The axis along which the seismometer is sensitive to motion is parallel to the axis of the hole in the rock. The frictional force connecting the torpedo and seismometer to the sides of the hole is equal to seven times the weight of the assembly.

The diamond-drilled holes pass through fractured rock, and it is not possible to slide the torpedo past cracks across the hole whilst the two halves are forced apart. The torpedo has, therefore, to be held together whilst the seismometer is being installed.

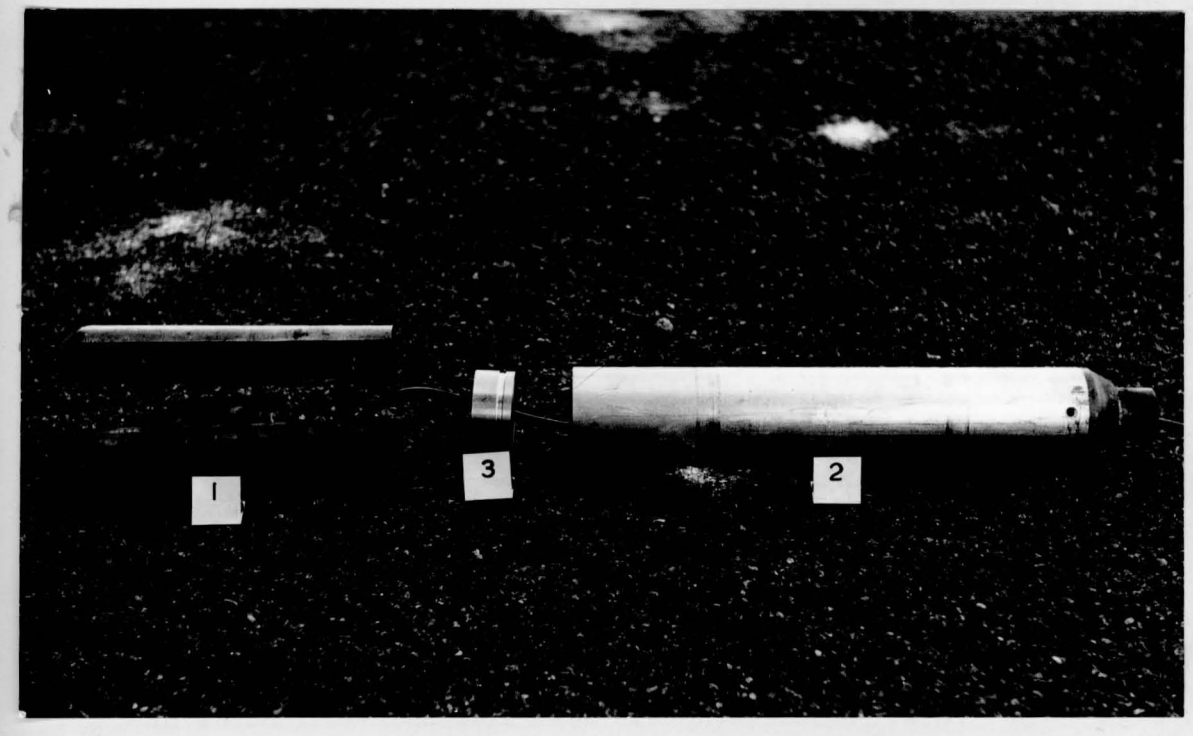
2 is a two-inch diameter tube which contains the torpedo whilst it is being inserted into the hole.

3 is a piston which fits in the containing tube behind the torpedo.

The containing tube is screwed to 10-foot lengths of steam pipe which are used to push the assembly to the back of the hole.

The seismometer cable passes through the piston, through the containing tube and down the steam pipe to the collar of the hole. "O" rings seal the joints between the piston and the seismometer cable, and the piston and the containing tube.

/MACHANISM....



MECHANISM FOR INSTALLING THE SEISMOMETER IN THE BACK OF LONG HOLES

FIGURE 1. 9

1. The seismometer and mounting torpedo
2. Containing tube
3. The ejection piston

When the assembly has been pushed to the back of the hole, it is withdrawn a foot or two. Water under pressure is then pumped down the steam pipe to force the piston and split torpedo out of the containing tube. As the torpedo emerges from the tube, it springs apart and attaches the seismometer to the sides of the hole. The steam pipe and the containing tube are then withdrawn a short distance so as not to interfere with the seismometer. The steam pipe remains in the hole to protect the cable against damage due to failure of portions of the hole. The rest of the cable from the seismometer to the recorder is protected by electric conduit piping.

All the seismometers on the F Shaft site were successfully installed with this technique.

The positions of the seismometers and the details of the region in which locations were made are shown in the Plan, Figure 1. 11 (page 37), and the Section, looking West, Figure 1.12 (page 38), of a portion of F. and G. longwalls, East Rand Proprietary Mines, Ltd.

Two horizontal seismometers, 58H and 60H, were installed in the ends of 200-foot holes drilled horizontally ahead of the face from the footwall drives. 57H is a horizontal seismometer installed in the end of a hole drilled from 57 reef drive.

Two vertical seismometers, 58R and 60R, were installed in the ends of 100-foot holes, drilled vertically into the hanging from reef drives on 58 and 60 levels respectively. 57R is a vertical seismometer installed in the end of a 150-foot hole drilled vertically into the hanging from 57 reef drive.

58V is a vertical seismometer installed in the bottom of a 100-foot hole, drilled vertically into the footwall from 58 footwall drive. 60V is a vertical seismometer installed in the footwall from 60 footwall drive.

/The....

The horizontal seismometers 57H and 60H are approximately at right-angles to oneanother. It is therefore possible to determine amplitude of the seismic waves along three perpendicular axes, using these two seismometers and the vertical seismometers.

b) The Determination of the Velocities of Propagation

The velocities of propagation of seismic waves in the rock around the excavation were measured as follows:-

Two or three pounds of explosive were detonated in a hole drilled into the face. The position of this hole was known. The instant of detonation, and the arrival at the seismometers of the seismic waves radiating from the explosion, were recorded on the magnetic tape. The lengths of the seismic paths from the point of detonation to the seismometers were determined.

These lengths, and the time taken for the waves to travel from the origin of the explosion to the seismometers, were used to compute the average velocities of propagation over those paths. In the first attempts to do this, the shot was detonated electrically. The instant of detonation was measured by the interruption of a current flowing in a wire wrapped around the explosive. This method was not successful because the voltage from the electric exploder generated an earth current which swamped the amplifiers. Subsequently, these calibration shots were successfully detonated with a conventional fuse. The instant of detonation was measured by recording the output of a seismometer placed within 10 feet of the charge. Allowance was made for the travel time between the shot and this seismometer.

Three calibrations were done with this method at points along the face between 57 and 60 levels on the East longwall of F Shaft. A fourth calibration was done by exploding a charge on the West longwall of G Shaft.

/The....

The position of the shot was determined to an accuracy of ± 10 feet, and the seismic travel times were determined to ± 1 millisec. Therefore, when the path length exceeded 500 feet the average velocity of propagation over the path could be determined to ± 5%.

In three shots on F Shaft, nine values of the velocity of propagation of P waves from points along the face to the seismometers with an accuracy better than ± 5% were obtained. The 90% confidence limits, determined from these, using Student's distribution, were 18.1 ft./millisec. and 18.9 ft./millisec.

The average velocities obtained for 22 different paths from these shots are shown in Table 1. 1.

In general, the velocities over paths which traversed the immediate footwall tended to be low and those which traversed the more solid rock ahead of the face tended to be high. However, the velocities over different paths similarly situated with respect to the excavation differed by as much as 2 ft/millisec. As the rock around the excavation is reasonably uniform, the velocity depends largely on the extent to which the rock is fractured. The extent of the fracturing changes as mining proceeds, and it is not possible to ascribe precise velocities to all the different paths. Therefore, a mean value of 18.5 ft./millisec. was used as the velocity of propagation of P waves in the vicinity of the seismometer network. The positions of the paths can be seen during location and suitable corrections to this velocity because of the position of the path can be made.

A fourth calibration on G Shaft showed that the 90% confidence limits for the velocity of propagation of P waves through the solid rock betwen the two Shafts were 20.1 ft/millisec. and 20.9 ft/millisec.

/The....

TABLE 1. 1

VELOCITY CALIBRATIONS

Date: 20/12/60

Position: 5 feet ahead of the face: 15 feet South of 60 Reef Drive

SEISMOMETERS	PATH LENGTH (FEET)	TRAVEL TIME (MILLISECS.)	VELOCITIES IN FT/ MILLISEC.
57H	850	45	18.9 ± .6
58R	660	35	18.8 ± .7
58H	670	36	18.6 ± .8
60V	200	12	16.7 ± 2.0
58V	640	39	16.4 ± .6
60R	180	10	18.0 ± 2.5
60H	120	9	13.4 ± 2.4

Date: 18/1/61

Position: 5 feet ahead of face: 40 feet South of 57 Reef Drive.

SEISMOMETERS	PATH LENGTH (FEET)	TRAVEL TIME (MILLISECS) .	VELOCITIES IN FT/ MILLISEC.
57H	330	18	18.4 ± 1.5
58R	210	11	19.1 ± 2.4
58H	150	7	21.4 ± 2.9
60V	690	37	18.6 ± .7
58V	250	16	15.7 ± 1.5
60R	730	40	18.3 ± .7
60H	690	38	18.2 ± .7

Date: 8/3/61

Position: 5 feet ahead of face: 25 feet South of 59 Reef Drive.

SEISMOMETERS	PATH LENGTH (FEET)	TRAVEL TIME (MILLISECS.)	VELOCITIES IN FT/ MILLISEC.
57H	560	31	18.1 ± .9
58R	340	17	20.0 ± 1.6
58V	310	16	19.4 ± 1.7
60V	250	13	19.3 ± 2.0
58H	330	19	17.4 ± 1.4
60R	300	14	21.5 ± 2.2
57R	710	35	20.2 ± .6
60H	230	11	20.9 ± 2.5

The shots did not generate a noticeable S wave, so that it was not possible to measure the velocity of propagation of S waves direct. However, the Poisson's ratio, ν, for quartzite is about 0.15, and this was used to calculate the velocity of propagation of S waves.

$$C_S = C_P\sqrt{\frac{1 - 2\nu}{2(1 - \nu)}} = 13 \text{ ft/millisec.}$$

(Timoshenko 1934 eqn. 259 p.398)

where $C_P = 20.5$ ft/millisec.

c) Location

Assume that seismic waves propagate with uniform velocity in straight lines from the focus to the seismometers.

Let a system of rectangular co-ordinates, x, y, z, define any point in the rock. Seismometers are situated at points x_n, y_n, z_n, where n = 1, 2....m and m = total number of seismometers.

If a failure occurs at a point, x,y,z, then the length of the seismic path between the focus and seismometer 1 is:-

$$r_1 = \sqrt{(x_1 - x)^2 + (y_1 - y)^2 + (z_1 - z)^2} \qquad (1)$$

If the time of arrival of both the P and the S waves can be determined for each seismometer, the distance, r_1 is:-

$$r_1 = \frac{t_{1S} - t_{1P}}{\frac{1}{C_S} - \frac{1}{C_P}} \qquad (2).$$

where $(t_{1S} - t_{1P})$ is the difference in the times of arrival of the S and P waves respectively, and C_S and C_P are the velocities of propagation of S and P waves.

When m = 3, three equations of the type of (2) are obtained.

/Using....

Using equation 1, these may be written in terms of x, y, z, and solved to determine two possible positions of the focus. symmetrical about the plane of the three seismometers. A fourth seismometer outside the plane of the other three is necessary to resolve this ambiguity.

If the times of arrival of the P waves only can be determined, the following analysis can be used. The time taken for the P waves to travel from the focus to seismometer 1 is:-

$$t_{1P} = \frac{r_1}{C_P} \qquad (3)$$

The difference between the times of arrival at seismometers 1 and n is

$$t_{(1 - n)P} = t_{1P} - t_{nP} \qquad (4)$$

When m = 4, three equations of the type of 4 are obtained. These equations may be written in terms of x, y, z, using equations 3 and 1 to find the focus.

Again, one of the seismometers must lie outside the plane of the other three.

The co-ordinates of any focus can be computed using the above equations. Such computation is laborious, and for this reason a mechanical device was developed to locate the foci.

The locator consists of a spatial scale model of the seismometer network. The seismic paths between the focus and the seismometers are represented in position and length by strings emerging from the positions of the seismometers. The locator, therefore, represents graphically the seismic paths. The times of arrival of the seismic waves at the seismometers are converted to distances. These distances are set up on the locator to obtain a three-dimensional graphical solution to the above equations.

/Figure....

Figure 1. 10 shows the locator for the F Shaft seismometer network. The positions of the seismometers correspond to the ends of the tubes extending downwards from the base-board. The perspex sheet represents a portion of the stope extending back from the face towards the shaft. String can be pulled out from each tube, to represent a seismic path. This string runs over some pulleys and is kept under tension by the weights hanging against the wall. The length of string pulled out from each tube is measured by the movement of a paper clip attached to the string across a graduated scale on the wall, each division of which is equivalent to 20 feet.

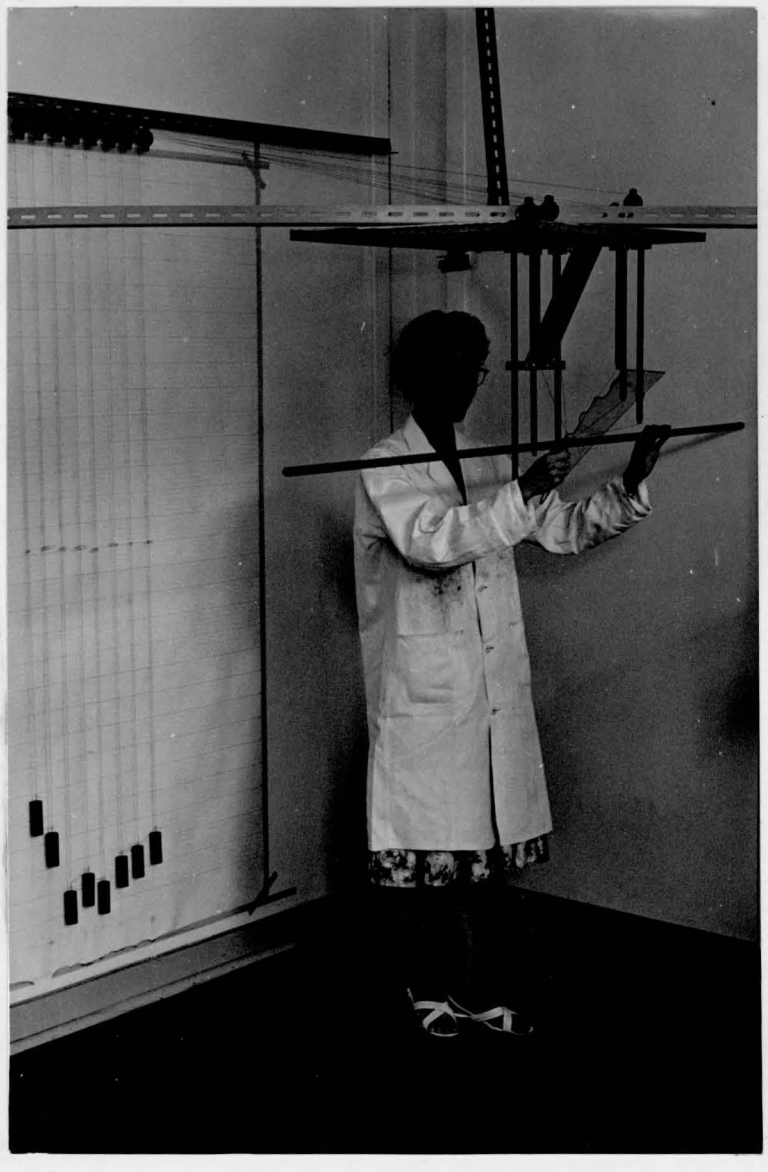
When the times of both the P and the S arrivals can be determined, the seismic path lengths can be calculated. These lengths can be set up for each seismometer on the paper clips of the locator. The strings can be pulled out by this distance and arranged to meet in a point, the focus.

The paper clips will then all line up on the datum from which the path lengths were measured.

If the times of arrival of only the P waves can be determined, only the differences in the seismic path lengths can be calculated; to locate a focus these differences are set up on the paper clips of the locator. The ends of all the strings are joined to a common point which is moved about until the paper clips line up. This point is the focus, and the extensions of the strings are, to scale, the total seismic path lengths. The paper clips line up in what corresponds to the 'time of origin' position. The co-ordinates of the focus are measured from each wall and the floor with a graduated scale.

The graphical locator has many advantages:-

/THE....



THE LOCATOR

FIGURE 1. 10

(i) It is rapid to use.

(ii) The position and length of the seismic path, and the angle at which it approaches the seismometer can be seen.

(iii) Any correction to the assumed velocity, because of the position of the seismic path, can readily be made.

(iv) The locator automatically precludes paths from passing through the excavation.

(v) It is easy to see when and where an error has been made in determining a time of arrival.

(vi) The scatter in the best line-up of the paper clips enables the accuracy of each location to be estimated.

To check the accuracy of location, the co-ordinates of the foci of the three velocity calibration shots were found, using the locator and the mean velocity of 18.5 ft/millisec. The co-ordinates determined in this way were compared with the known co-ordinates of the shots. The 90% confidence limits of location, using Student's distribution, were found from the differences between these two sets of co-ordinates to be $\pm$ 16 feet.

1. 3 The Results obtained from the Seismic Network on F Shaft

a) General

The installation of the equipment on F Shaft was started in August, 1960, and by November sufficient seismometers had been installed to enable locations to be made. Originally it had been planned to sample only a few days each week. However, it soon became apparent that it could not be assumed that the seismometers and cables would remain undamaged for long periods, and that many failures other than those reported by the mine occurred. So as to obtain a comprehensive picture of the development of the failures, and to make full use of the equipment whilst it remained operative, it was decided to record continuously every day, and to transcribe all these records.

/Continuous....

Continuous recording and transcription was started on 13th January, 1961, and was continued until 30th June, 1961. The duration of this period was 4,060 hours, during 2,280 of which recordings were made. On some days it was not possible to change the recording tapes, and other records were lost because of damaged seismometer cables, power failures and faulty magnetic tape.

b) The Location of Failure Foci and the Seismic Energy Radiated from the Failures.

The seismometer network was planned to locate only the foci of those failures which occurred within the network. The lengths of the seismic paths from the failures to the seismometers in this region are less than 1,000 feet. Over paths of this length, the separation in the times of arrival of the P and S waves is less than their period, and it is not possible to distinguish the S arrival clearly. The location in this region has, therefore, to be done on the basis of the times of arrival at the seismometers of the P waves only.

The accuracy with which the time of arrival of the initial seismic pulse can be determined is set by the rise-time and the amplification. With high frequency emphasis and an amplification of 5×10^4 on the sensitive channels, it was possible to read the times of arrival of the P waves to one millisecond.

The failures from which the seismic waves radiate occur across areas from a few square feet to hundreds of square feet. The precise location of each focus depends upon the points from which the first wave to reach each seismometer radiated. Presumably the failure progresses at a speed at or less than the P velocity. In this case, the first pulse to arrive at each seismometer originates at the start of the failure. If the first pulse is smaller than

/subsequent....

subsequent waves, it may be too attenuated to be detected at the seismometer. In this event, the first pulse to arrive at close and distant seismometers might not have originated at the same point.

A continuous recorder and seismic network designed to locate all the foci within a large region is necessarily limited in frequency responses and resolution. It is therefore not suitable for a detailed analysis of the progression of a failure. The failure foci located by this network are therefore points close to, and are probably the start of, each failure.

It was found that failure foci on the West side of G Shaft could be located with reduced accuracy. The length of the seismic paths for failures in this region was about 2,000 feet. Although the period of the S waves and the interval between the P and S arrivals were both about 50 milliseconds, it was possible to determine the P - S interval to within 5 milliseconds. The locations in this region are, therefore, accurate to only about 200 feet.

"Bursts", or sudden releases of seismic energy, were selected from each magnetic tape record for transcription on to photographic paper. The trigger circuit was set to select all those events within the seismometer network radiating seismic energy in excess of 10^3 ft.-lbs. This appeared to be roughly the seismic energy radiated by a pound of dynamite. It was the smallest burst which could be detected above the background noise on sufficient seismometers for location. With this sensitivity, nearly all the shots which occurred during blasting of the face were transcribed. This was done for only ten days, so as to

/obtain....

obtain a picture of all the events during blasting. The remaining records were transcribed with a lower trigger sensitivity during blasting, so as to select only the larger bursts during that time.

With this triggering arrangement, about twenty bursts were transcribed each day, of which an average of seven occurred within the location region. Continuous transcription of portions of the magnetic tapes indicated that some 10^4 minor bursts radiating energy less than 10^3 ft.-lbs. occur each day.

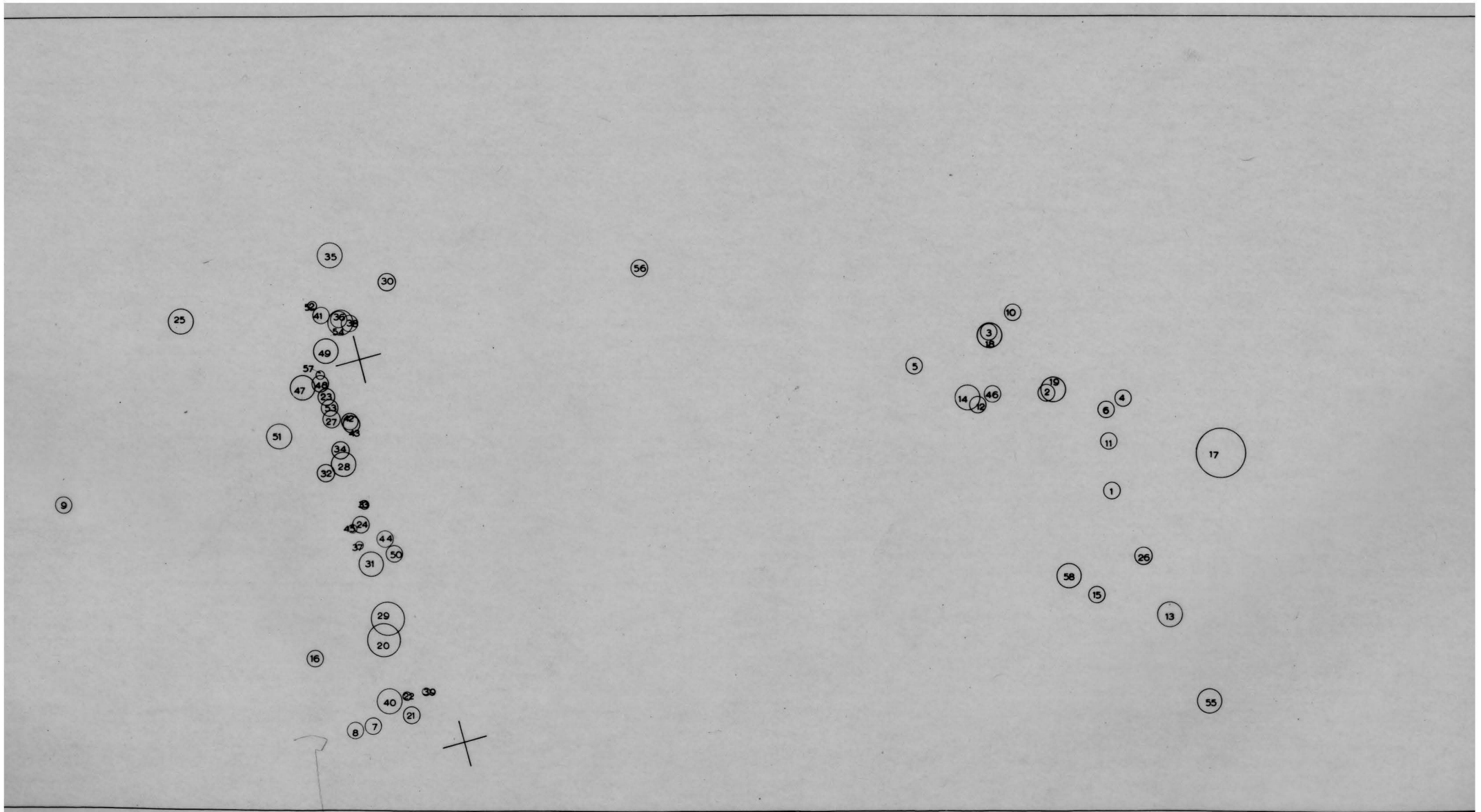
The location of each transcribed burst was found and the co-ordinates of those foci falling within the location region were determined. The position in plan of each focus is plotted as the centre of a circle in Figure 1.11. The elevations of those foci within the seismometer network are plotted as the centres of the circles in Figure 1.12. The diameters of the circles represent to an approximately logarithmic scale, as shown in the reference of Figure 1.12, the seismic energy radiated between 15 c.p.s. and 150 c.p.s.

Seismic energy radiated between 15 c.p.s. and 300 c.p.s. was recorded on the oscillograph records. Most of the energy in the larger bursts was radiated at about 20 c.p.s.

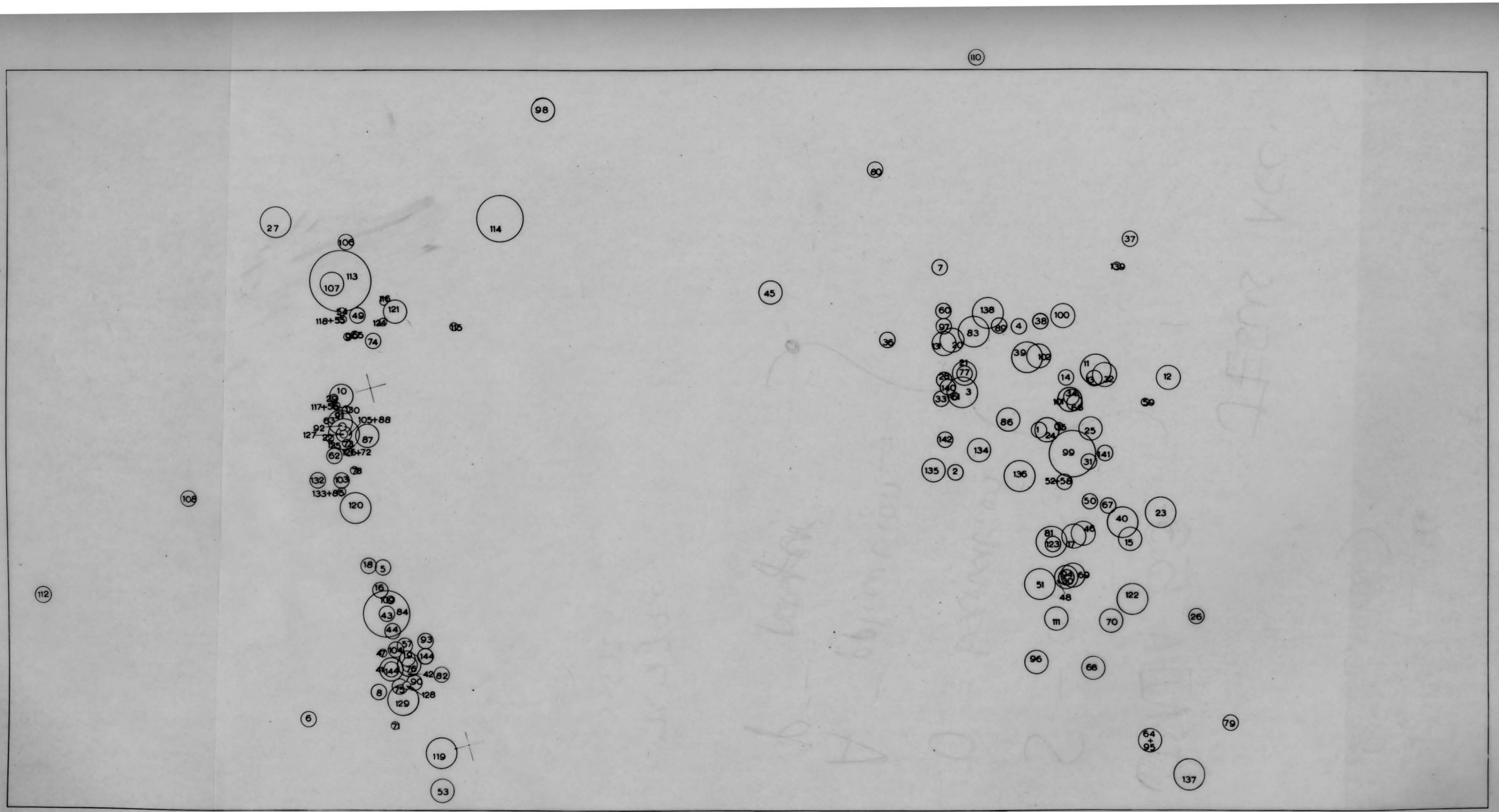
The amplitudes of the seismic waves detected by the seismometers varied inversely as the distance from the focus to the seismometers, indicating that the seismic waves radiated from a limited region not exceeding a few hundred feet around the focus.

Assuming that the seismic energy crossing a sphere of radius r, with the focus as its centre, is mainly a series of sine waves, then the radiated energy is:-

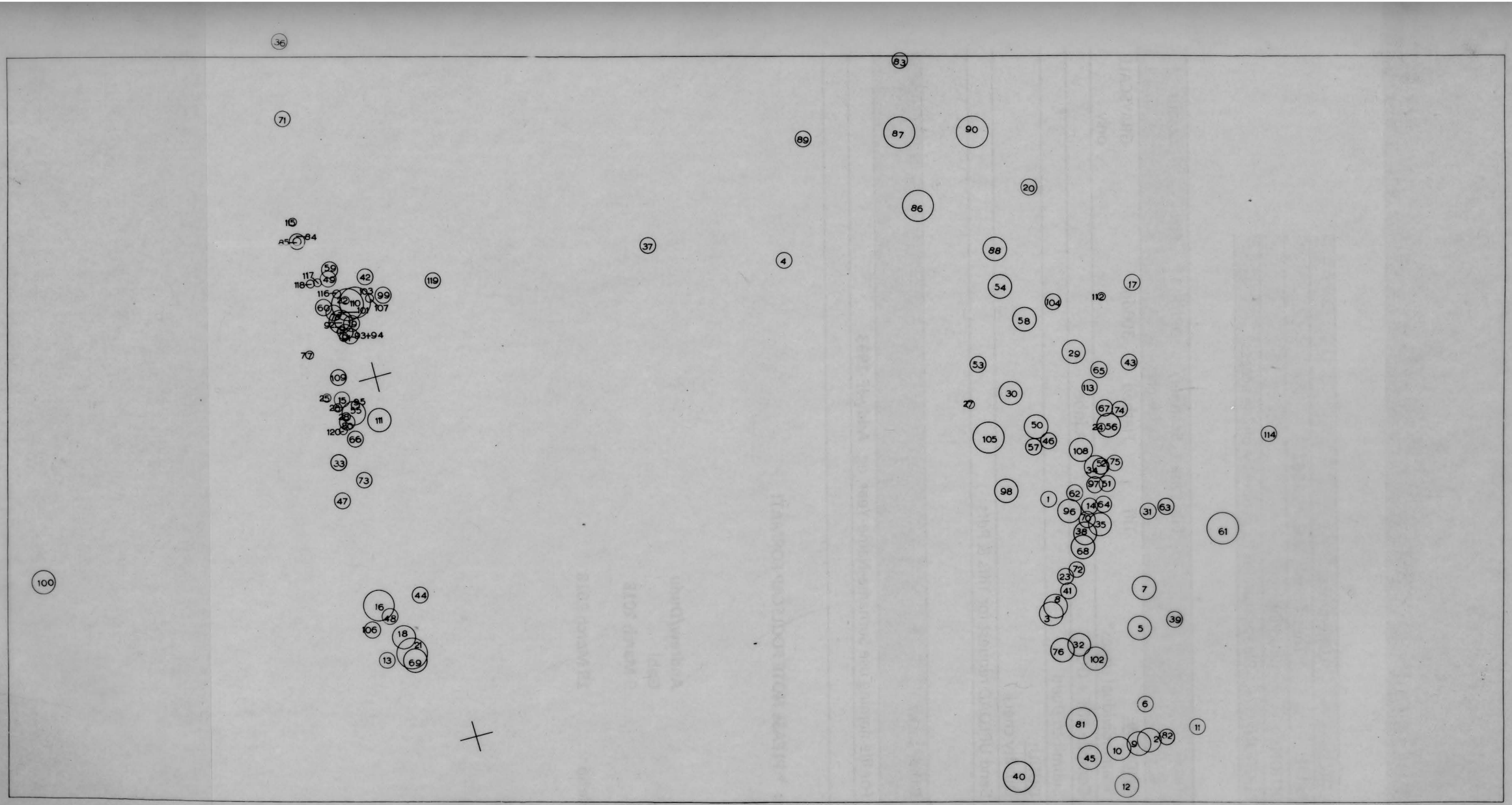
/PLAN....



BURST PLOTS FROM 1st.—30th. JUNE 1961



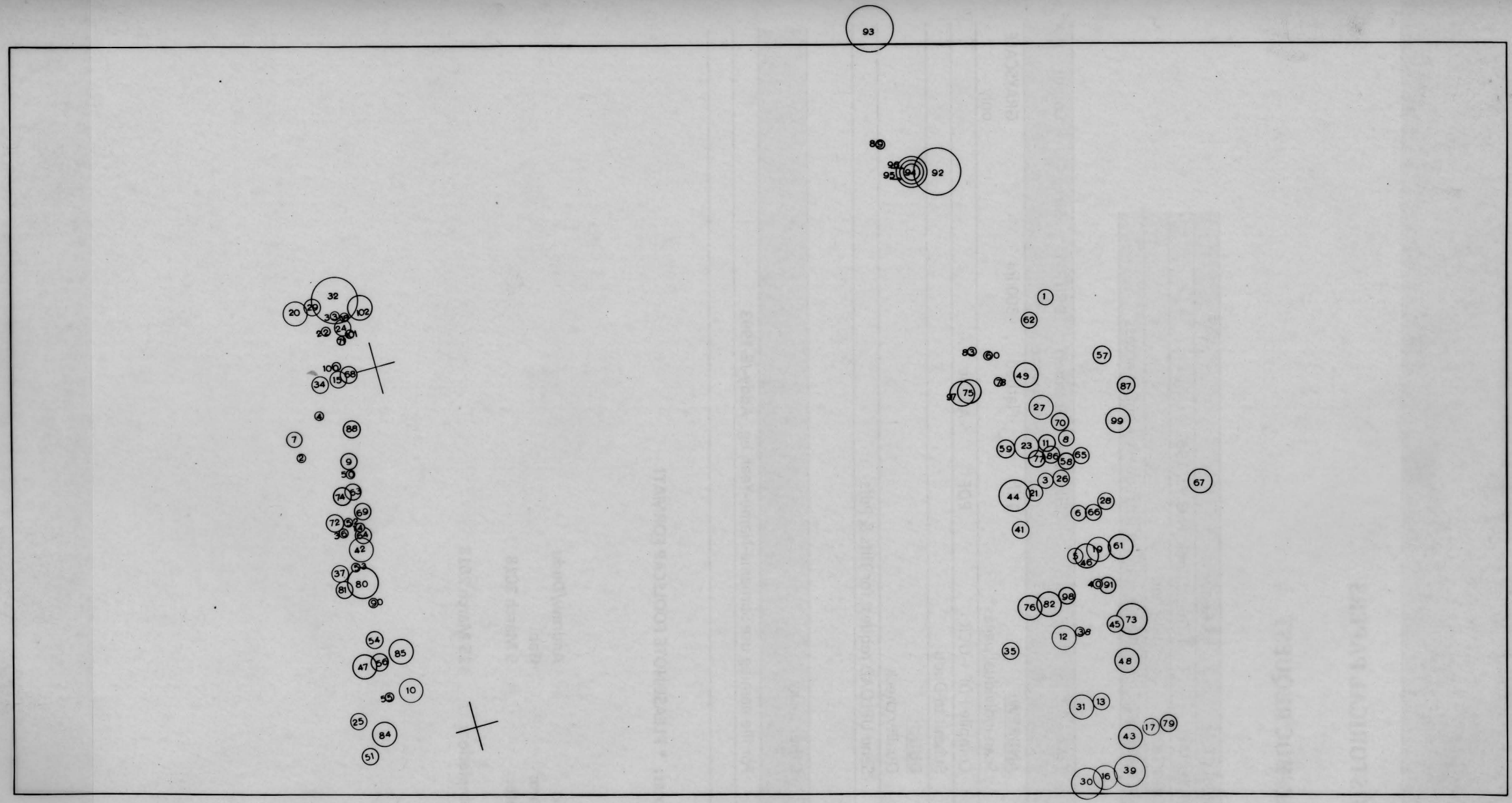
BURST PLOTS FROM 1st.-31st. MAY 1961.



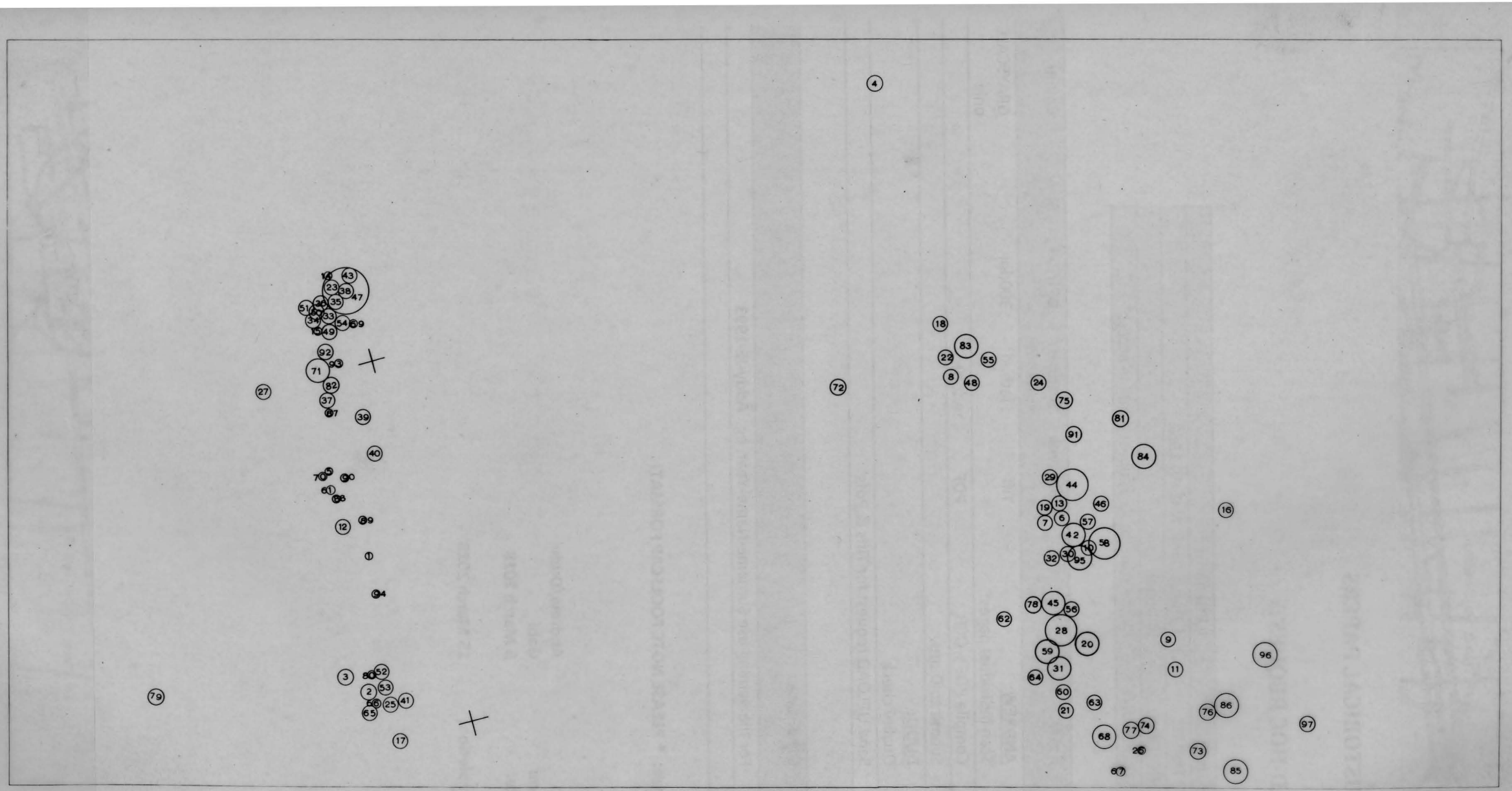
BURST PLOTS FROM 1st. – 30th. APRIL 1961



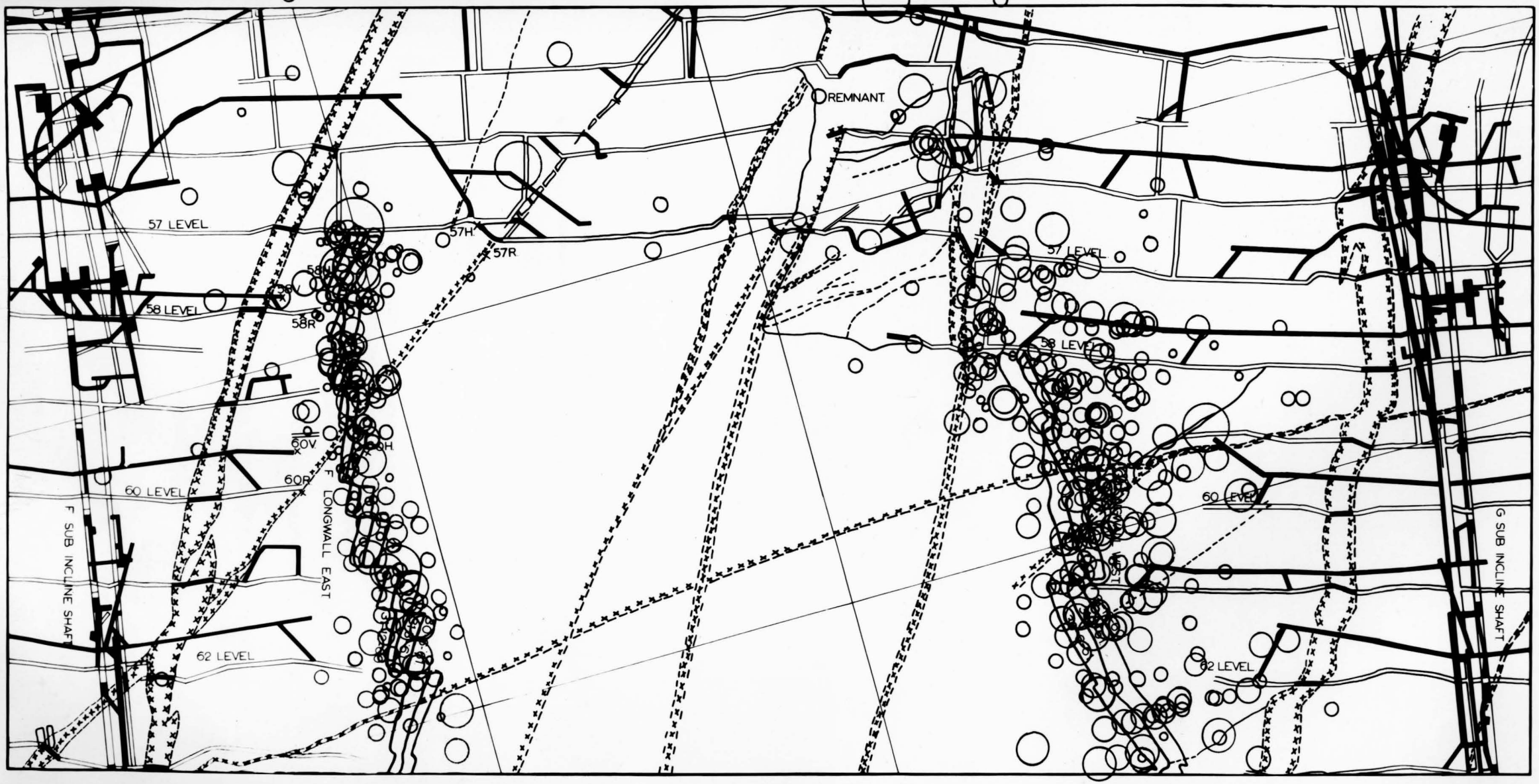
BURST PLOTS FROM 1st. – 31st. MARCH 1961.



BURST PLOTS FROM 1st FEB – 28th FEB 1961

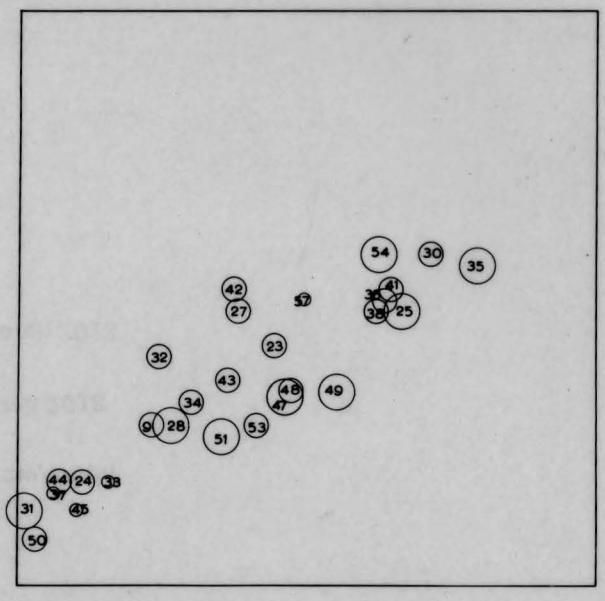


BURST PLOTS FROM 13th JAN. – 31st JAN. 1961

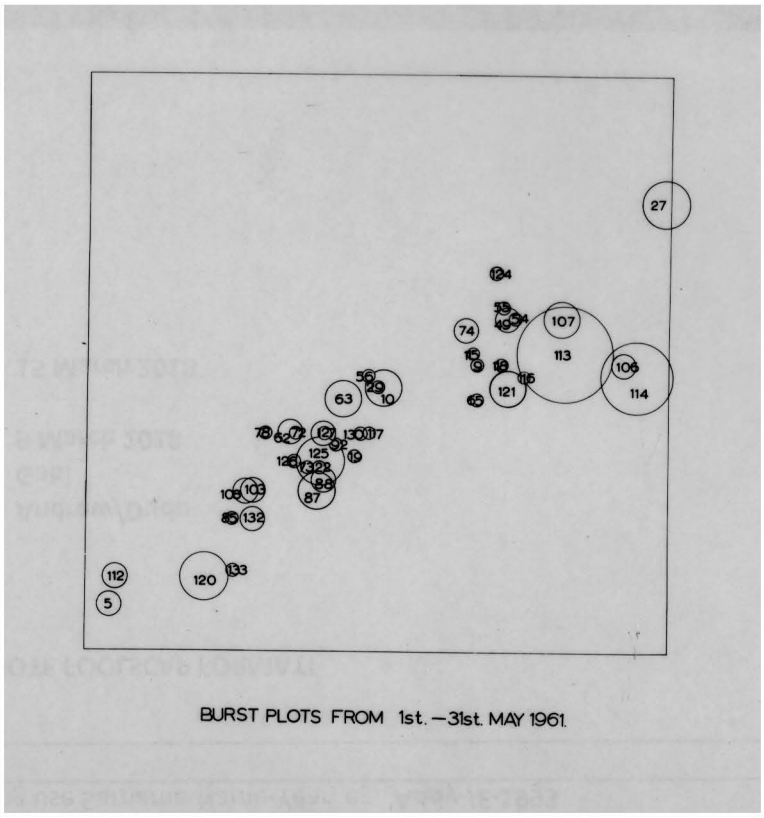


PLAN OF PORTION BETWEEN 'F' AND 'G' SUB INCLINE SHAFTS E.R.P.M.

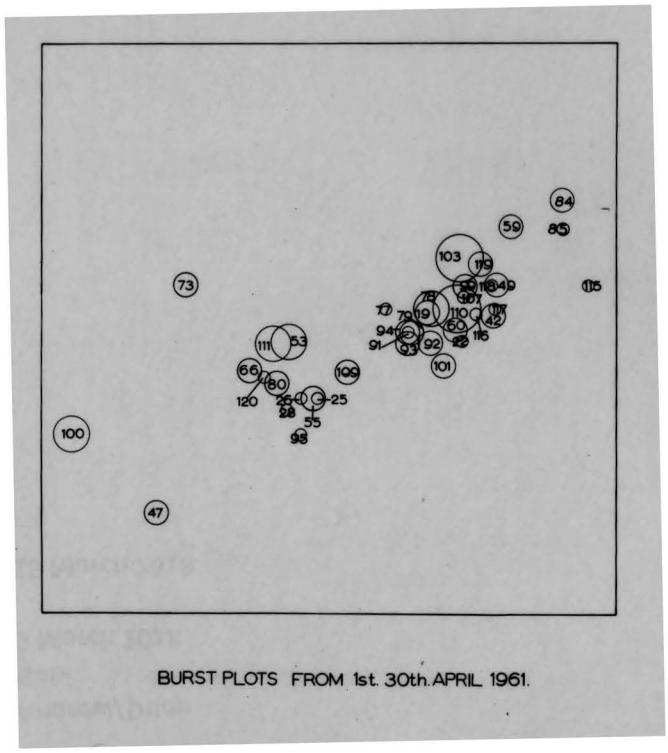
1000' GRID



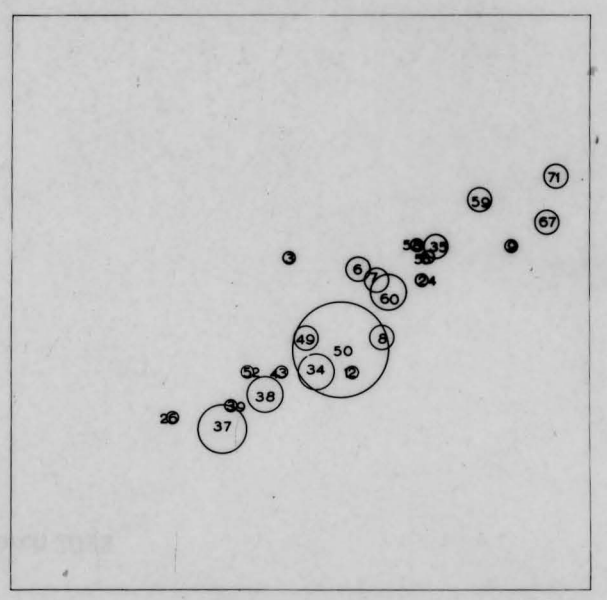
BURST PLOTS FROM 1st.–30th. JUNE 1961



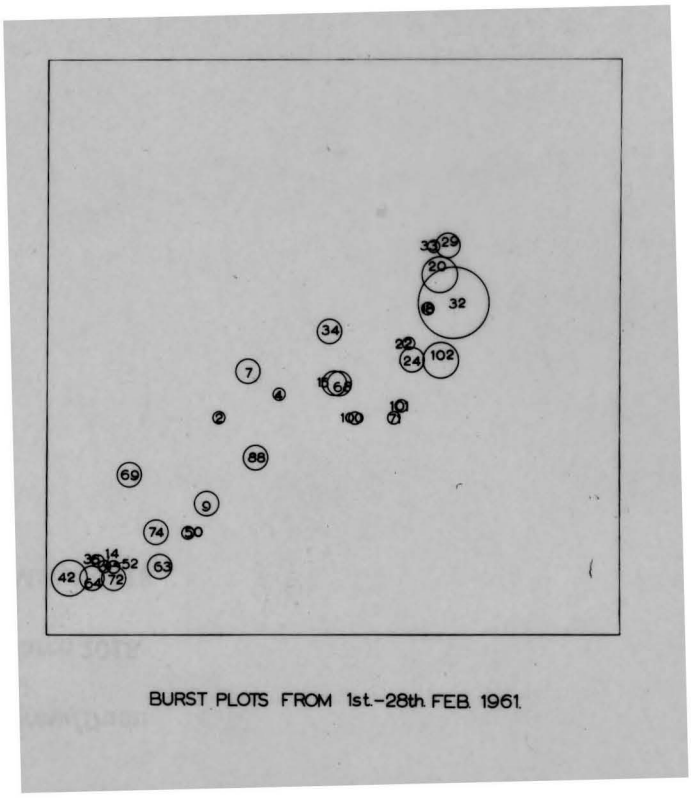
BURST PLOTS FROM 1st. — 31st. MAY 1961.



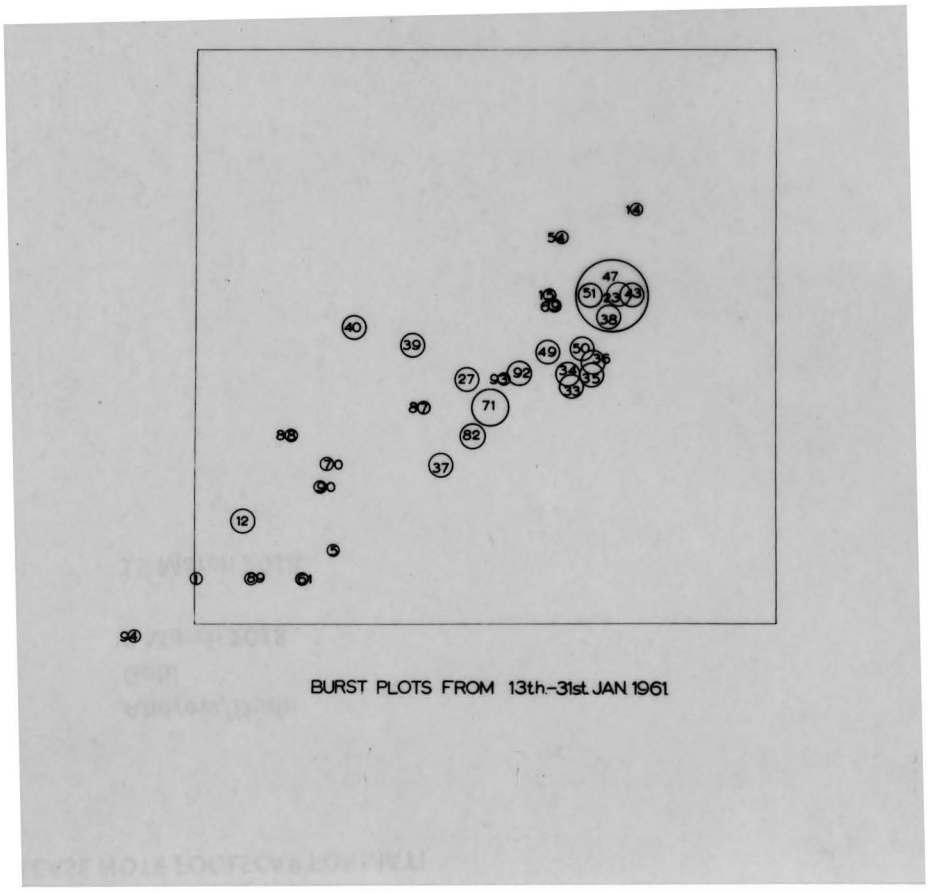
BURST PLOTS FROM 1st. 30th. APRIL 1961.



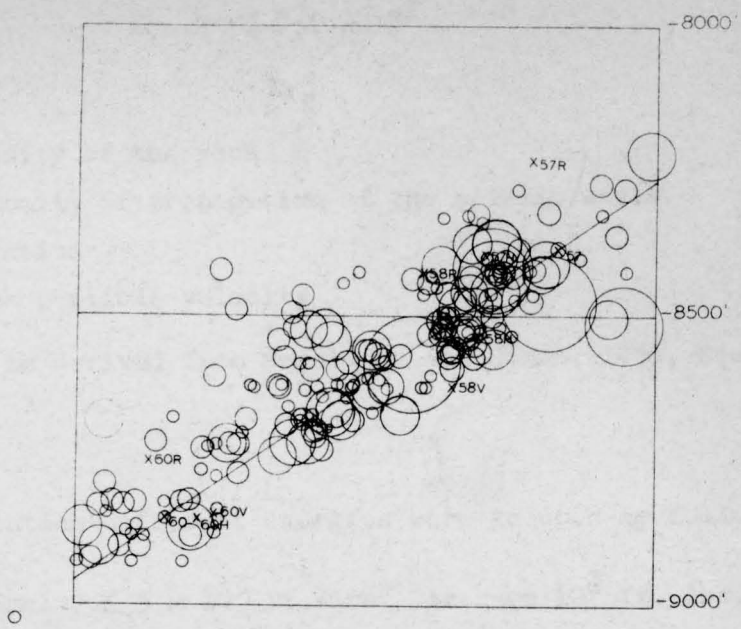
BURST PLOTS FROM 1st.–31st. MARCH 1961



BURST PLOTS FROM 1st.-28th. FEB. 1961.



BURST PLOTS FROM 13th.-31st. JAN 1961



SECTION THROUGH FACE OF PORTION OF 'F' LONGWALL EAST

SCALE 1=4000

1000 500 0 1000 FEET

REFERENCE:

- FOOTWALL DRIVES.
- REEF DRIVES.
- DYKES.
- FAULTS.
- X SEISMOMETER.
- H HORIZONTAL SEISMOMETER.
- R VERTICAL SEISMOMETER IN HANGING.
- V VERTICAL SEISMOMETER IN FOOTWALL.
- VERY SMALL BURST 10^3 FT.-LBS. (10^{10} ERGS.)
- SMALL BURST 10^4 FT.-LBS. (10^{11} ERGS.)
- MEDIUM BURST 10^5 FT.-LBS. (10^{12} ERGS.)
- LARGE BURST 3×10^6 FT.-LBS. (3×10^{13} ERGS.)
- VERY LARGE BURST 10^8 FT.-LBS. (10^{15} ERGS.)
- VERY VERY LARGE BURST 10^9 FT.-LBS. (10^{16} ERGS.)

$$E = 2\pi d\, C\, T\, r^2\, \hat{v}^2$$

where:-

d = density of the rock

C = velocity of propagation of the seismic waves

T = duration

$\hat{v}$ = peak particle velocity

(This equation is derived from Macelwane and Sohon, 1936, Equation 7.94, p.177).

Bursts radiating different energies were grouped as follows:-

1. (Very Small) $< 5 \times 10^3$ ft.-lbs. Average 10^3 ft.-lbs. (10^{10} ergs)
2. (Small) (5×10^3 to 5×10^4) ft.-lbs. Average 10^4 ft.-lbs. (10^{11} ergs)
3. (Medium) (5×10^4 to 5×10^5) ft.-lbs. Average 10^5 ft.-lbs (10^{12} ergs)
4. (Large) (5×10^5 to 5×10^7) ft.-lbs. Average 3×10^6 ft.-lbs. (3×10^{13} ergs)
5. (Very Large) (5×10^7 to 5×10^8) ft.-lbs. Average 10^8 ft.-lbs. (10^{15} ergs)
6. (Very, Very Large) 5×10^8 to 5×10^9 ft.-lbs. Average 10^9 ft.-lbs. (10^{16} ergs)

The average energy in each group is nearer the lower limit because burst frequency increases as the energy decreases (See Table 1.3, page 49).

The largest bursts were felt as "tremors", and were recorded on the seismograph at Pretoria, 60 km. away, with a ground amplitude betwen 10^{-4} mm. and 10^{-3} mm.

During the course of the investigation, it was suggested that there might be some seismic warning of an impending rockburst. The background noise in the mine was predominantly low frequency, and it was decided to examine seismic radiation above a kilocycle. A seismometer was modified to make its suspension stiffer and damp it

/with....

with oil. As high frequencies cannot be recorded on the tape, the output of this seismometer was rectified and the rectified envelope was recorded on the tape. The records obtained in this way showed that there was a great deal of seismic radiation at high frequencies. This radiation came in distinct bursts, of which there were about 10^4 per day. Often these bursts were separated by less than a second, and formed an almost continuous period of activity, lasting for several seconds. Sometimes high frequencies were radiated about a second before a major burst. This was not always the case, and many large bursts occurred without prior high frequency radiation. High frequency radiation was also detected during periods free from major bursts. There appeared to be no obvious correlation between high frequency radiation and major bursts.

c) A Discussion of the Burst Location

The bursts plotted in Figures 1.11 and 1.12 show that most of the burst foci are close to the working faces - that is, the two long-walls and the remnant. All but a few of the foci on the East side of the F Shaft follow the contour of the face very closely. Those bursts removed from the face tend to be small, and those towards the Shaft tend to fall more in the hanging. The foci on the West side of G Shaft fall in a broad band close to the face. This scatter is probably due to the less accurate location in this region.

All the rockbursts noticed by the miners on East Rand Proprietary Mines, Ltd. are reported and classified. The positions and severity of the reported rockbursts are assessed from the damage observed in the stopes. Table 1.2 gives a list of those rock-bursts which were reported whilst the seismic network was operating.

/TABLE....

TABLE 1.2

ROCKBURST CLASSIFICATION				SEISMIC CLASSIFICATION		
SECTION	WORKING PLACE	DATE AND TIME OF BURST	CLASSIFICATION	IDENTIFICATION No. OF BURST.	SIZE	LOCATION
1. Angelo	61 W/L/W	26/1/61 09.25	Medium to Slight Extra Dosal.	58	Large 3×10^6 ft.-lbs.	60/61
2. Angelo	60/61 W/L/W	20/2/61 10.25	Medium to Slight Intra Dosal.	49	Medium. 10^5 ft.-lbs.	58/59
3. Angelo	60/61 W/L/W	23/2/61 02.40	Medium to Slight Intra Dosal.	67	Medium 10^5 ft.-lbs.	60
4. Angelo	West Remnant	28/2/61 08.00	Medium to Slight Extra Dosal.	92 & 93	Very large 3×10^8 ft.-lbs.	West Remnant
5. Driefontein	59 E/L/W	28/3/61 Between Shifts	Medium to Slight Intra Dosal.	50	Very, very large 10^9 ft.-lbs.	58/59
6. Angelo	61 W/L/W	19-20/4/61 Between Shifts	Slight Intra Dosal.	81	Large 3×10^6 ft.-lbs.	62
7. Driefontein	58 E/L/W	26/5/61 22.50	Severe Extra Dosal.	113	Very, very large 10^9 ft.-lbs.	57/58

Note: This table refers to seven rockbursts which occurred whilst the seismic network was operating.

It can be seen that the positions determined from the damage agree with those determined seismically. All the reported rockbursts radiated seismic energy in excess of 5×10^4 ft.-lbs., but there is no relation between the seismic energy and the severity determined from the damage.

A total of 187 bursts radiating seismic energy in excess of 5×10^4 ft.-lbs. were located by the network. In the same region, over the same period of time, only seven rockbursts were reported by the miners. Therefore only a small proportion of those failures radiating a large amount of seismic energy cause noticeable damage to the workings. It appears that only the larger bursts can cause noticeable damage, but that many of the larger bursts pass unobserved. There appears to be no difference in location between those larger bursts which are noticed as rockbursts and those which are not.

Mr. A.J. White, of East Rand Proprietary Mines, Ltd., has noticed that a face where a rockburst has occurred may appear to be no different from a face which has been blasted. It appears that failures of similar magnitude cause varying degrees of damage to a stope. It is suggested that the degree of damage is determined by the stability of the rock in the immediate hanging and footwalls. In this respect, two very, very large bursts which occurred within the seismometer network on 28th March and 26th May are of interest. Both of these bursts radiated seismic energy of 10^9 ft.-lbs. and were similarly situated. However, the damage caused by them to the stope was vastly different, as is shown by their classification in Table 1.2 (page 41).

The burst in May was followed after 36 minutes by a very large burst, removed from the face but near a fault in the worked-out area above the F East longwall. It was probably caused by a

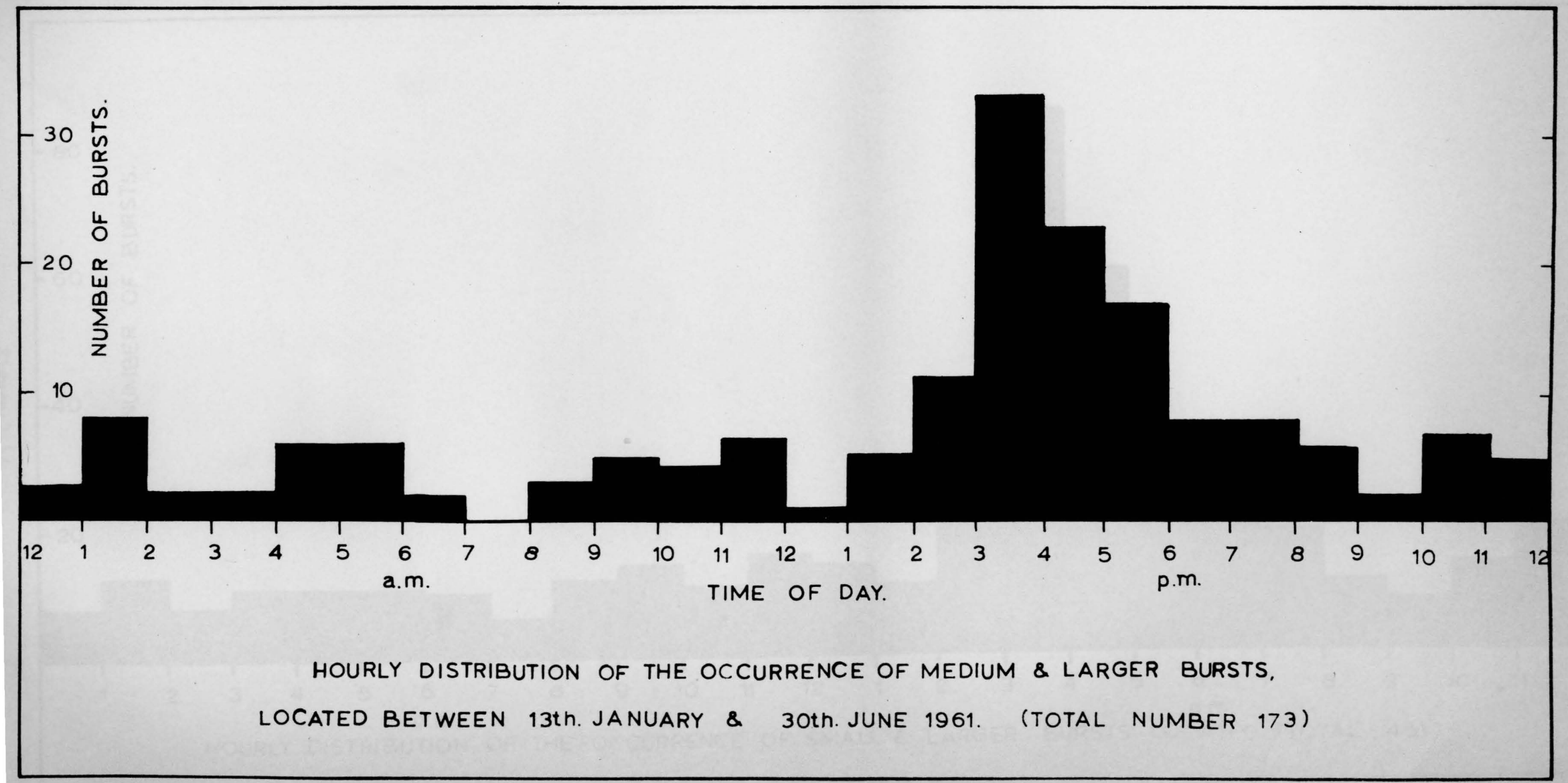
/redistribution....

redistribution of the stress on the fault after the first burst. Large bursts are often followed by other bursts which may occur several hours after the first one.

Two very large bursts occurred in February, on opposite sides of the remnant above G West longwall. This remnant was being mined at the time. The bursts were separated by an interval of four seconds. They were followed during the succeeding few hours by a series of smaller bursts. The incident was classified by the mine as a single rockburst.

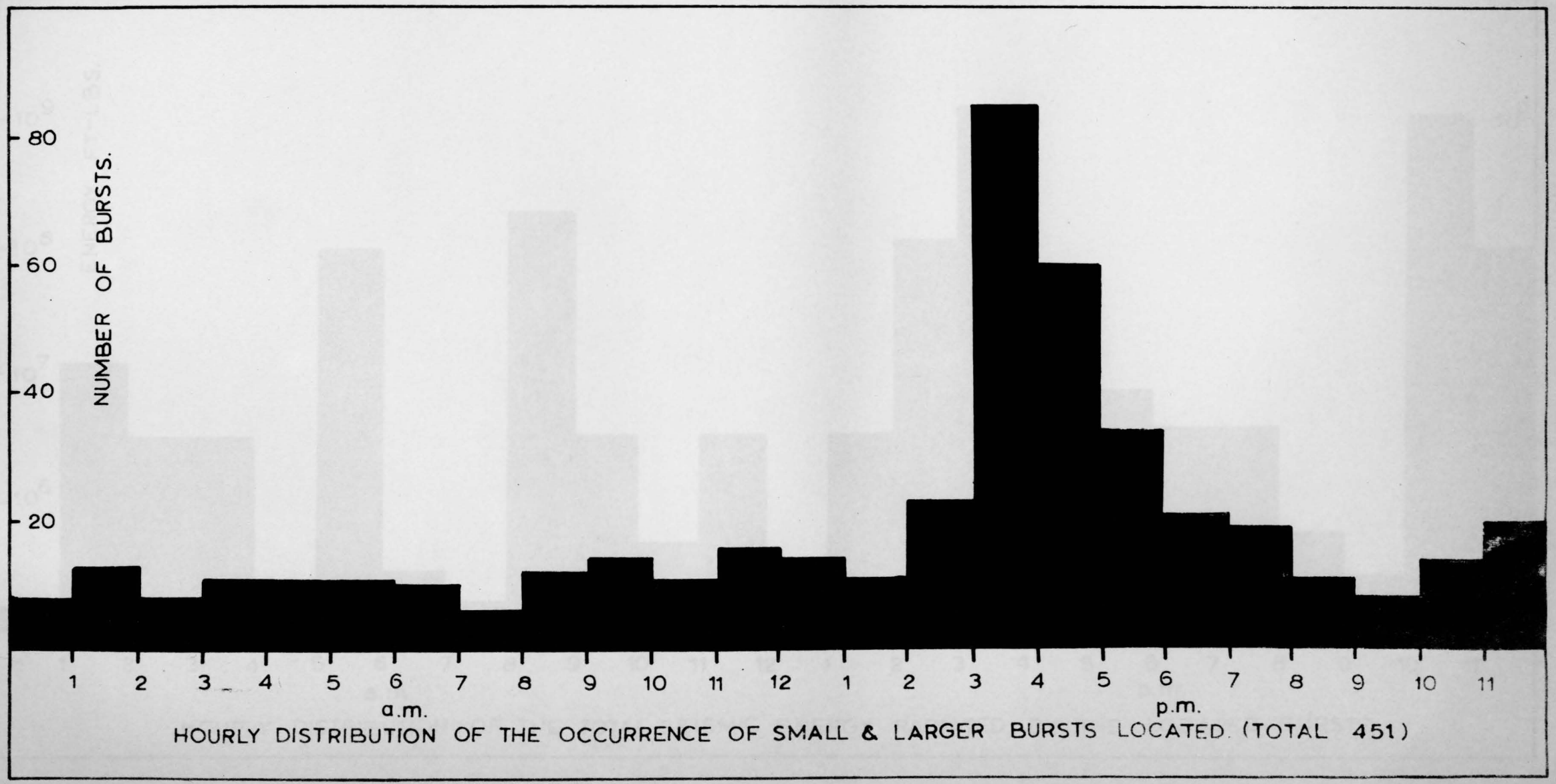
The same mining operations take place at the same time each day. For this reason, it was felt that it might be useful to plot some of the data against the time of the day. All these plots are based on the information obtained from the seismic network between 13th January and 30th June, 1961. It should be noted that the seismic network was operative for only 56% of this period. In Figure 1.13, the diurnal distribution of the number of medium and larger bursts located by the network is plotted. Figure 1.14 is a similar plot, including the small bursts. The diurnal distribution of the seismic energy radiated by the located bursts is plotted on a logarithmic scale in Figure 1.15. All these plots show a similar distribution. There is a very marked increase in the occurrence of bursts between 3 p.m. and 6 p.m., during which time blasting of the faces covered by the network takes place. These plots also show an increase between 1 p.m. and 2 p.m., when blasting of the reclamation areas some thousands of feet away starts. Another increase seems to occur at 10 p.m., when night shift cleaning of the blasted stopes starts. These last two increases seem to indicate that relatively small disturbances can trigger bursts.

/HOURLY....

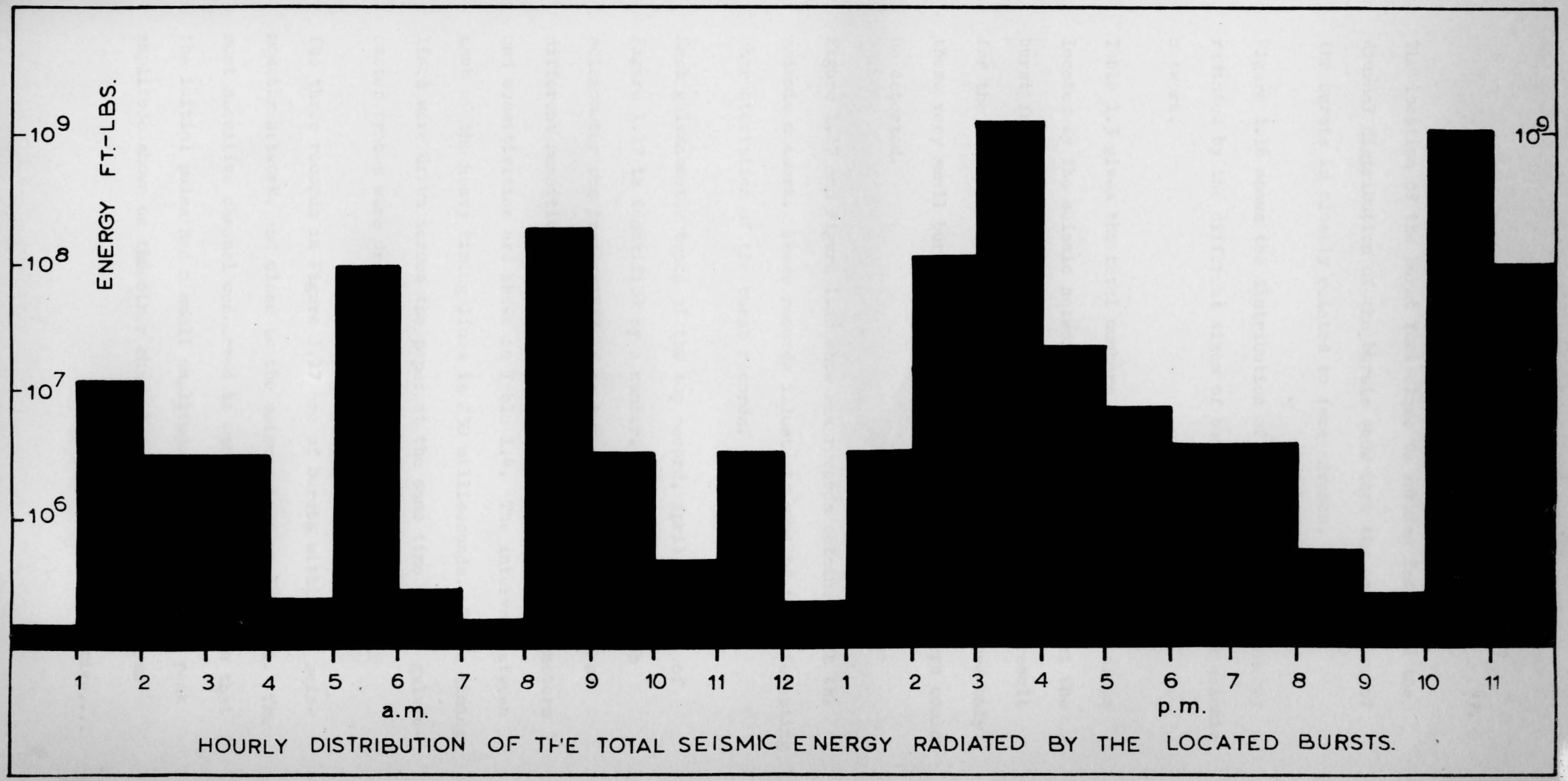


HOURLY DISTRIBUTION OF THE OCCURRENCE OF MEDIUM & LARGER BURSTS,

LOCATED BETWEEN 13th. JANUARY & 30th. JUNE 1961. (TOTAL NUMBER 173)



HOURLY DISTRIBUTION OF THE OCCURRENCE OF SMALL & LARGER BURSTS LOCATED. (TOTAL 451)



HOURLY DISTRIBUTION OF THE TOTAL SEISMIC ENERGY RADIATED BY THE LOCATED BURSTS.

The location of the burst foci close to working faces and the diurnal distribution of the bursts show that the occurrence of the bursts is closely related to face advance.

Figure 1.16 shows the distribution of the total seismic energy radiated by the different sizes of bursts, located by the seismic network.

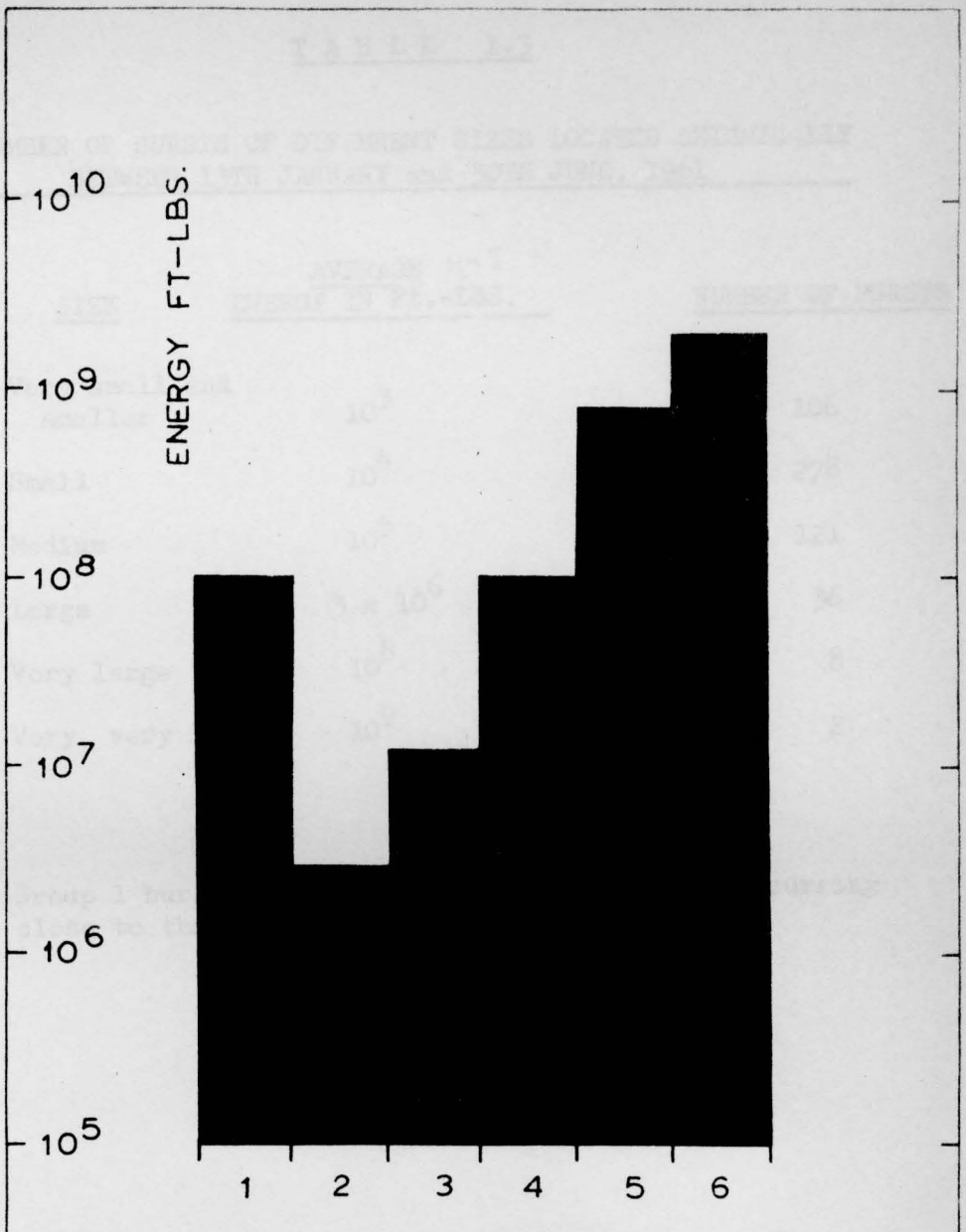
Table 1.3 gives the total numbers of bursts of differenc sizes located by the seismic network, from which it appears that the burst frequency increases as the energy decreases. The result for the smallest bursts, Group 1, is not anomalous, because only those very small bursts occurring close to the seismometers could be detected.

Figure 1.17 and Figure 1.18 show six records obtained with the seismic network. These records illustrate most of the interesting characteristics of the burst records.

Each galvanometer trace of the top record, April No. 101, of Figure 1.17 is identified by a number. The output of each seismometer was transcribed on to two galvanometer traces of different sensitivities. The galvanometer traces, seismometers and sensitivities are shown in Table 1.4. The interval between each of the heavy timing lines is 230 milliseconds. These timing lines were drawn across the paper at the same time as the galvanometer traces were drawn.

The three records in Figure 1.17 are of bursts within the seismometer network, and close to the seismometers on 58 level. The most sensitive channel connected to each seismometer shows that the initial pulse has a small amplitude compared with the peak amplitude shown on the other channel, which is 30 times less

/sensitive....



1 VERY SMALL & SMALLER $<10^3$ FT-LBS.

2 SMALL 10^4 FT-LBS.

3 MEDIUM 10^5 FT-LBS.

4 LARGE 3×10^6 FT-LBS.

5 VERY LARGE 10^8 FT-LBS.

6 VERY VERY LARGE 10^9 FT-LBS.

TOTAL ENERGY RADIATED BY DIFFERENT SIZED BURSTS BETWEEN 13th. JANUARY 30th. JUNE 1961.

Figure 1.16

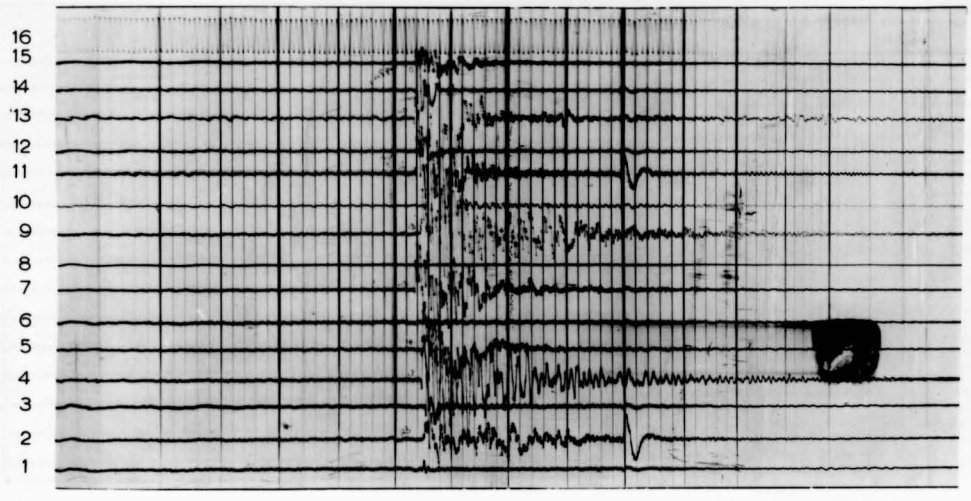
TABLE 1.3

THE NUMBER OF BURSTS OF DIFFERENT SIZES LOCATED SEISMICALLY BETWEEN 13TH JANUARY and 30TH JUNE, 1961

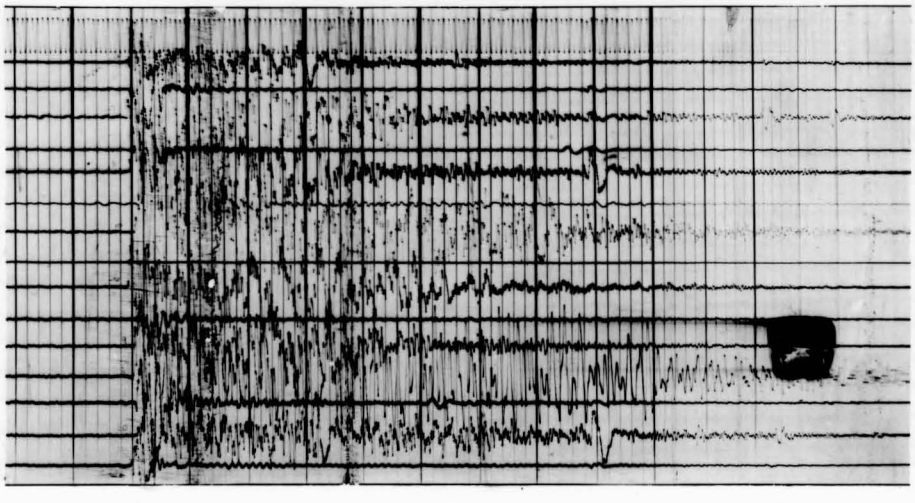
	SIZE	AVERAGE ENERGY IN Ft.-LBS.	NUMBER OF BURSTS
1.	Very small and smaller	10^3	106
2.	Small	10^4	278
3.	Medium	10^5	121
4.	Large	3×10^6	36
5.	Very large	10^8	8
6.	Very, very large	10^9	2

NOTE:

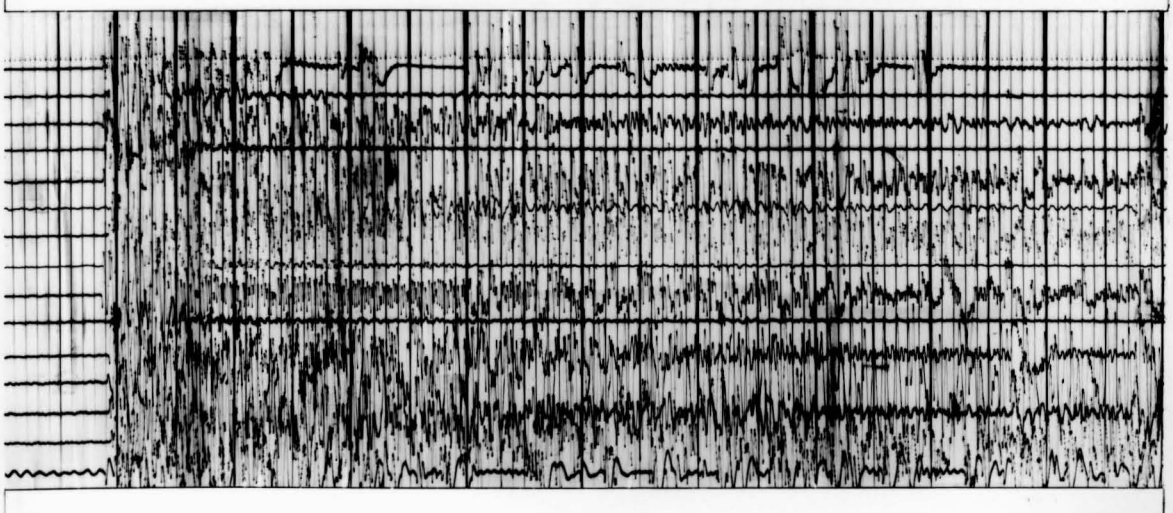
Group 1 bursts were so small that only those occurring close to the seismometers were located



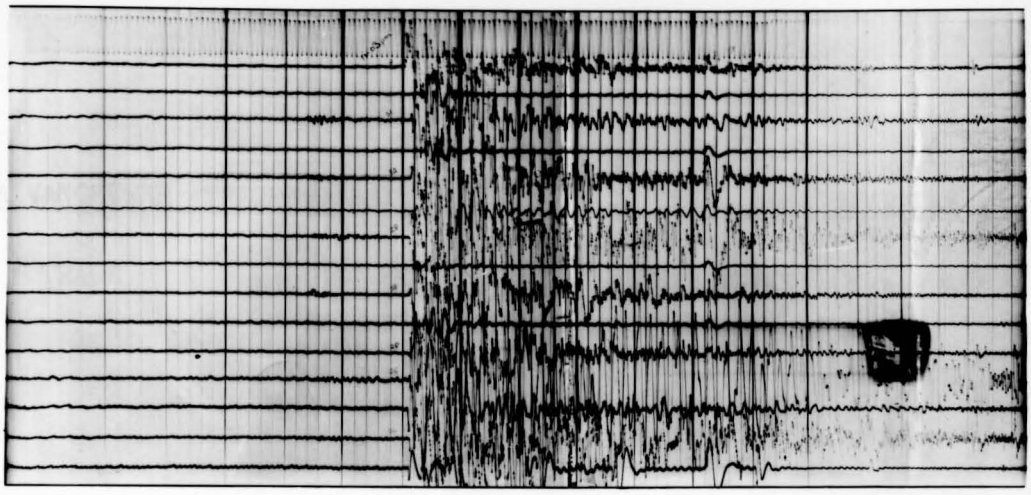
APRIL 1961. Nº 101. MEDIUM.



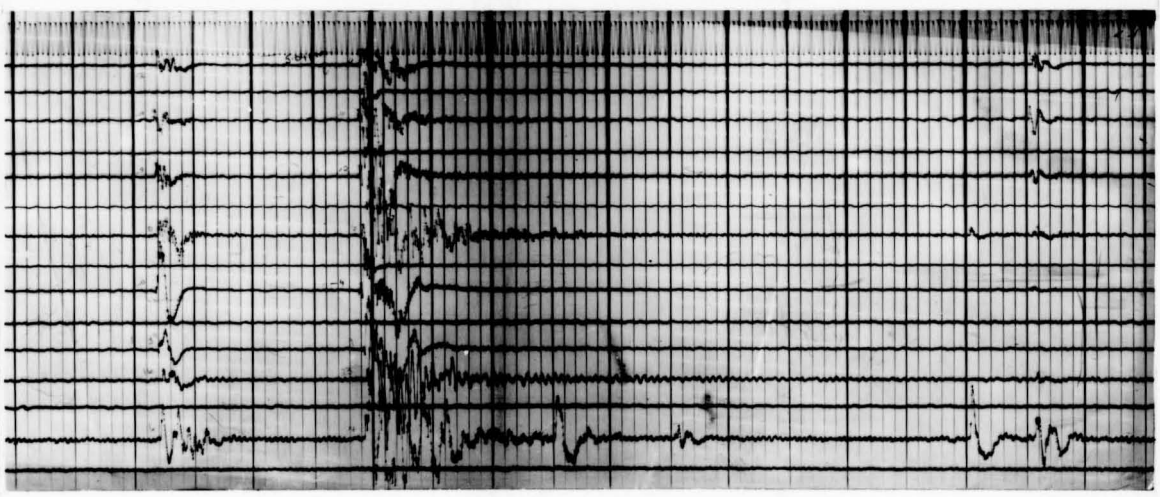
APRIL 1961. Nº 103. LARGE.



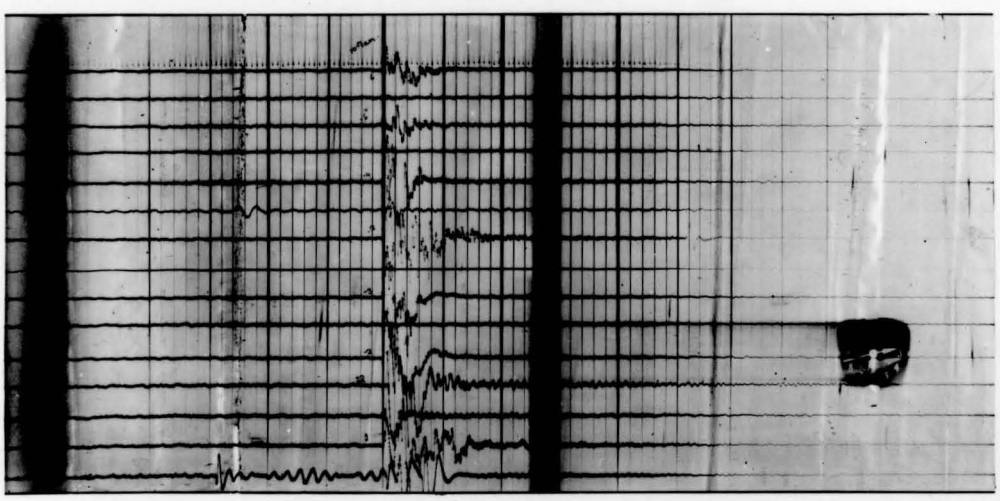
MAY 1961. Nº 113. VERY, VERY LARGE.



MAY 1961. VERY LARGE. Nº 99.



MAY 1961. MEDIUM. Nº 63.



MAY 1961. SMALL. Nº 105.

TABLE 1.4

GALVANOMETER TRACES, SEISMOMETERS AND THEIR SENSITIVITIES

TRACE	SEISMOMETER	SENSITIVITY (Max = 1)
1	57H *	$\frac{1}{450}$
2	60H	$\frac{1}{3}$
3	60H	$\frac{1}{45}$
4	57R	$\frac{1}{3}$
5	60R	$\frac{1}{15}$
6	60R	$\frac{1}{450}$
7	58H	$\frac{1}{15}$
8	58H	$\frac{1}{450}$
9	60V	$\frac{1}{10}$
10	60V	$\frac{1}{150}$
11	58V	$\frac{1}{15}$
12	58V	$\frac{1}{450}$
13	58R	$\frac{1}{15}$
14	58R	$\frac{1}{450}$
15	57H	$\frac{1}{15}$
16	50 c.p.s. time trace	

* Channel 1 was connected to the high frequency seismometer and rectifier for records May 99; 105; 113.

sensitive. The initial pulse is probably radiated at the start of the failure, and the maximum energy is probably only radiated when the failure has developed fully.

Burst No. 113 in May cut the seismometer cable to Channel 15. The effect of this is seen in the waveform of that channel. In this burst, Channel 1 was connected to the high frequency seismometer and some high frequency noise can be seen preceding the burst.

In Figure 1.18, Burst No. 99, in May, occurred on 59 level G West longwall. On the less sensitive channels the S arrival can be seen. Burst No. 63, in May, occurred on F East longwall, 59 level, following a blast which can be seen preceding it by less than a second. This blast was one of several on 59 level face. The low frequency of the blast record is due to overloading of the amplifiers by the high frequency compressional pulse of the blast. Burst No. 105, in May, shows typical high frequency radiation on Channel 1, preceding a burst. The high sensitivity channels are also overloaded.

An analysis of the distribution of energy amongst the different phases for major bursts at some distance from the network is shown on Table 1.5. This indicates that shear forms a major part of the failure in each burst.

1.4 Summary

The seismic network was installed on F Shaft of East Rand Proprietary Mines, Ltd., at a depth between 8,000 feet and 9,000 feet below surface, where it was operated continuously over a period of six months. The foci of all the bursts releasing seismic energy in excess of 10^3 ft.-lbs. which occurred between 56 level and 62 level on F East longwall were located to within 20 feet. The foci

/of....

TABLE 1.5

PHASE DISTRIBUTION OF ENERGY

ENERGY FT.-LBS.	DIRECTION OF BURST FROM SEISMOMETERS	RELATIVE P.	PHASE S.V.	ENERGY S.H.
		.02 ?		
3×10^6	South	.12	.59	.39
3×10^6	South East	.06	.71	.23
10^8	East)On G	.01	.69	.30
10^8	East)West)Remnant	.01	.59	.40
10^7	West	.05	.76	.19
10^8	South East	.01	.69	.30
10^{10}	East	.04	.67	.29

of the bursts releasing seismic energy in excess of 10^4 ft.-lbs. which occurred between 54 and 62 levels West of G Shaft were located to within 200 feet.

The foci of 458 bursts were located, and the data indicate that in both position and time the occurrence of bursts is closely related to the advance of the working faces - that is, nearly all the bursts occur close to those faces and fall during blasting time. Of 187 bursts radiating seismic energy in excess of 5×10^4 ft.-lbs., only 7 caused observed damage to the workings. There appear to be no differences in energy or location between those 7 bursts and the others. The extent of the observed damage does not seem to be related to the seismic energy release.

Major bursts often start a series of bursts and relatively small disturbances such as distant blasting seem to trigger bursts.

Most of the seismic energy radiated from a burst is in the form of shear waves.

PART II SOME MECHANICAL PROPERTIES OF QUARTZITE AND ROCK STRESS

2.1 The Failure of Quartzite

a) A Failure Criterion for Quartzite

The Council for Scientific and Industrial Research has done comprehensive compression tests on cylindrical specimens 1 inch long by 1 inch diameter of rock taken from mines on the Witwatersrand (Denkhaus, Roux, Grobbelaar, 1958) (Grobbelaar, 1958). The results form a basis for the comparison of the strength of different rocks, but the information obtained from them is insufficient to establish a failure criterion. Robertson (1955) established an empirical failure criterion for silicate rocks defined by the equality of the maximum shear stress and the mean stress. Certain anomalies exist in such a definition; for example, under uniaxial compression the maximum shear stress always exceeds the mean stress. Most of Robertson's tests were done on hollow cylinders, the outsides of which were subject to hydrostatic pressure. This results in a non-uniform stress distribution in the specimen, and failure must first start on the inside surface of the hollow cylinder. In these circumstances it is difficult to determine the stresses when the whole specimen fails. The results which fit the Robertson criterion best are those obtained from hollow cylinders.

Some further knowledge of the stresses which produce failure in quartzite, particularly at the stresses likely to be encountered around a mining excavation - that is, less than 50,000 p.s.i. - seemed necessary. It was decided that it would be best to investigate failure under conditions of uniform stress distribution. This facilitates interpretation of the results and reduces the

/effects....

effects of heterogeneities in the sample, which are accentuated in a non-uniform stress system where failure starts in a small region of the specimen.

In most multi-axial tests on rock specimens, an axial load is applied to the specimen in a testing machine and confining pressure is applied to its lateral surfaces hydraulically through an impervious jacket. In some cases lateral stresses have been applied to the specimens by surrounding them with metal jackets, or by compressing them laterally between additional jacks. These last two methods suffer from the disadvantage that frictional forces arise between the sides of the specimen and the jackets or jack platens.

Some thought was given to other means of applying multi-axial stresses to rock specimens, and it seemed that lateral stresses of several thousand pounds per square inch could be applied to specimens by winding them with piano wire under tension. The maximum lateral stress which can be applied to a cylindrical specimen by winding it with a single layer of wire is:-

$$P_{max} = \frac{\pi P_{ult} J}{2D}$$

P_{ult} = ultimate tensile strength of the wire
J = diameter of the wire
D = diameter of the specimen

This stress cannot be attained in practice. The diameter of the wire must be small in relation to the diameter of the specimen so that the stress distribution on the surface of the specimen can be regarded as uniform. In order that the stress on the wire should not be relieved by creep after winding, the wire should not be stressed to its ultimate tensile strength. The wire should be

/wound....

wound with a pitch slightly greater than its diameter, so that it cannot exert any axial forces. The lateral stress applied to a cylinder by a wire winding under these conditions, when it fails due to axial compression is:-

$$p_3 = \frac{\pi J^2}{2.u.D} \quad (p_w + p_1 \nu^{Y_w/Y})$$

where:

p_1 = axial stress in the rock at failure
p_w = winding stress in the wire
J = diameter of the wire
u = winding pitch
D = diameter of the rock cylinder
ν = Poisson ratio for rock
Y_w = Young's modulus of the wire
Y = Young's modulus of the rock

The simple technique of winding rock specimens with wire seemed to offer all the advantages of a hydraulic rig for applying small lateral stress. In addition, it provided scope for easily obtaining more complicated stress systems. For example, it is possible to wind only a portion of the axial length of the specimen, or with a suitable jig the winding can be arranged to lap only part of the circumference of the specimen. Cross sections, other than circular, can be used to obtain non-uniform lateral stress distribution.

All the specimens were cut from cores drilled from the solid rock ahead of the excavation between 8, 000 feet and 10, 000feet, below surface. Specimens of two different types of quartzite were tested. The first type was a pebbly quartzite, with a grain size of about a twentieth of an inch, from the central section of East Rand Proprietary Mines, Ltd - an extensively mined area, prone to rockbursts. The second type was a very fine grained shaly quartzite, from the South-East section of East Rand Proprietary Mines, Ltd. - an area not yet extensively mined and which appears to be relatively free from rockbursts.

/Initially....

Initially, several specimens of the pebbly quartzite about 1 inch in diameter and between 1 inch and 2 inches long, were broken by uniaxial compression between hard steel plates. Most of these specimens failed in the middle, leaving two cones based on the ends of the specimens. This seemed to indicate that frictional forces between the ends of the specimen and the steel plates were strengthening the portions which remained intact at the ends. To study these end effects, some further specimens were compressed between $\frac{1}{4}$ inch thick aluminium plates. These plates were annealed so as to deform plastically over a range of stresses which extended below and above the stress at which the specimens failed. The extent of the lateral flow of the aluminium could be determined from the depth of the depression left by the specimen. It was found that when the lateral flow exceeded the Poisson expansion of the specimen the rock tended to fail (at a lower axial stress) in tension along many surfaces running right through the specimen nearly parallel to its axis. When the lateral flow was comparable with the Poisson expansion, the specimen failed along planes inclined at about 25° to the axis of the specimen. These planes often formed wedges some of which pointed towards, and others away from, the centre.. The sequence of the failures could be determined from the depth of the indentations in the aluminium plate. The first portion to fail leaves the shallowest indentation in the plate. It appeared that the first failures took place across shear planes inclined at about 25° to the axis of the specimen. These failures often formed wedges which split the specimen along planes at small angles to the axis. The shear planes were covered with a white powder of ground quartzite, whilst the tension planes were clean. No significant differences were observed in the strength or mode of failure between specimens $\frac{5}{8}$ inch and $1\frac{1}{4}$ inch in diameter and 2 to 3 times the diameter in length.

/The....

The tests between aluminium plates seemed to indicate that end effects may be significant. The Young's modulus and Poisson's ratio of steel are each nearly twice those of quartzite. Therefore, if a specimen of quartzite is compressed between pieces of steel of the same cross-section as the quartzite, the Poisson's expansion of the steel and quartzite would be almost identical, and any end effects on the quartzite would be eliminated. Hardened steel end-pieces employing this principle were made for compressing the specimens, and a simple bulk compressometer was clamped to them so as to measure the movement between the ends of the specimen. The compressometer consisted of a simple 20 : 1 mechanical lever with blade hinges. The magnified compression at the end of the lever was measured with a microscope and graduated eyepiece. The compressometer was sufficiently robust to withstand failure of the specimen.

The quartzite cores were machined in a lathe with a toolpost grinder and silicon carbide wheel to form standard specimens 7/8 inch diameter by three inches long. The over-all tolerance of the machined specimens was better than $\pm$ .0005 inches. These specimens were loaded between steel end-pieces, compressed between two sheets of blottingpaper, in a 50-ton Amsler compression tester. Some of the specimens were wound in a lathe with 30 gauge (.0124 inch diameter) piano wire with a pitch of .0139 inch. During winding, the piano wire was tensioned by suspending a weight from it.

The results obtained with the specimens of pebbly and shaly quartzite are presented in Tables 2.1 and 2.2.

/TABLE....

TABLE 2.1

Strength of Pebbly Quartzite

p_1 p.s.i.		p_3 p.s.i.	No. of Specimens
Mean	Standard Deviation	Mean	
29,000	2,500	0	6
51,000	1,900	3,000	5
-1,570	100	0	2

In the region of compression these results are reasonably well represented by:

$$p_1 = 29{,}000 + 7.3\, p_3 \quad \text{p.s.i.}$$

TABLE 2.2

Strength of Shaly Quartzite

p_1 p.s.i.		p_3 p.s.i.	No. of Specimens
Mean	Standard Deviation	Mean	
36,200	5,000	0	7
42,600	2,700	1,100	5
55,000	2,500	3,200	3

These results are reasonably well represented by:

$$p_1 = 36{,}200 + 6p_3 \quad \text{p.s.i.}$$

Note: The rate of loading was about 3,000 p.s.i. per minute, and all the tests were done at room temperature.

/During....

During his visit to South Africa, Professor J.C. Jaeger kindly suggested testing some specimens in his triaxial hydraulic rig, so that the results obtained with piano wire could be compared with those from the rig. Identical specimens were cut in contiguous pairs from the same core of shaly quartzite. One member of each pair was tested with piano wire and the other was tested under similar load in the hydraulic rig. The hydraulic rig has a spherical seat at one end, whilst the piano wire tests were done without a spherical seat. The results are shown in Table 2.3, and those with lateral constraint seem comparable.

Hysteresis curves obtained from the bulk compressometer are shown in Figure 2.1 and Figure 2.2. For comparison, curves for steel are included with those for shaly quartzite in Figure 2.1. Young's modulus for shaly quartzite obtained from Figure 2.1 is 1.3×10^7 p.s.i. A lateral stress of 3,000 p.s.i. was applied to the specimen of pebbly quartzite (Figure 2.2) with a wire winding. The secant Young's modulus from the first hysteresis loop for this specimen is 1.1×10^7 p.s.i. The dynamic Young's modulus of solid quartzite in situ can be found using the velocity of propagation of compressional waves.

This modulus is:

$$Y = \frac{C_P^2 \, d \, (1 + \nu) \, (1-2\nu)}{(1 - \nu)}$$

Where: C_P = velocity of propagation of compressional waves
d = density
ν = Poisson's ratio

(This equation is derived from Timoshenko, 1934 equation 258 p. 398)

For C_P = 20.5 ft./millisecond, d = 1695 lbs./Cu.ft. and ν = 0.15

$Y = 1.45 \times 10^7$ p.s.i.

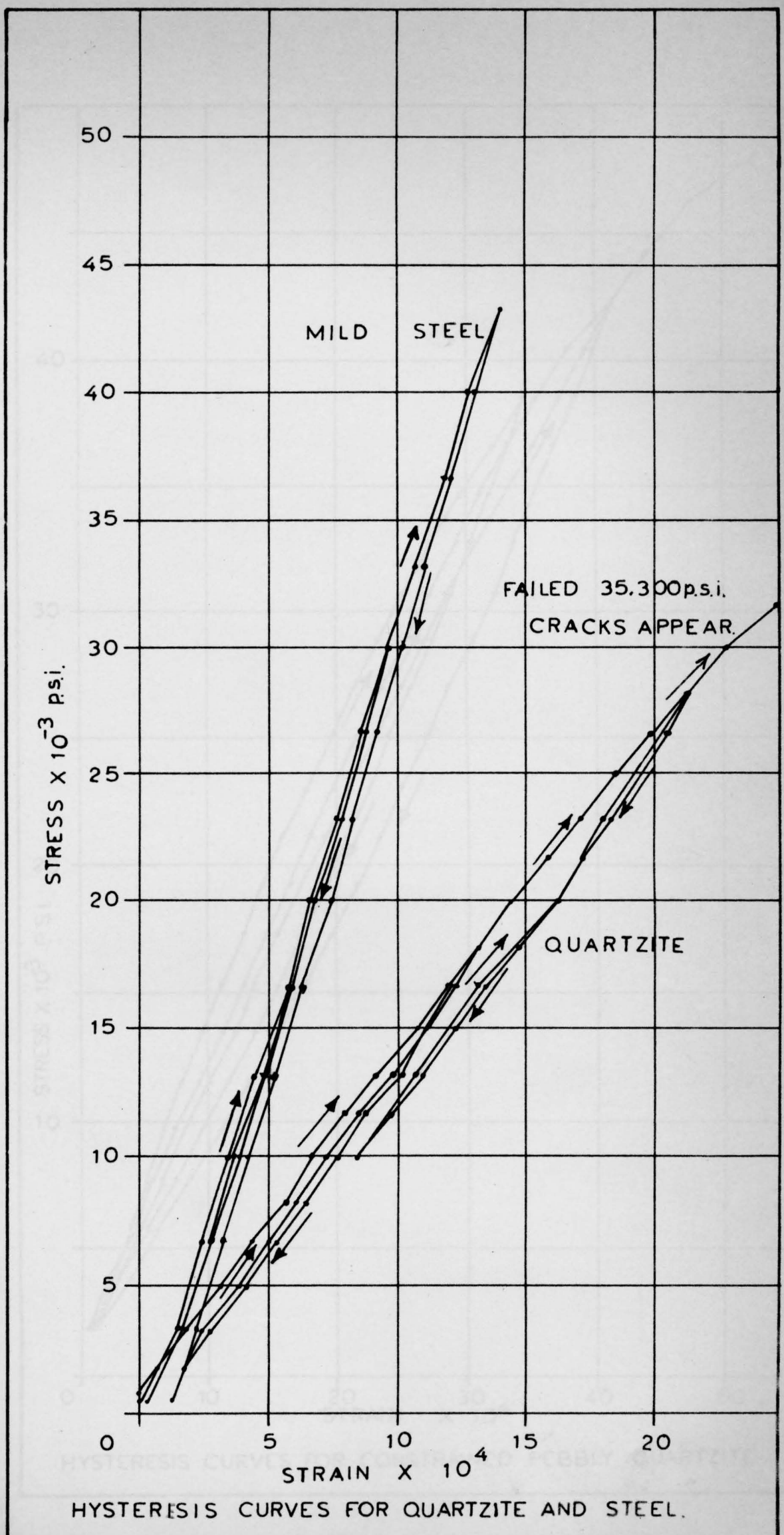
TABLE 2.3

PIANO WIRE TESTS ON SHALY QUARTZITE

Specimen	p_1 p.s.i.	p_3 p.s.i.	Failure
S_1	29,000	0	Multiple shear and longtitudinal tensile
S_2	35,600	0	Multiple shear into platen
S_3	47,500	1250	Single shear from edge of specimen
S_4	39,500	1200	Multiple shear into platen
S_5	59,000	3300	Diagonal shear across specimen
S_6	43,300	—	Wire came loose

HYDRAULIC RIG TESTS ON SHALY QUARTZITE

Specimen	p_1 p.s.i.	p_3 p.s.i.	Failure
A_1	35,000	0	Shear into platen
A_2	44,300	0	Shear into platen
A_3	43,200	1000	Double shear to edge of platen
A_4	41,000	1000	Shear into platen
A_5	54,000	3000	Shear into platen
A_6	53,300	3000	Shear into platen



HYSTERESIS CURVES FOR QUARTZITE AND STEEL.

Figure 2.1

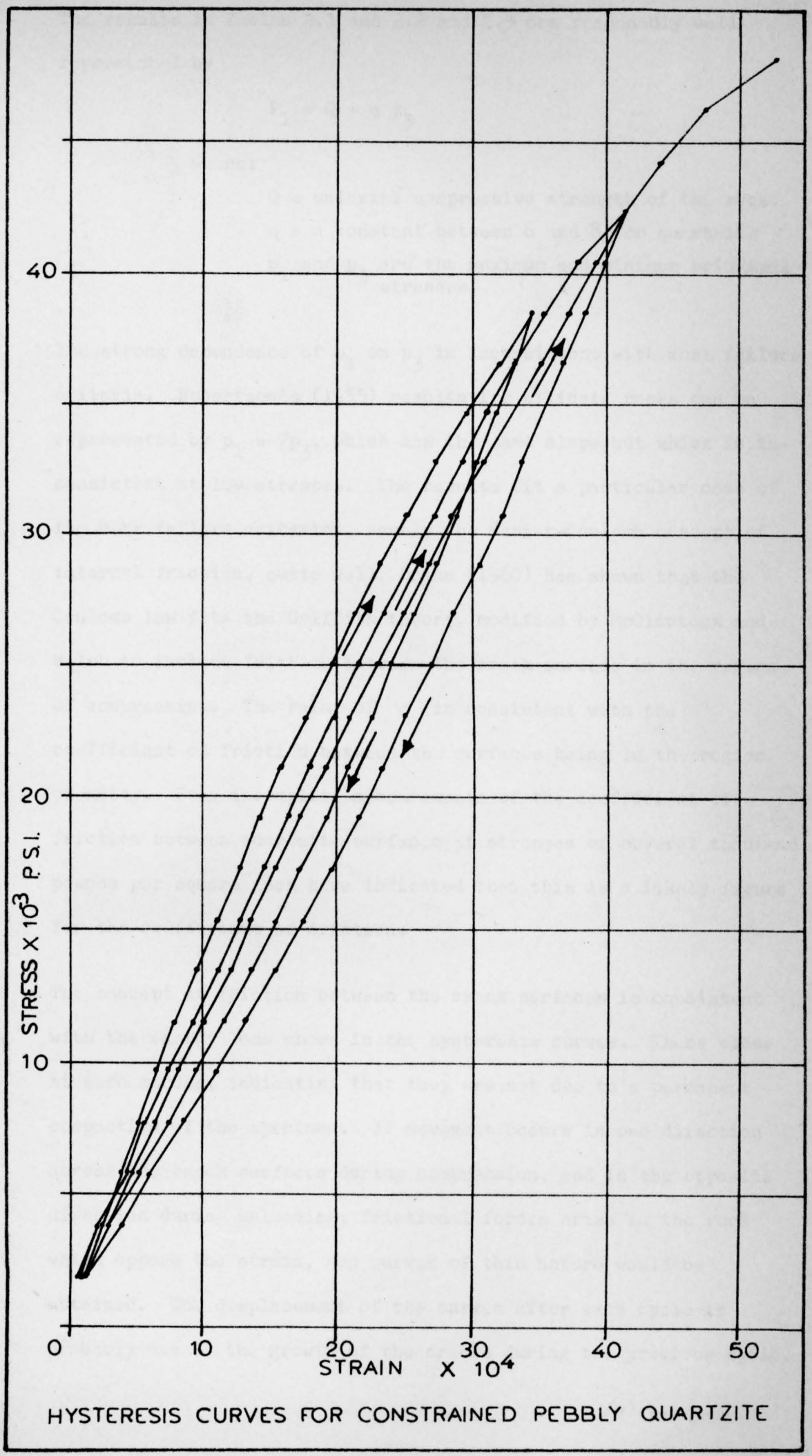

40
30
20
10
STRESS X 10^3 P.S.I.
0
10
20
30
40
50
STRAIN X 10^4
HYSTERESIS CURVES FOR CONSTRAINED PEBBLY QUARTZITE

Figure 2.2

The results in Tables 2.1 and 2.2 and 2.3 are reasonably well represented by

$$P_1 = Q + q\, p_3$$

where:

Q = uniaxial compressive strength of the rock.

q = a constant between 6 and 8 for quartzite

p_1 and p_3 are the maximum and minimum principal stresses.

The strong dependence of p_1 on p_3 is inconsistent with most failure criteria. Robertson's (1955) results for silicate rocks can be represented by $p_1 = 7p_3$, which has the same slope but which is inconsistent at low stresses. The results fit a particular case of the Mohr failure criterion, namely the Navier-Coulomb concept of internal friction, quite well. Brace (1960) has shown that the Coulomb law fits the Griffith theory, modified by McClintock and Walsh to include friction between the crack surface in the region of compression. The value of q is consistent with the coefficient of friction between the surfaces being in the region of unity. Some incomplete measurements of the coefficient of friction between quartzite surfaces at stresses of several thousand pounds per square inch have indicated that this is a likely figure for the coefficient of friction.

The concept of friction between the crack surfaces is consistent with the energy loss shown in the hysteresis curves. These close at zero stress, indicating that they are not due to a permanent compaction of the specimen. If movement occurs in one direction across the crack surfaces during compression, and in the opposite direction during unloading, frictional forces arise in the rock which oppose the strain, and curves of this nature would be obtained. The displacement of the curves after each cycle is probably due to the growth of the cracks during the previous cycle.

/b)....

b) Fractures in Quartzite

The primary failures in most of the specimens of shaly and pebbly quartzite consisted of shear across one or more planes inclined at angles of about 25° to the axis of the specimen. These shear planes often formed wedges which split the specimen in tension, leaving characteristically clean tension failure planes. The shear planes in the pebbly quartzite tended to follow the bedding, but specimens cut at different angles to the bedding indicated that this tendency was usually slight and did not have a significant effect on the uniaxial strength. To further investigate this effect, cylindrical specimens of pebbly quartzite with their axes parallel to the bedding were prepared. These were broken across a diameter by compressing them diametrically between steel plates. The bedding was inclined at different angles to the direction of the load, but no marked tendency for the failures to follow the bedding, nor any significant change in strength were detected. The failure surfaces were covered with thin flakes of quartzite similar to those found on disc failure surfaces produced by diamond drilling (See 2.3b, page 93).

In these tests, the maximum and minimum principal stresses occur on the diameter along which the load is applied. The minimum principal stress is tensile and perpendicular to the direction of the applied load. If the applied load per unit length of the specimen is L, then the minimum stress is:- $2L/\pi D$, and the maximum stress at a distance ℓ from the end of the diameter is:

$$\frac{2L}{\pi D} \cdot \frac{a^2 - a + 1}{a - a^2}$$

where: D = diameter of the specimen

and $a = \ell/D$

(These equations are derived from Timoshenko, 1934, page 104)

/High....

High compressive stress concentrations and a small tensile stress exist towards the ends of the diameter along which the load is applied. According to the failure criterion in Tables 2.1 and 2.2, this is sufficient to produce shear failure with very small normal stresses in this region. The direction and propagation of the failure are complicated by the highly non-uniform stress field. It is possible that the flaky appearance of the failure surfaces is characteristic of shear failure in the absence of a normal compressive stress.

The specimens of shaly quartzite were all cut from the same core which was drilled on strike. Some of these specimens had fine veins running across them, which did not seem to affect the strength in any way. In general, the results obtained from the pebbly quartzite were more consistent than those obtained from the shaly quartzite.

Some of the pebbly quartzite specimens were held under a constant stress (to 1 part in 10^3), very close to their uniaxial strength. Failure occurred in these specimens one to twenty minutes after the application of the load. To investigate this phenomenon further, constantin electrical resistance strain gauges were cemented to the surfaces of some specimens. These enabled strains of 10^{-5} to be measured (see Appendix A3). These specimens were compressed axially. At stresses greater than about two-thirds of the ultimate uniaxial stress, the elastic strain in the specimen was followed by a decreasing exponential creep strain of about 10^{-5}, with a time constant of about a minute. If the stress was increased to very near the strength of the specimen, the creep strain increased and failure occurred. The surfaces of some specimens were finely finished, and it appeared that at the start of creep behaviour fine cracks developed and could be seen spreading

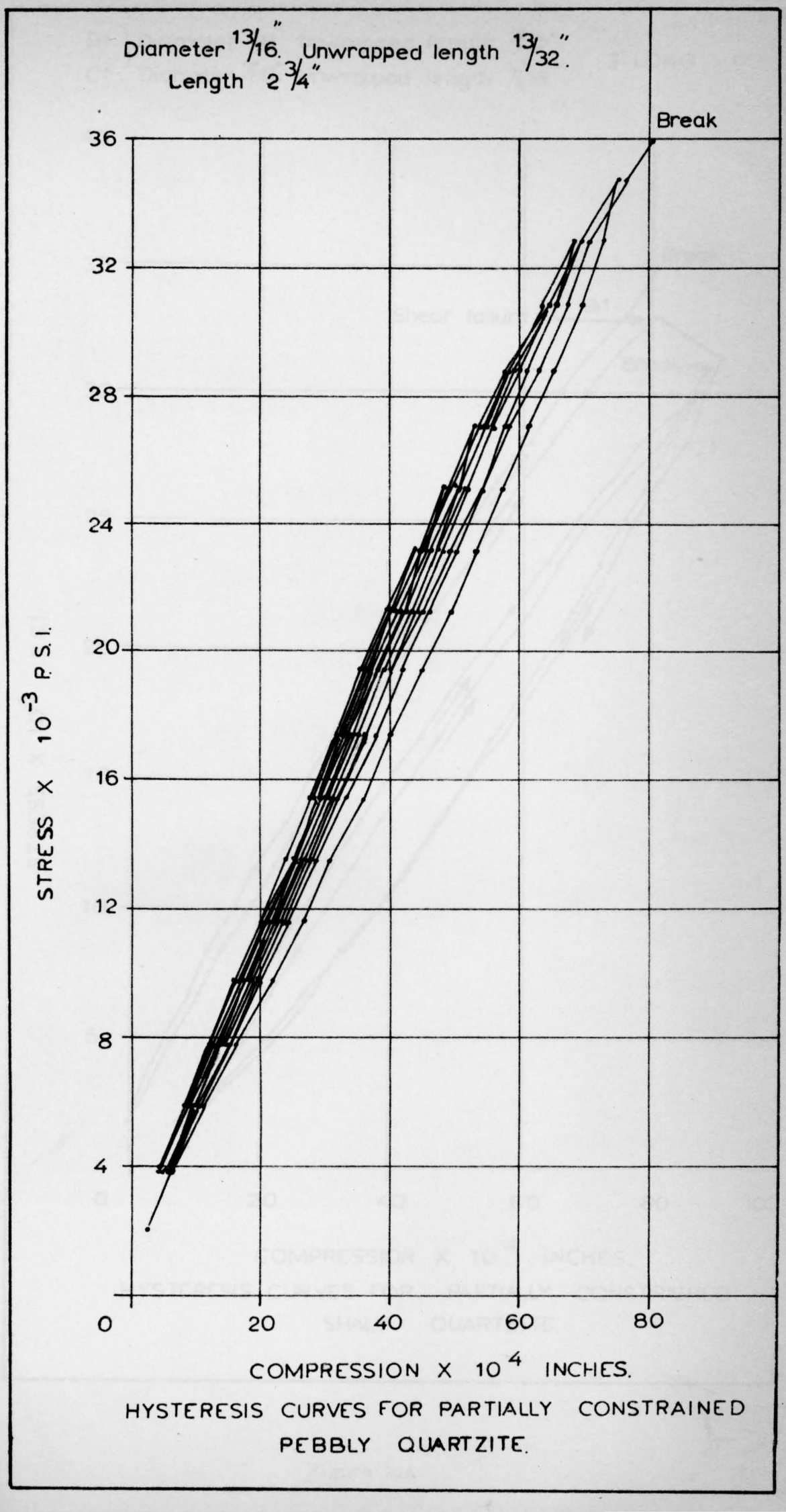
/between....

between the grains of quartz. At high stresses, the whole surface of the specimen turned a milky white with a multitude of intergranular cracks. An attempt was made to detect seismic radiation from these cracks. A crystal pick-up was connected to the specimen, and to a tape recorder and an oscilloscope with a pass band from 50 c.p.s. to 20 Kc.p.s. No radiation was detected, but if there is any it is likely to be at a much higher frequency. If the intergranular cracks develop in discrete steps, it appears that each step must usually be of the order of a thousandth of a foot. Assuming that the steps propagate at a velocity of the order of the velocity of seismic propagation, then each step takes place in less than a micro-second and frequencies of the order of megacycles might be expected.

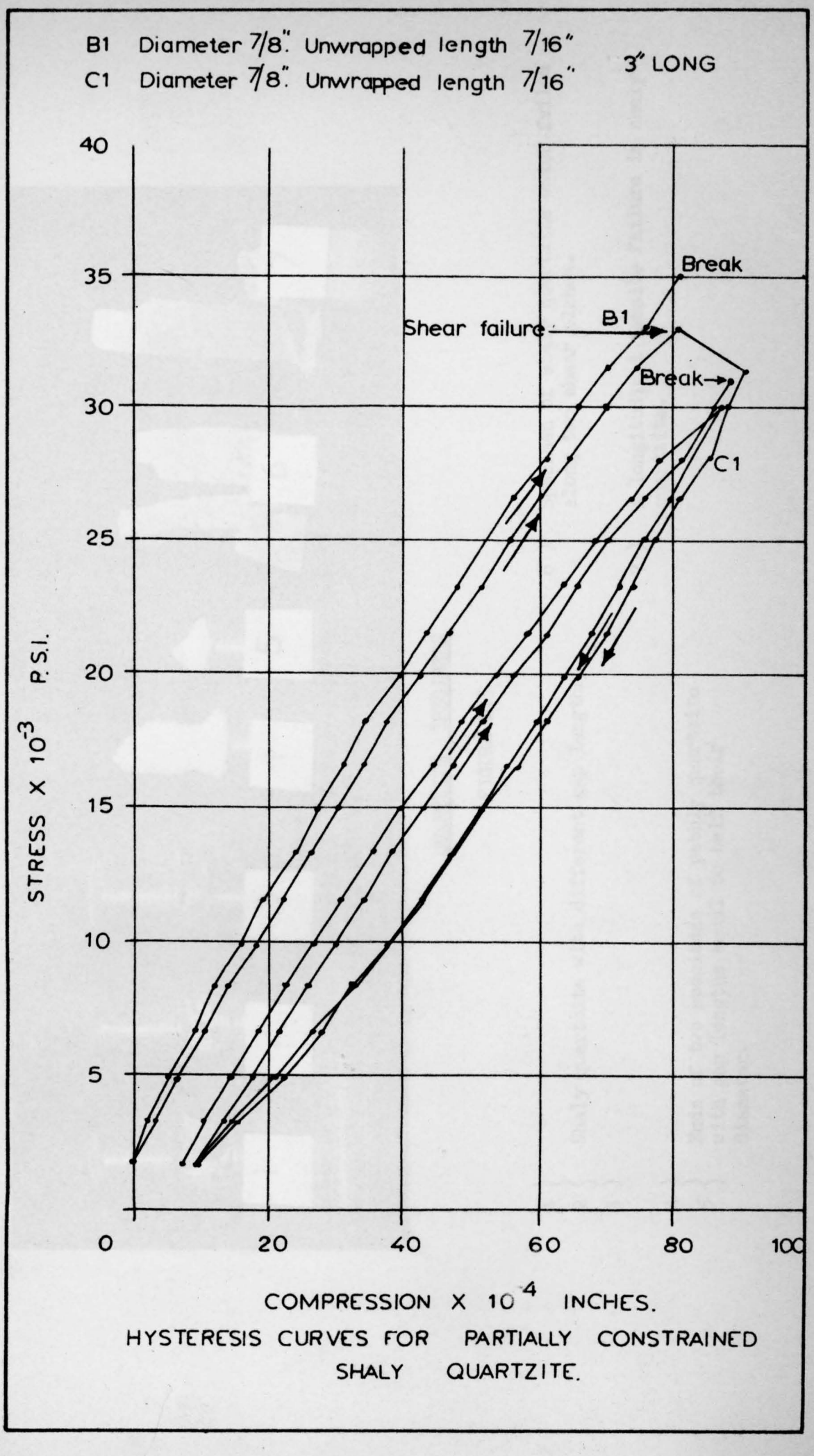
Cylindrical specimens of shaly and pebbly quartzite were partially wound with piano wire. The winding started from each end, applying a stress of 3,000 p.s.i., and left a gap in the middle. A series of compression tests was made, the gap being reduced progressively.

The strength of the partially wrapped pebbly specimens began to exceed the uniaxial strength appreciably when the length of the unwrapped gap was reduced to the diameter of the specimen. When the gap length was reduced to half the diameter, the average axial stress at failure was 40,000 p.s.i. Noticeable cracks occurred in the gap at loads near the uniaxial strength. As the stress increased, flakes spalled from the gap. The specimens failed violently and most of the material in the gap disintegrated into fine white powder, leaving a rough cone standing on each of the wrapped portions of the specimen (Specimens 4 and 5 of Figure 2.5, page 72).

/The....

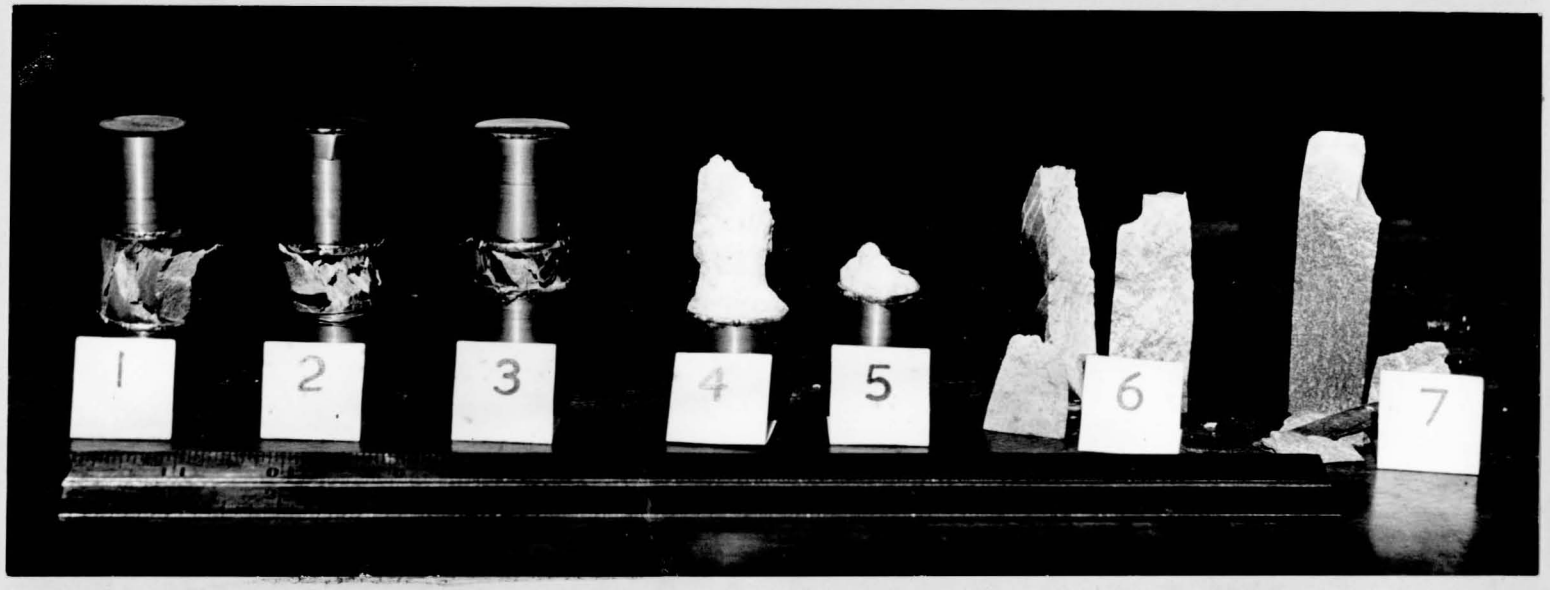


HYSTERESIS CURVES FOR PARTIALLY CONSTRAINED PEBBLY QUARTZITE.



HYSTERESIS CURVES FOR PARTIALLY CONSTRAINED SHALY QUARTZITE.

Figure 2.4



QUARTZITE SPECIMENS

FIGURE 2.5

1)
2) Shaly quartzite with different gap lengths
3)

4)
5) Ends of two specimens of pebbly quartzite with gap lengths equal to half their diameter.

6) Specimen of shaly quartzite which failed along two shear planes.

7) A longitudinal tensile failure in shaly quartzite.

The behaviour of the shaly quartzite was less consistent. Significant strengthening of the specimens did not seem to start until the gap length was reduced to half the diameter. Cracks began to appear in the gap soon after the load exceeded the uniaxial strength. Sometimes flakes spalled from the gap, but a crack often spread from the gap diagonally through one of the wound portions of the specimen. Even when the material in the gap spalled this was the ultimate mode of failure.

Hysteresis curves for partially constrained pebbly and shaly quartzite are shown in Figure 2.3 and Figure 2.4. Figure 2.5 shows some of the specimens after failure, with a foot rule to indicate scale. Specimens 1, 2 and 3 are of shaly quartzite with different gap lengths, showing clearly the spalling which occurred in the gap. Specimens 4 and 5 are the ends of two specimens of pebbly quartzite with gap lengths equal to half their diameters. The portions protruding above the wire winding are covered in a powder of ground quartzite. Specimen 6 is a specimen of shaly quartzite which failed along two shear planes. The white powder of ground quartzite can be seen on the shear surfaces. Specimen 7 shows a longitudinal tensile failure in shaly quartzite which followed the shear failure at the top end of the specimen. The relatively clean tensile failure can be seen.

2. 2 Information about Rock Stresses obtained from Diamond Drilling

Whilst drilling the holes for installing the seismometers, a log of diamond drilling progress and core recovery was kept. A study of the data obtained from this has revealed some details of the stresses and failures ahead of an advancing face.

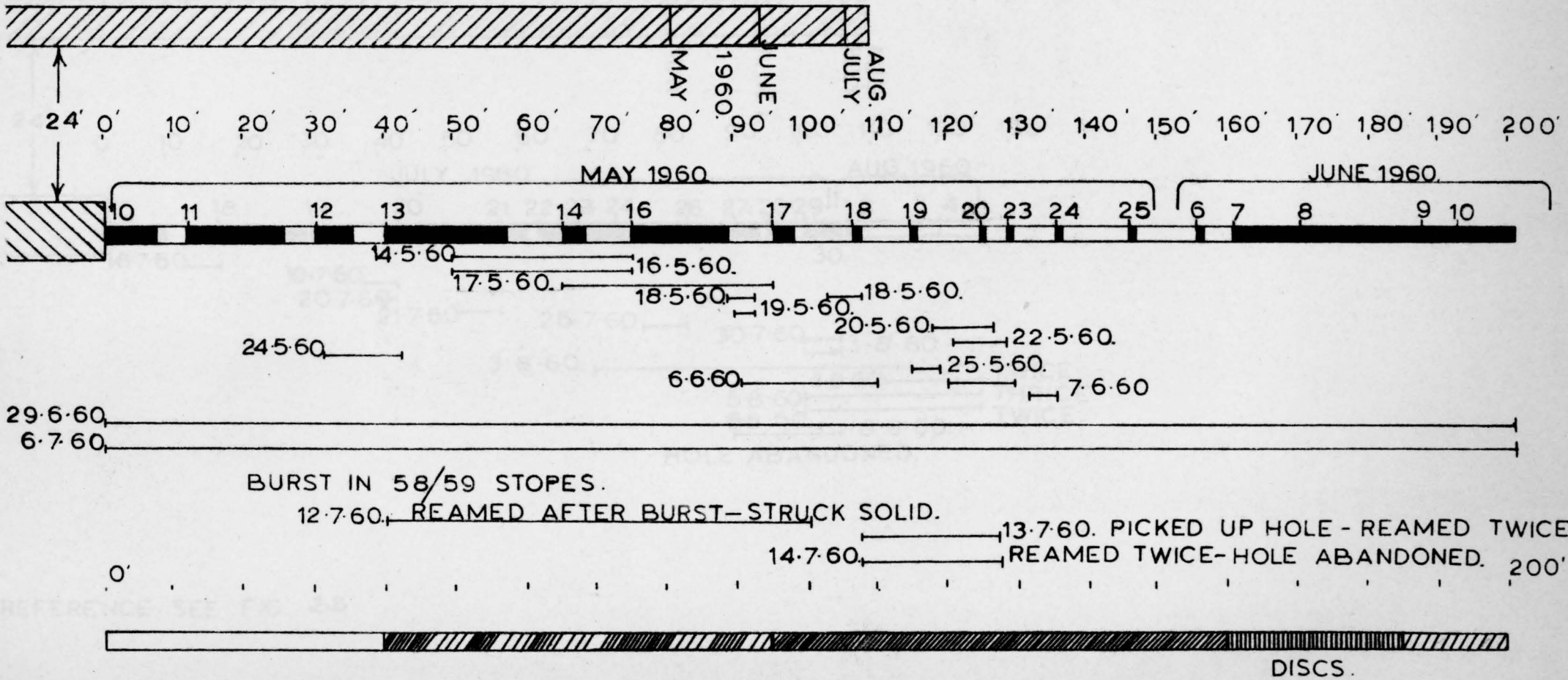
/the....

The results obtained from the long horizontal holes drilled on strike ahead of the face from the footwall drives on 58 level and 60 level are shown graphically in Figures 2.6, 2.7 and 2.8.

When drilling through intensely fractured rock, pieces of rock fall into the hole and it is necessary to ream often to keep the hole open. In very highly stressed rock, the hole deforms and it is again necessary to ream frequently to keep the hole open. These two conditions can be distinguished from oneanother. In fractured rock, the hole usually closes when drilling is not in progress and the drill rods are removed. The proportion of core recovered during the initial drilling of fractured rock, which is not under high stress, is high. In rock subject to high stress, closure takes place all the time, and frequently jams the drilling crown and core barrel while drilling is in progress. Core recovery in highly stressed rock is poor. In rock subject to very high stress, the core breaks off in thin discs which usually break up in the core barrel. As the stress decreases the discs become thicker, and complete discs are recovered.

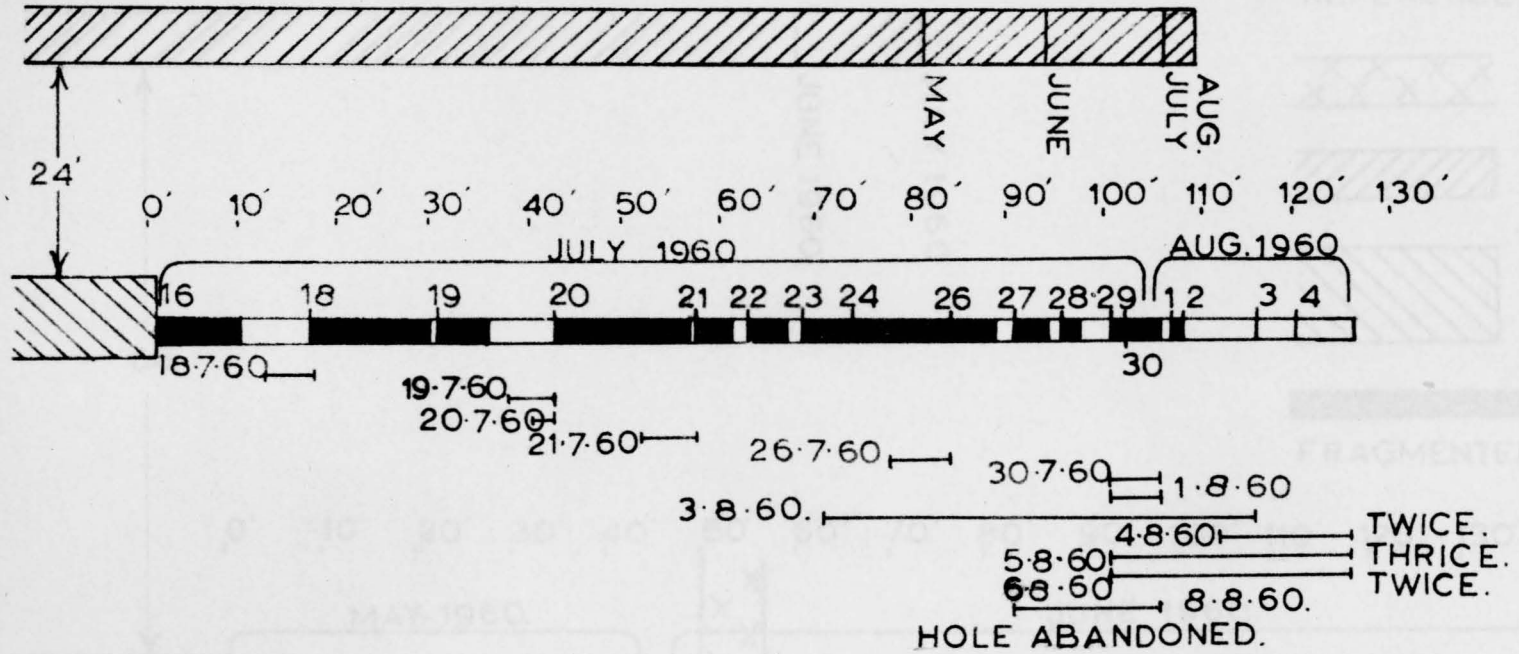
A rockburst occurred in 58/59 level stopes of F East longwall after the drilling was completed. After the rockburst, it was necessary to ream the hole on 58 level open from 60 feet behind the face. At the face position, the drill struck and drilled through 7 feet of solid rock before intersecting the original hole again. This indicates a major displacement caused by the rockburst. Hole deformation caused by high stress was rapid for 20 feet ahead of the face, and it was necessary to ream almost continuously. Further than 20 feet ahead of the face, the stresses were so high and hole closure was so extensive that the core barrel and crown jammed severely and it was impossible to continue drilling. A second hole was started after the rockburst had damaged the first hole, removed a few feet from, but parallel to, the first hole. Very high stresses were again encountered

/ahead....



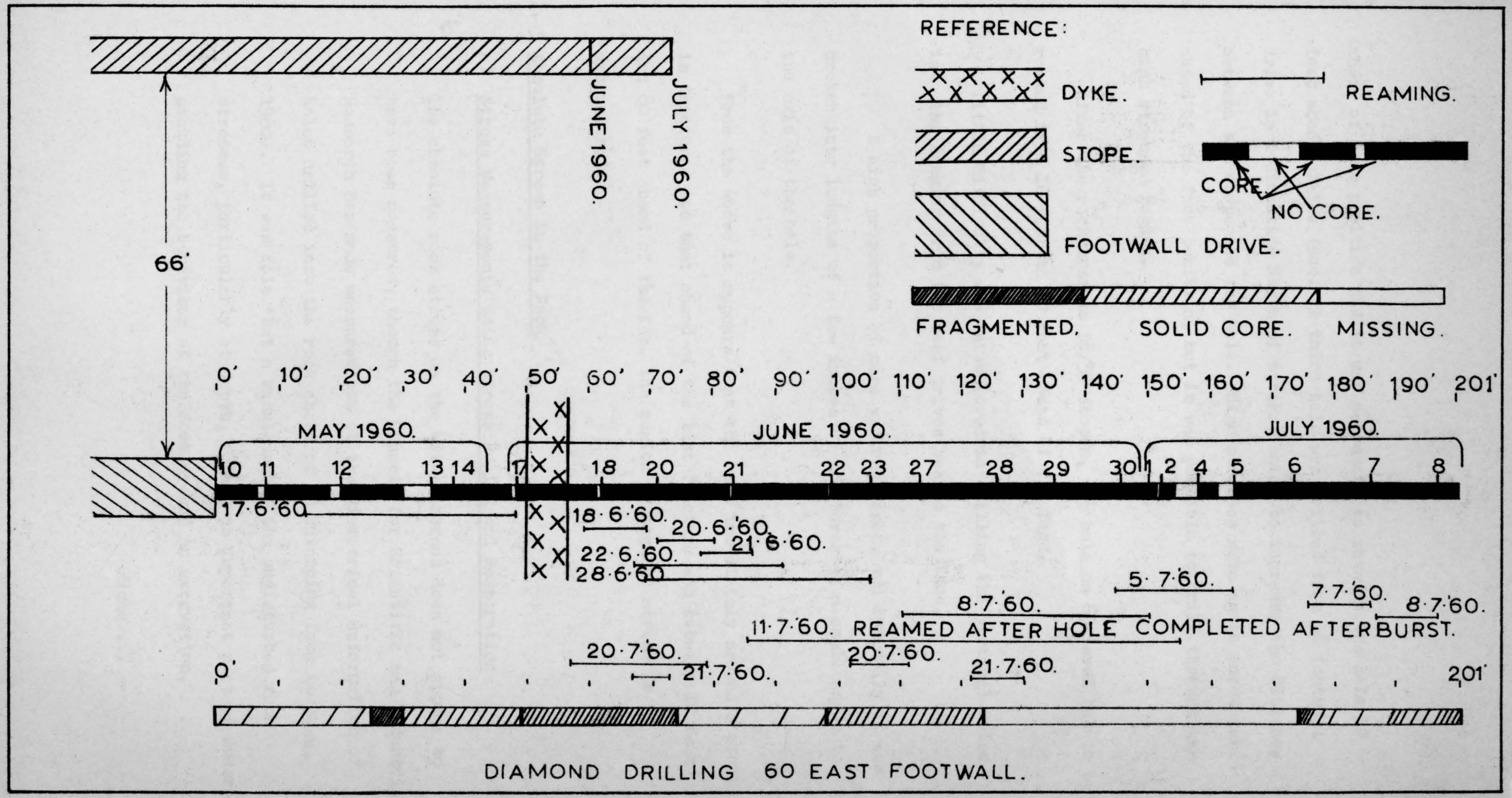
REFERENCE: SEE FIG. 2·8

DIAMOND DRILLING 58 EAST LONGWALL. (FIRST HOLE.)



REFERENCE: SEE FIG. 2.8

DIAMOND DRILLING 58 EAST LONGWALL. (SECOND HOLE.)



DIAMOND DRILLING 60 EAST FOOTWALL.

ahead of face position and it was necessary to abandon the hole 17 feet ahead of the face. A third hole was drilled from 58 footwall drive in a direction North of strike, so as to increase the distance between the stope and the hole. High stresses were again encountered ahead of the face position, but it was possible to drill through the high stressed region.

After the rockburst in 58/59 stopes, the hole on 60 level had to be reamed from 10 feet to 80 feet ahead of the face.

Little difficulty was encountered in drilling the vertical holes into the hanging from the reef drives behind the face.

A high proportion of core was recovered, and typically it was broken into lengths of a few inches by fractures at a small angle to the axis of the hole.

From the above it appears that the rock immediately around a stope is fractured and that ahead of the last fracture and between 10 feet and 80 feet ahead of the face the region of highest stress is encountered.

2.3 Absolute Stress in the Rock

a) Stress Measurements using Stress Relief and Restoration

The absolute rock stress on the Witwatersrand does not appear to have been measured, though the Council for Scientific and Industrial Research has made measurements of the diametrical deformation of holes drilled into the rock ahead of an advancing face (Leeman, 1960). It was felt that a knowledge of the undisturbed rock stresses, particularly at depth, formed an important part of understanding the behaviour of the rock around an excavation.

/None....

None of the properties of quartzite appears to change with stress in such a way as to enable indirect measurements of stress to be made. It seems, therefore, that any stress measurement has to be based on the deformation of the quartzite produced by the stress. In general, two methods of measuring rock stress, based on deformation, have been devised. One method is based on stress relief and the other method on stress restoration.

In the stress relief method, a hole is drilled into the rock under stress, and a suitable deformation sensing cell is placed in the hole. The stresses in the rock surrounding the deformation cell are relieved by cutting an opening around the rock surrounding the cell. The deformation measured by the cell is then related to the stress change produced by stress relief, and hence to the original stress in the rock.

In the stress restoration method, the positions of points on the surface of an excavation are measured and an opening is made between these points. A jack is installed in this opening, and the stress is restored until the points regain their original positions. The restoration stress is then related to the rock stress.

At depths of the order of 10,000 feet, the quartzite around an opening fails, and it is difficult to relate stresses in the failed rock to stresses in the solid rock removed from the opening. For this reason, stress restoration measurements in the wall of the excavation were not considered suitable at these depths. Small holes have been drilled into the solid rock from an excavation, and deformation cells have been installed in these. The stresses around these cells have been relieved by overdrilling

/them....

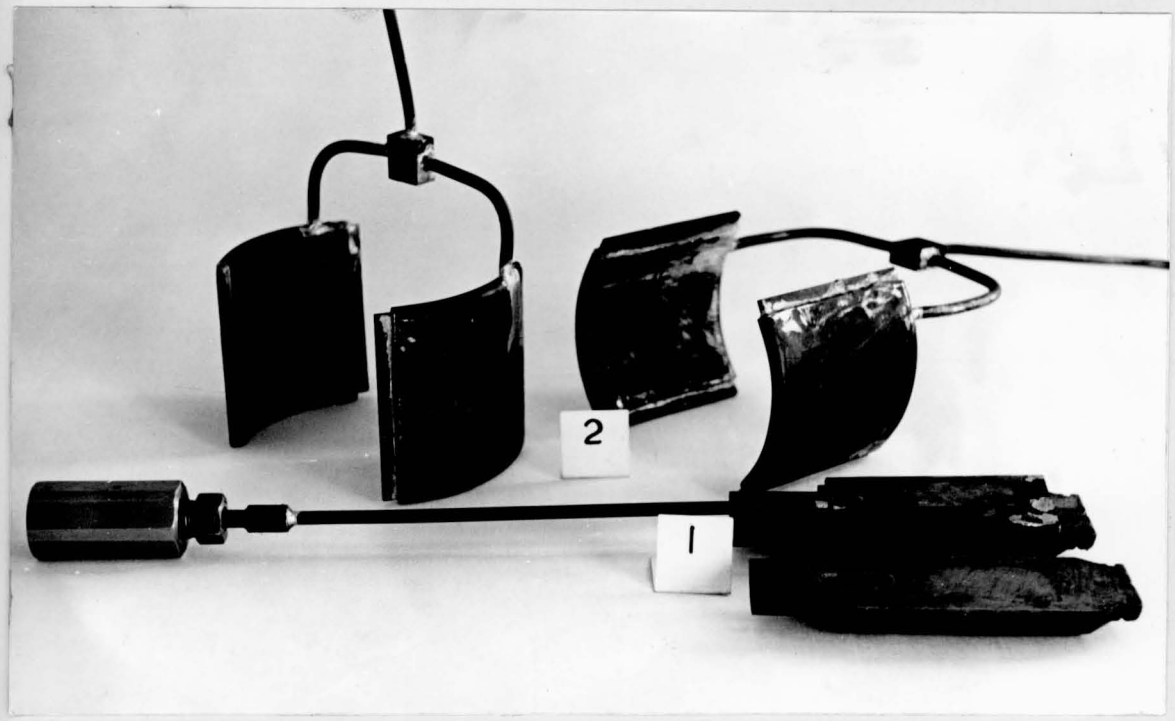
them with a larger annular opening. Stress measurement by this technique has proved difficult at depth because the quartzite around the small hole fails, making it difficult to relate deformation to stress. Failure of the rock around the cell, particularly during overdrilling, causes spurious movements of some types of deformation cell.

The following technique to measure high stresses in rock removed from an excavation was devised:

A hole can be drilled from the excavation into solid rock. When fractured rock is subject to compressive stresses, it behaves, in many respects, like a solid material. It seemed that a pre-stressed deformation cell installed in a hole so as to apply a compressive stress to the inside of the hole would measure deformation related to the bulk of the rock around the hole even if the rock immediately surrounding the hole failed. The stress in the rock around such a cell can be relieved by drilling a concentric annulus around the cell. The original stress in the rock could be established without making any assumptions about the properties of the rock or the centre-cell by restoring the stress across the annular opening. To do this, jacks could be installed in the annulus and stressed until the original deformation measured by the centre-cell was restored. The stress generated by the annular jacks could be closely related to the original stress existing in the rock.

The cells were based on conventional hydraulic flat jacks used for stress restoration measurements, and are shown in Figure 2.9. The centre-cell, 1, is a flat jack, $1\frac{1}{4}$ inch wide by 3 inches long, made from 16-gauge copper tube. Two steel pieces of almost semi-circular cross-section are used to fit this to a $1\frac{1}{2}$ inch-diameter borehole. The cell is most sensitive to deformation perpendicular

/to....



CENTRE-CELL (1) AND ANNULAR JACKS (2)

FIGURE 2.9

to its flat surfaces. The annular jacks, 2, consist of four quadrants to fit an annulus of 4 inches internal diameter and 4.650 inches external diameter. The dimensions of the annulus were chosen so that the jacks were reasonably removed from the high stress concentrations caused by the 1½ inch centre-cell hole, but the annulus was sufficiently small not to present a major drilling difficulty.

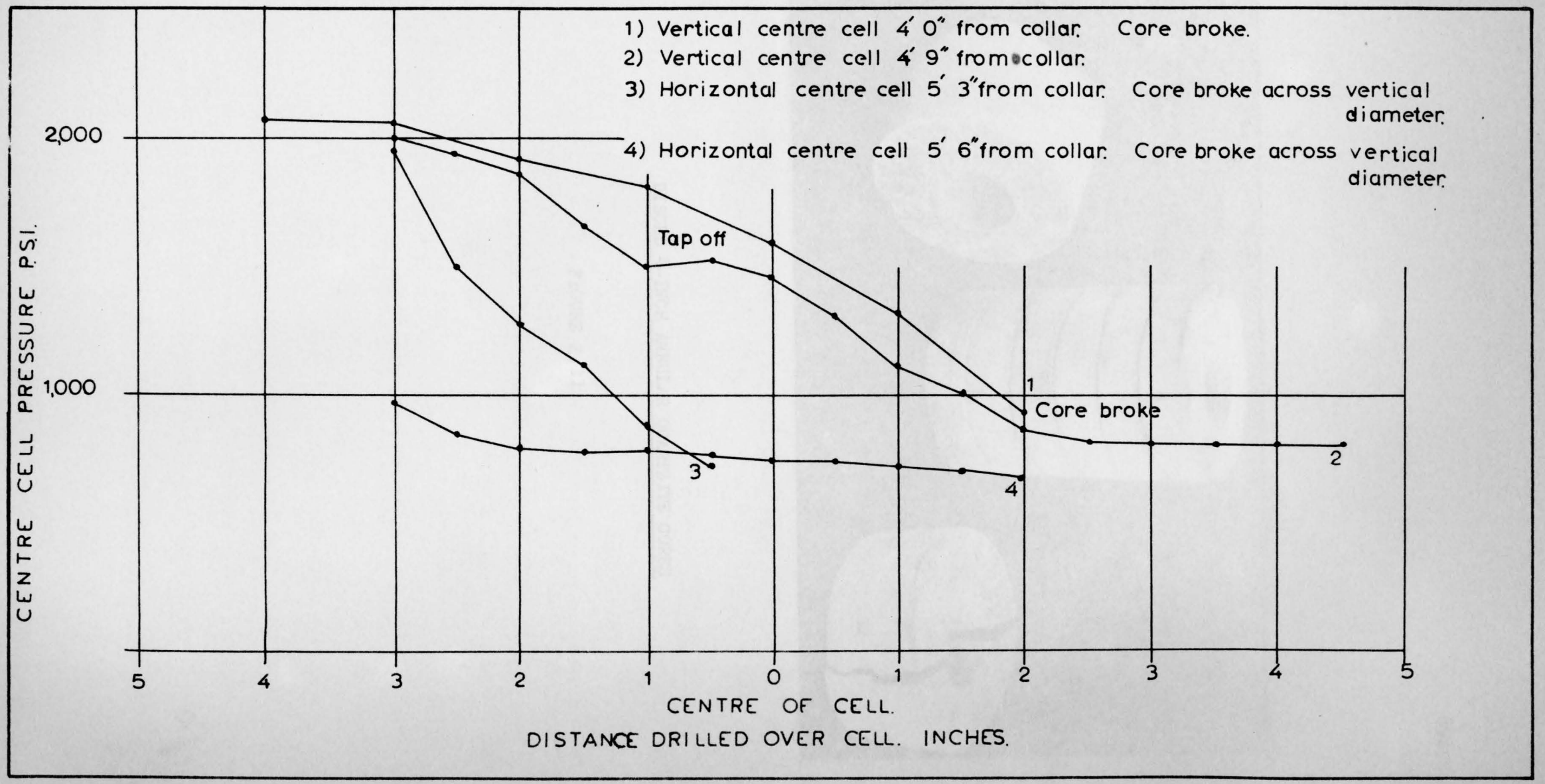
A site in a main haulage 8,000 feet below surface and removed from stoping by several thousand feet was selected for the stress measurements. Holes for installing the stress cells were drilled horizontally into the solid rock, at right-angles to the axis of the haulage. The rock to a depth of three or four feet was fractured, beyond which it became solid. The procedure was to drill the 4.650 inch hole to the depth at which the stress measurement was to be made. The core was broken off at the back of this hole. A concentric 1½ inch-diameter hole was drilled in the bottom of the 4.650 inch hole. The centre-cell was installed in the 1½ inch hole and oriented to detect either vertical or horizontal deformation. The hydraulic pressure-pipe from the centre-cell was led through a 4.650 inch-diameter crown and core barrel, then through the drilling rods and out through the water swivel of the drill. A pressure gauge, tap and hyrdaulic pump were connected to this pipe. The centre-cell was pre-stressed and allowed to settle with the drilling water supply flowing. Overdrilling of the centre-cell with the 4.650 inch crown was started and drilling depth and centre-cell pressure were recorded throughout overdrilling.

The first centre-cells were 6 inches long. Trouble was experienced when overdrilling these because the core disced, broke off and jammed in the core barrel, before overdrilling could be completed.

/This....

This made it impossible to instal the annular cells. The changes in centre-cell pressure during overdrilling are shown in Figure 2.10 When the centre-cell, pre-stressed to 2,000 p.s.i., was oriented to detect horizontal deformation, the core broke across a vertical diameter soon after overdrilling started. Curve 4 was obtained by overdrilling a horizontal centre-cell pre-stressed to 1,000 p.s.i. None of the cores obtained from overdrilling vertically-oriented centre-cells was broken other than by disc-failure. This seemed to indicate that the horizontal stress must be much less than the vertical stress, and that a pre-stress of 2,000 p.s.i. in the centre-cell was sufficient to cause tensile failure at the top and bottom of the hole. To confirm this, a centre-cell was installed so as to exert a vertical force. This cell was stressed to 15,000 p.s.i. and released several times, after which the stress was completely relieved and the cell was over-drilled with the 4.650 annulus. The core was disced, but was otherwise free from failures or cracks. The $1\frac{1}{2}$ inch centre hole was extended, and the same centre-cell installed so as to exert a horizontal force. The cell was stressed to 3,000 p.s.i., and released several times, after which the stress was completely relieved and the cell was overdrilled with the 4.650 inch crown. The core was again disced, but in each disc a crack appeared across a vertical diameter. Three cores are shown in Figure 2.11 The core n the left was recovered from overdrilling the vertical centre-cell which had been stressed to 15,000 p.s.i. The discs of this core remained joined to oneanother. The right-hand core, from overdrilling the horizontally-oriented cell with a pre-stress of 2,000 p.s.i., shows the diametrical failures. The core in the centre was obtained from overdrilling the horizontal centre-cell which had been pre-stressed to 3,000 p.s.i. and then released. This core is

/shown....


1) Vertical centre cell 4′ 0″ from collar. Core broke.
2) Vertical centre cell 4′ 9″ from collar.
3) Horizontal centre cell 5′ 3″ from collar. Core broke across vertical diameter.
4) Horizontal centre cell 5′ 6″ from collar. Core broke across vertical diameter.
2,000
1,000
CENTRE CELL PRESSURE P.S.I.
Tap off
Core broke
1
2
3
4
5 4 3 2 1 0 1 2 3 4 5
CENTRE OF CELL.
DISTANCE DRILLED OVER CELL. INCHES.



DISCED 4-INCH ANNULAR QUARTZITE CORES

FIGURE 2.11

shown in detail in Figure 2.12 where the arrow indicates the line of tensile cracks at the top of the core. These cracks have been shown up by a penetrating dye.

The small decrease in centre-cell pressure in Curve 4 of Figure 2.10 and the incipient tensile failures at the top and bottom of the $1\frac{1}{2}$ inch hole indicate that the ratio between the vertical and horizontal stresses is in the region of 3 : 1.

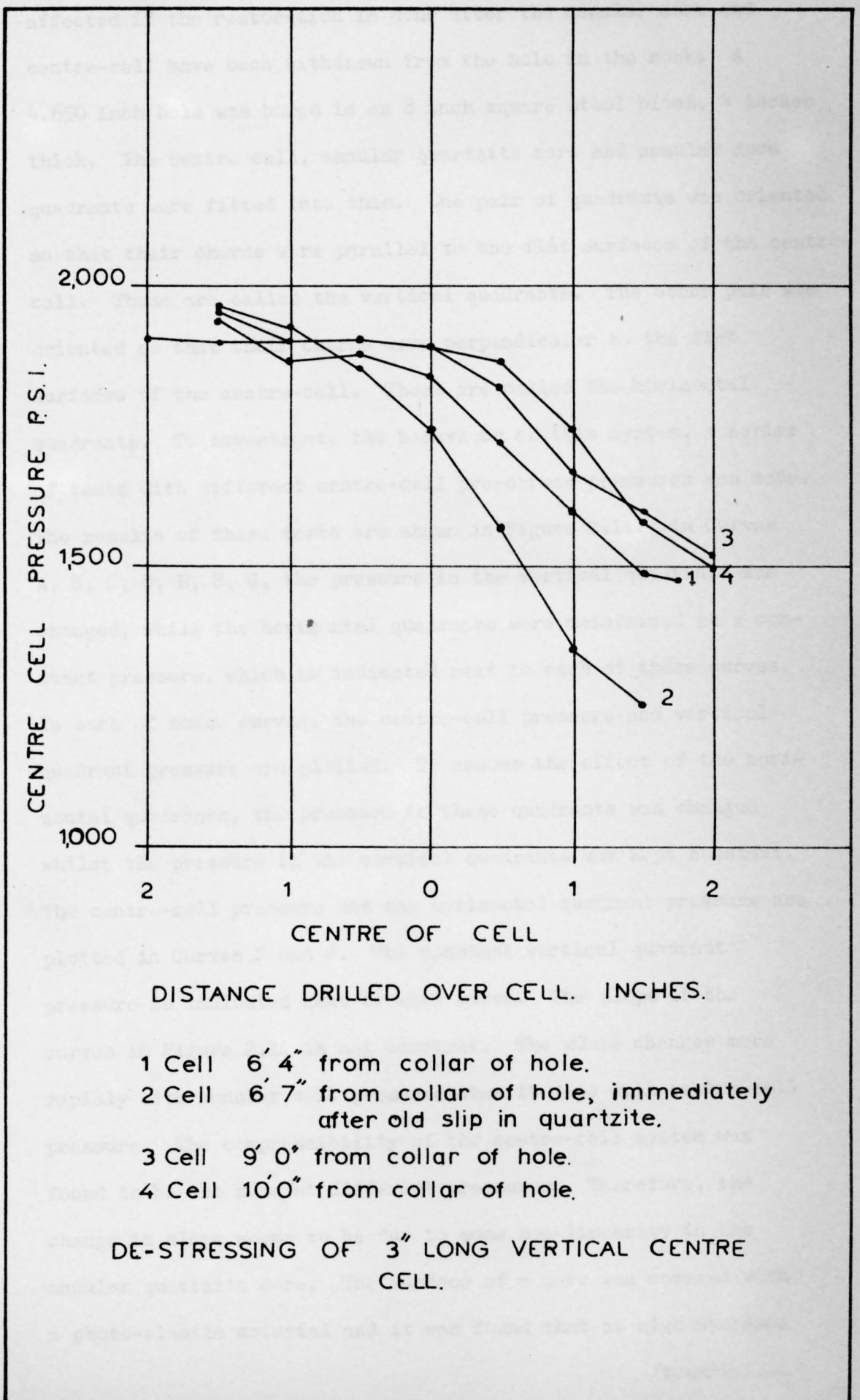
To reduce the probability of the cores breaking before complete overdrilling of the centre-cell, the length of the centre-cell was reduced to 3 inches. It was felt that the shorter cells might introduce errors due to end effects. Hast (1958) has noted the stress measured by a centre-cell while the concentric annulus is drilled towards, and then passes, the centre-cell. His results indicate that the stress at the end of the borehole does not increase, but that the stress in the centre-cell starts decreasing when the annulus comes within a distance of the centre-cell equal to the annular radius; and that the centre-cell stress stops decreasing when the annulus has passed the centre of the centre-cell by a similar distance. It seems that there should be some stress concentration at the end of a hole, but these results indicate that it is small, and it was felt that in initial experiments it could be neglected. The changes in centre-cell pressure during overdrilling vertically-oriented 3-inch centre-cells are plotted in Figure 2.13. Complete overdrilling of these cells proved to be possible, but the core always broke off on a disc failure when the 4.650 inch crown was withdrawn, and it was not possible to restore the centre-cell pressure with the annular quadrants, in the back of the hole.

/The....



ANNULAR QUARTZITE CORE, SHOWING DIAMETRICAL TENSILE CRACKS

FIGURE 2.12

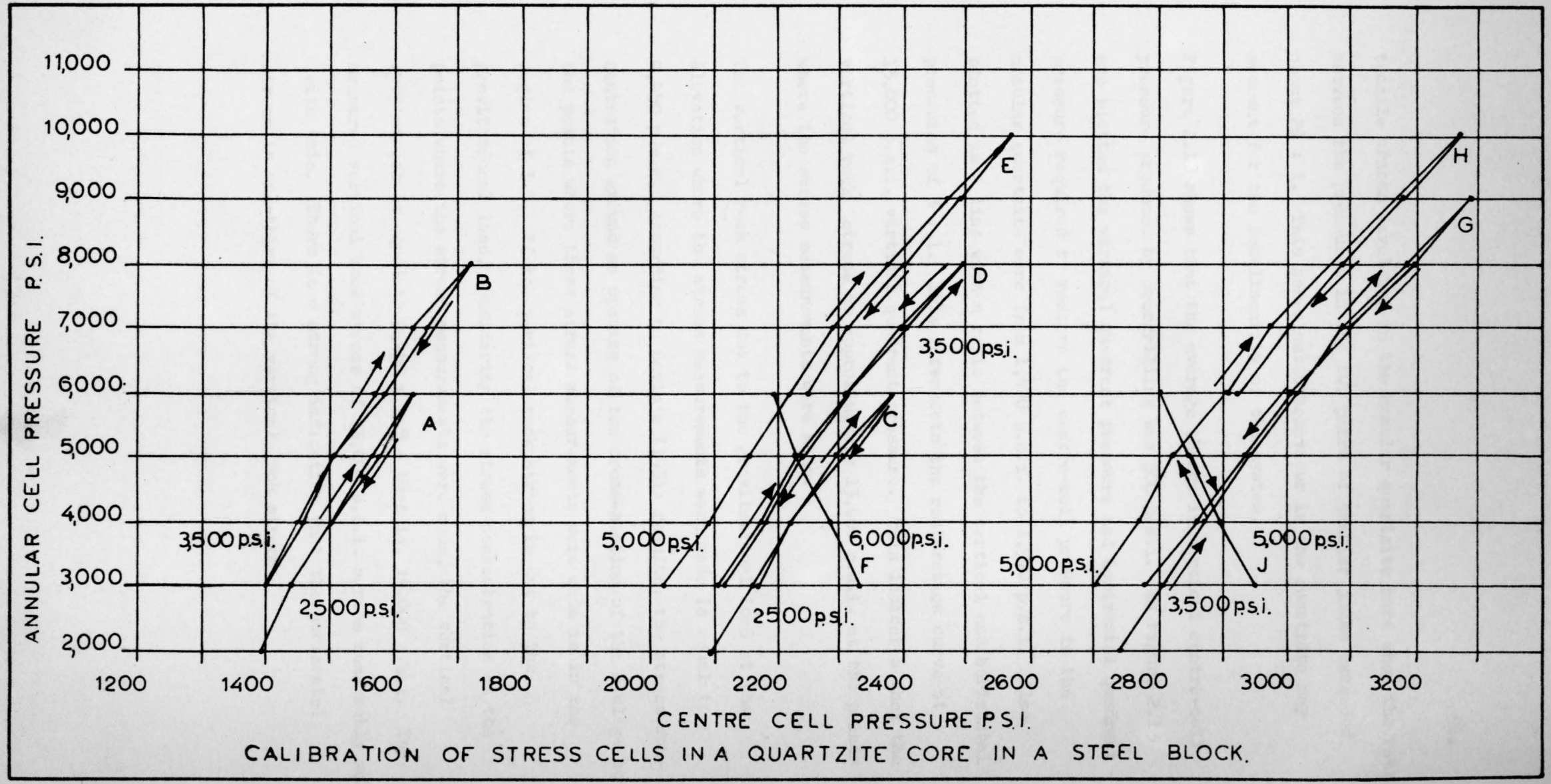


1 Cell 6′ 4″ from collar of hole.
2 Cell 6′ 7″ from collar of hole, immediately after old slip in quartzite.
3 Cell 9′ 0″ from collar of hole.
4 Cell 10′ 0″ from collar of hole.

DE-STRESSING OF 3″ LONG VERTICAL CENTRE CELL.

The only important factor in restoring the stress in the annular quartzite core surrounding the centre-cell is the restoration stress on the outside surface of the quartzite. This is not affected if the restoration is done after the annular core and centre-cell have been withdrawn from the hole in the rock. A 4.650 inch hole was bored in an 8 inch square steel block, 4 inches thick. The centre cell, annular quartzite core and annular jack quadrants were fitted into this. One pair of quadrants was oriented so that their chords were parallel to the flat surfaces of the centre-cell. These are called the vertical quadrants. The other pair was oriented so that their chords were perpendicular to the flat surfaces of the centre-cell. These are called the horizontal quadrants. To investigate the behaviour of this system, a series of tests with different centre-cell pre-stress pressures was made. The results of these tests are shown in Figure 2.14. In Curves A, B, C, D, E, H, G, the pressure in the vertical quadrants was changed, while the horizontal quadrants were maintained at a constant pressure, which is indicated next to each of these curves. In each of these curves, the centre-cell pressure and vertical quadrant pressure are plotted. To assess the effect of the horizontal quadrants, the pressure in these quadrants was changed whilst the pressure in the vertical quadrants was kept constant. The centre-cell pressure and the horizontal quadrant pressure are plotted in Curves F and J. The constant vertical quadrant pressure is indicated next to each curve. The slope of the curves in Figure 2.14 is not constant. The slope changes more rapidly with annular cell pressure than it does with centre-cell pressure. The compressibility of the centre-cell system was found to be the same at different pressures. Therefore, the change in slope seems to be due to some non-linearity in the annular quartzite core. The surface of a core was covered with a photo-elastic material and it was found that at high stresses

/tensile....



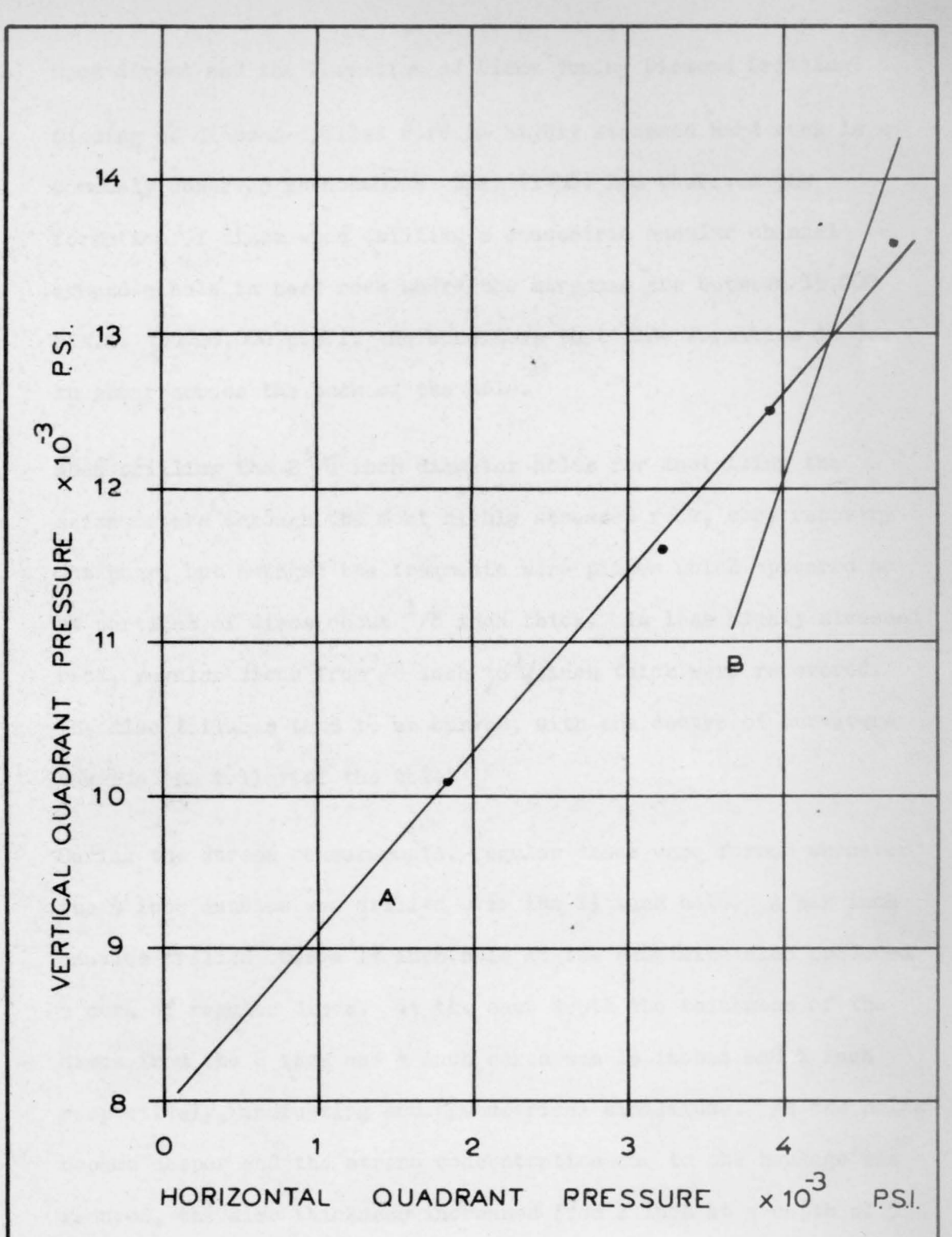
CALIBRATION OF STRESS CELLS IN A QUARTZITE CORE IN A STEEL BLOCK.

Figure 2.14

tensile cracks developed in the annular quartzite core when the ratio between the pressures in the two pairs of annular jacks exceeded about $2\frac{1}{2}$: 1. This non-elastic behaviour in the quartzite may account for the non-linearity of the system.

Figure 2.13 shows that the average change in vertical centre-cell pressure produced by overdrilling was 500 p.s.i. In Figure 2.15 are plotted the vertical quadrant pressure and horizontal quadrant pressure required to restore the centre-cell pressure in the annular quartzite core from 1,470 p.s.i. to 1,970 p.s.i. Also plotted is a line with a ratio between the vertical and horizontal pressures of 3 : 1. This intersects the restoration curve at 13,000 p.s.i. vertical quadrant pressure. This indicates that the vertical rock stress is approximately 13,000 p.s.i. at the points where the stress measurements were made.

The vertical rock stress due to the gravitational load at the elevation where the stress measurements were made is equal to 9,450 p.s.i. According to Savin's (1951) results, the stress concentration around an opening of the cross-section of the haulage at the points where these stress measurements were made is in the region of 1.5. If the vertical rock stress is due to the gravitational load, considering the stress concentration at the points where the stress measurements were made, the vertical rock stress is equal to 9,450 x 1.5 - that is, 14,000 p.s.i. The measured vertical rock stress of 13,000 p.s.i. agrees reasonably well with this. There is a strong indication that the horizontal stress is one-third of the vertical rock stress.



A Constant vertical centre cell pressure of 1970psi.

B Vertical pressure : Horizontal pressure = 3:1

RESTORATION OF CENTRE CELL PRESSURE BY ANNULAR QUADRANTS.

Figure 2.15

b) Rock Stress and the Formation of Discs during Diamond Drilling

Discing of diamond-drilled core in highly stressed hard rock is a commonly observed phenomenon. Hast (1958) has observed the formation of discs when drilling a concentric annular channel around a hole in hard rock where the stresses are between 15,000 p.s.i. and 20,000 p.s.i. He considers that disc formation is due to shear across the back of the hole.

When drilling the $2\frac{3}{8}$ inch diameter holes for installing the seismometers through the most highly stressed rock, core recovery was poor, but amongst the fragments were pieces which appeared to be portions of discs about $\frac{1}{8}$ inch thick. In less highly stressed rock, regular discs from $\frac{3}{8}$ inch to $\frac{1}{2}$ inch thick were recovered. The disc failures tend to be curved, with the centre of curvature towards the collar of the hole.

During the stress measurements, regular discs were formed whenever the 4 inch annulus was drilled over the $1\frac{1}{2}$ inch hole. A six inch annulus drilled over a $1\frac{1}{2}$ inch hole at the same site also produced a core of regular discs. At the same depth the thickness of the discs from the 6 inch and 4 inch cores was $1\frac{1}{2}$ inches and 1 inch respectively, indicating some geometrical similitude. As the holes became deeper and the stress concentration due to the haulage was reduced, the disc thickness increased from 1 inch at a depth of 5 feet to $1\frac{1}{2}$ inches at a depth of 10 feet. Neither the $1\frac{1}{2}$ inch core nor the solid 4 inch core broke into discs, indicating that the presence of the centre hole results in disc formation at stresses lower than those necessary to produce discs in solid core. The discs can be fitted closely to oneanother, so that the failure can hardly be detected on the surface of the centre hole, but there is usually a distinct gap on the outside. When the 4 inch annulus was drilled over the $1\frac{1}{2}$ inch hole, several discs firmly joined to

/oneanother....

oneanother were often recovered. In such cases the failure on the outside of the core could be seen as a distinct gap, but could often only be traced all the way around the inside with the aid of a penetrating dye. A force of about fifty pounds was necessary to separate such discs, and the disc surfaces were covered with thin flakes of quartzite which could be prized loose.

It seemed that a measure of the stress at which discing occurs in quartzite would be interesting. It is almost impossible to obtain an unfractured, homogeneous block of quartzite bigger than a few inches. Therefore, 15 inches of 4 inch core were drilled from a hole at depth in solid quartzite. A 1½ inch diameter hole was drilled 12 inches along the axis of the 4 inch core, and 1 inch of 1 inch diameter core was left at the back of this hole. The 4 inch core was tested with a penetrating dye, and found to be free from cracks. A piece 4 inches long was cut from this core, with the end of the 1½ inch hole in the middle. A 4 1/4 inch diameter hole was bored in an 8 inch square steel block, 4 inches thick. This block was split parallel to two of its sides through the axis of the hole. The piece of 4 inch core, wrapped in a layer of blotting-paper, was carefully fitted to the steel block with two pieces of soft aluminium 1/8 inch thick. The whole assembly was compressed between two sheets of plywood. At a load of 280,000 pounds, the 1 inch core broke off with a distinct snap. The cross section of the 4 inch core was 16 square inches, giving an average stress of 17,500 p.s.i. over the horizontal diameter when the core broke. The steel block and 4 inch quartzite core are shown in Figure 2.16, and the 1 inch core which broke from the centre of the 4 inch core is shown in Figure 2.17. The end of the 1 inch core which failed is surrounded by a fin. The failure was slightly curved, and was covered with characteristic thin flakes of quartzite. Presumably

/the....



THE SPLIT STEEL BLOCK AND 4 INCH QUARTZITE CORE WITH THE END OF THE 1½ INCH HOLE IN THE CENTRE

FIGURE 2.16



THE 1 INCH DIAMETER QUARTZITE CORE, SHOWING THE END WHICH BROKE FROM THE BOTTOM OF THE HOLE IN THE 4 INCH CORE

FIGURE 2.17

the fin breaks off when the discs are produced by diamond drilling and this leaves the gap on the outside of the core and accentuates the curvature of the disc failure. The observations indicate that the disc length decreases as the stress increases. When the disc length is equal to, or greater than, the disc diameter, the stress must be close to the lower limit of the stresses necessary to cause discing. In the above experiment, the length of the core was equal to its diameter, and the stress of 17,500 p.s.i. must closely represent the minimum stress which will produce discs in a solid quartzite core.

When diamond drilling in rock which is subject to stress, the maximum compressive stress concentration takes place at the outside corner of the bottom of the annular cut. The compressive principal stress trajectories at the bottom of the hole curve into the core. The minimum principal stress trajectories are perpendicular to these, and tensile stresses, which are a maximum at the centre, must arise across the bottom of the hole. When a core discs, the disc surfaces are covered with thin flakes of quartzite and appear very similar to the failure surfaces produced by diametrical compression of cylindrical samples of quartzite. These diametrical failures occur on a surface subject to a tensile stress (See 2.1b, page 67). The absence of any ground quartzite powder on the disc surfaces certainly indicates that they are not due to shear on a surface subject to a compressive normal stress. When discing occurs, corresponding failures do not propagate outwards into the solid rock from the bottom of the annular cut, even though the maximum stress concentration occurs in this region. Thus, the disc failures are seen to be related to tensile forces across the bottom of the hole.
At the site of the stress measurements, the vertical rock stress was in the region of 13,000 p.s.i. A sample of quartzite from this site showed that discing of a solid core

/occurred....

occurred at a minimum stress of 17,500 p.s.i. Solid core did not disc at this site, but a 6 inch diameter core drilled concentrically over a $1\frac{1}{2}$ inch diameter hole disced regularly. Savin (1951) shows that the maximum change in stress at a radius of 3 inches from a $1\frac{1}{2}$ inch diameter hole is less than 10% of the undisturbed stress. If disc failures start from the bottom of the annular cut, it seems unlikely that this 10% change in the stress would be sufficient to overcome the difference between the rock stress of 13,000 p.s.i. and the minimum stress necessary to produce discs of 17,500 p.s.i. However, if disc failures are largely dependent on tensile stresses, and start from the centre of the core, then even a very small hole in the centre can cause a stress concentration in this region sufficient to produce disc failures. The stress field at the bottom of the annular cut is complicated, and becomes more so as soon as failure starts. It is difficult to explain the curvature of the disc failures in detail, but if they start in the centre of the core a little ahead of the bottom of the annulus, they are almost certain to end in the region of high stress concentration at the bottom of the annular cut.

PART 3 CONCLUSION

3.1 The Theoretical Model

Over short periods of time, quartzite behaves almost elastically. Some idea of the initial displacements and stresses arising from underground excavations in quartzite can, therefore, be gained by analyzing them in terms of elastic theory.

In general, the stresses around an opening in an elastic medium, subject to hydrostatic stress p at infinity, can be found by superposing on the undisturbed hydrostatic stress the stresses around a similar opening, to the surface of which a normal stress -p is applied. Such a solution by superposition can be obtained for any opening, provided that the sum of the undisturbed and superposed stresses over the contour of the opening is zero. Consider a horizontal slit far below the surface of an elastic body subject to gravity. Assume that the undisturbed principal stresses in the body are vertical and horizontal, and that the vertical stress at the elevation of the slit is P. If the width of the slit can be neglected in comparison with the other dimensions, then the stresses over the surface of the slit will vanish if the solution for the stresses around a slit with internal pressure - P is superposed on the undisturbed gravitational field. Stresses from the superposed load will remain at the free surface of the body. If the surface is sufficiently removed from the slit, they will be small and can be cancelled by applying a distributed load to the surface equal in magnitude but opposite in sign to the residual stresses. Such a load has a negligible effect on the stresses around the slit, but depresses downwards that portion of the body beneath the load

A vertical strike section through a longwall stope on East Rand Proprietary Mines, Ltd., shows a narrow horizontal slit of about 2,000 feet span and 3 feet wide, 8,000 feet to 10,000 feet below the surface.

The stresses in plane strain around such a slit in an elastic body subject to gravity can be found by superposition.

Muskelishvili, making use of the Stress, or Airy, function and the transformation

/z....

$$z = w(\zeta) = R(\zeta + \frac{1}{\zeta})$$

has obtained a solution to the stresses around a slit of length 4R to the inside of which a pressure, P, is applied. Using the notation of Muskelishvili, the equations defining the stresses in curvilinear co-ordinates are:-

$$\hat{\rho\rho} = -P + \frac{P(\rho^2 - 1)^3 (\rho^2 + 1)}{(\rho^4 - 2\rho^2 \cos 2\theta + 1)^2}$$

$$\hat{\theta\theta} = -P + \frac{P(\rho^4 - 1)(1 + 2\rho^2 + \rho^4 - 4\rho^2 \cos 2\theta)}{(\rho^4 - 2\rho^2 \cos 2\theta + 1)^2}$$

$$\hat{\rho\theta} = \frac{2P\rho^2(\rho^2 - 1)^2 \sin 2\theta}{(\rho^4 - 2\rho^2 \cos 2\theta + 1)^2}$$

(Muskelishvili, 1951, page 340).

Note: ρ and θ are not the usual polar co-ordinates but curvilinear co-ordinates defined by $\zeta = \rho e^{i\theta}$ which gives

$$z = x + iy = R\left(\frac{\rho^2 + 1}{\rho} \cos\theta + \frac{\rho^2 - 1}{\rho} i \sin\theta\right)$$

from the transformation $z = R(\zeta + \frac{1}{\zeta})$

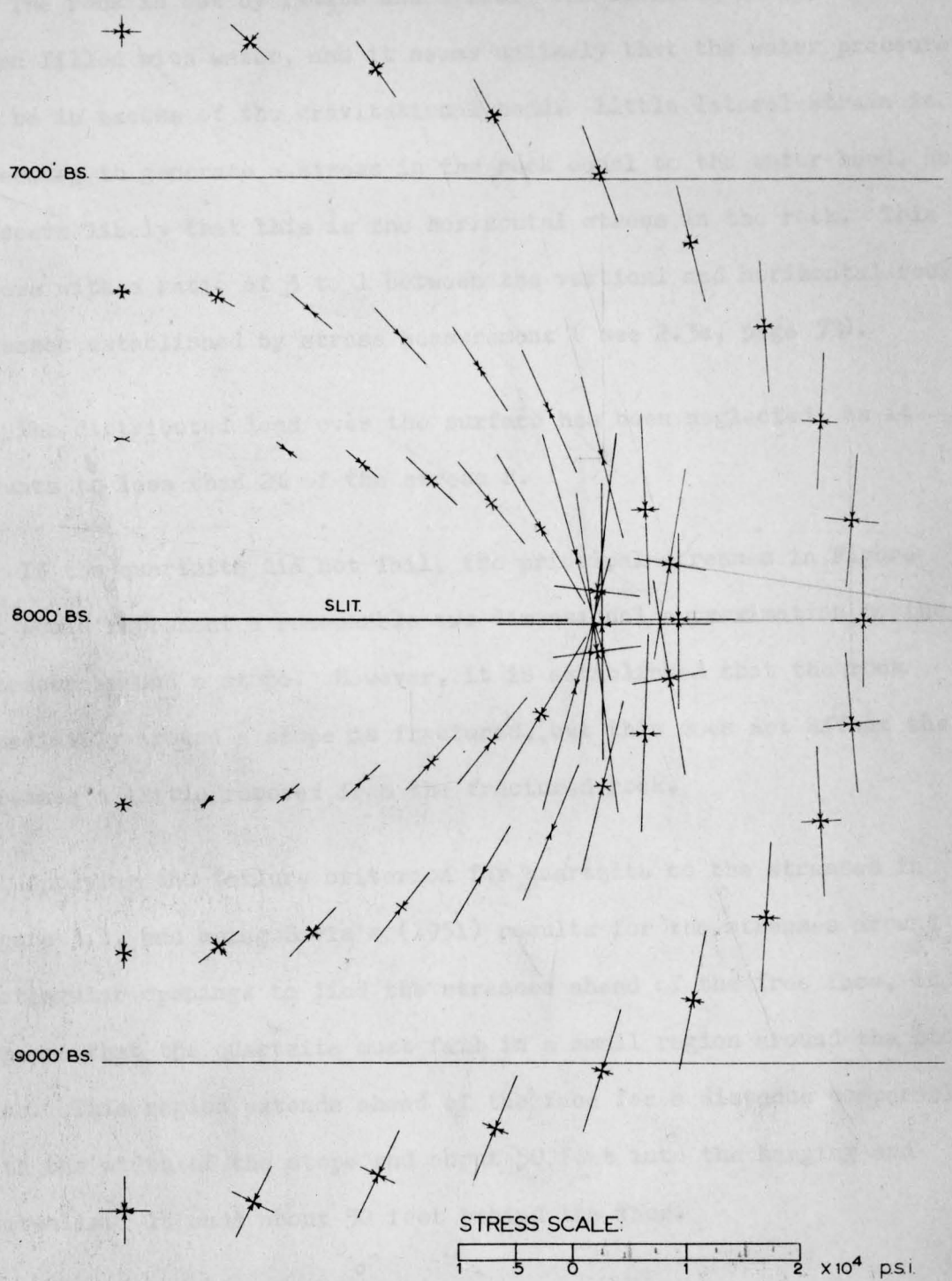
This transformation corresponds to the transformation to elliptic co-ordinates:-

$$Z = x + iy = c \cosh \zeta' = c \cosh (\xi + i\eta)$$

$$= c(e^{\zeta'} + \frac{1}{e^{\zeta'}})$$

This solution with - P = the undisturbed vertical gravitational stress, has been superposed on the undisturbed stress field to obtain the result in Figure 3.1. The undisturbed vertical stress has been assumed equal to dgh where: d = density of the rock and h = depth below the surface. The undisturbed horizontal stress has been assumed equal to gh - that is, the stress generated by an equal column of water or .37 of the vertical stress.

/The....



THE MAGNITUDES AND DIRECTIONS OF THE PRINCIPAL STRESSES IN PLANE STRAIN AROUND ONE HALF OF AN HORIZONTAL SLIT IN AN ELASTIC SOLID SUBJECT TO GRAVITY.

Figure 3.1

The rock is cut by faults and dykes. The fissures in the rock are often filled with water, and it seems unlikely that the water pressure can be in excess of the gravitational head. Little lateral strain is necessary to generate a stress in the rock equal to the water head, and it seems likely that this is the horizontal stress in the rock. This agrees with a ratio of 3 to 1 between the vertical and horizontal rock stresses established by stress measurement (see 2.3a, page 73).

The distributed load over the surface has been neglected, as it amounts to less than 2% of the stress P.

If the quartzite did not fail, the principal stresses in Figure 3.1 would represent a reasonable two-dimensional approximation to the stresses around a stope. However, it is established that the rock immediately around a stope is fractured, but this does not affect the stresses a little removed from the fractured rock.

Applying the failure criterion for quartzite to the stresses in Figure 3.1, and using Savin's (1951) results for the stresses around rectangular openings to find the stresses ahead of the free face, it appears that the quartzite must fail in a small region around the stope face. This region extends ahead of the face for a distance comparable with the width of the stope and about 50 feet into the hanging and footwalls. It ends about 50 feet behind the face.

Jaeger (1959) has shown that fractured rock sustains certain stresses without slipping. When the rock around a stope fails, the stresses change but the fractured rock still affords support to the solid rock further from the stope. Equilibrium is attained when the stresses in the fractured rock are less than those necessary to cause slipping, and the stresses in the solid rock are within the limits of the failure criterion. The maximum values of the equilibrium stresses in the solid rock immediately ahead of the fractured rock depend upon the support afforded to it by the fractured rock.

/Face....

Face advance removes the fractured rock, and hence the support of the solid rock. This lowers the maximum equilibrium stresses in the solid rock nearest the face. Three possible conditions arise from face advance:-

1. The maximum equilibrium stresses may be lowered, but may still remain above the actual stresses. In this case, no new fractures result.

2. The maximum equilibrium stresses may be reduced to values less than the actual stresses. In this case, new fractures occur during face advance. These reduce the actual stresses, fracture solid rock, and equilibrium is restored.

3. The maximum equilibrium stresses may be reduced to values slightly greater than the actual stresses. In this case, any further disturbances, or time dependency of the failure mechanism, can cause new failures.

The above discussion assumes that the rock around the stope is isotropic. In fact, it is cut by discontinuities in the form of bedding planes, dykes and sills.

Figure 3.1 shows that the vertical compressive stress in the hanging is less than the undisturbed vertical stress, and that relatively small disturbances could cause separation of the hanging along bedding planes.

The dykes are stronger and more rigid than the quartzite. Therefore, stress concentrations arise in the dykes when the quartzite surrounding them deforms. A large proportion of the strain energy from such stress concentrations is released when the dyke fractures whilst stoping through it.

/A....

A strong sill in the vicinity of a stope interrupts the continuous and uniform development of the fractures. Stress concentration occurs in such a sill as mining proceeds, and the sill may fail at intervals, releasing large amounts of strain energy.

Muskelishvili's equations defining the displacements around a slit are:-

$$v_\rho = -\frac{P R}{2\mu\rho} \cdot \frac{(1+K)\rho^2 \cos 2\theta + 1 - K - 2\rho^2}{\sqrt{\rho^4 - 2\rho^2 \cos 2\theta + 1}}$$

$$v_\theta = -\frac{P R \rho}{2\mu} \cdot \frac{(1 - K) \sin 2\theta}{\sqrt{\rho^4 - 2\rho^2 \cos 2\theta + 1}}$$

where, for plane strain:

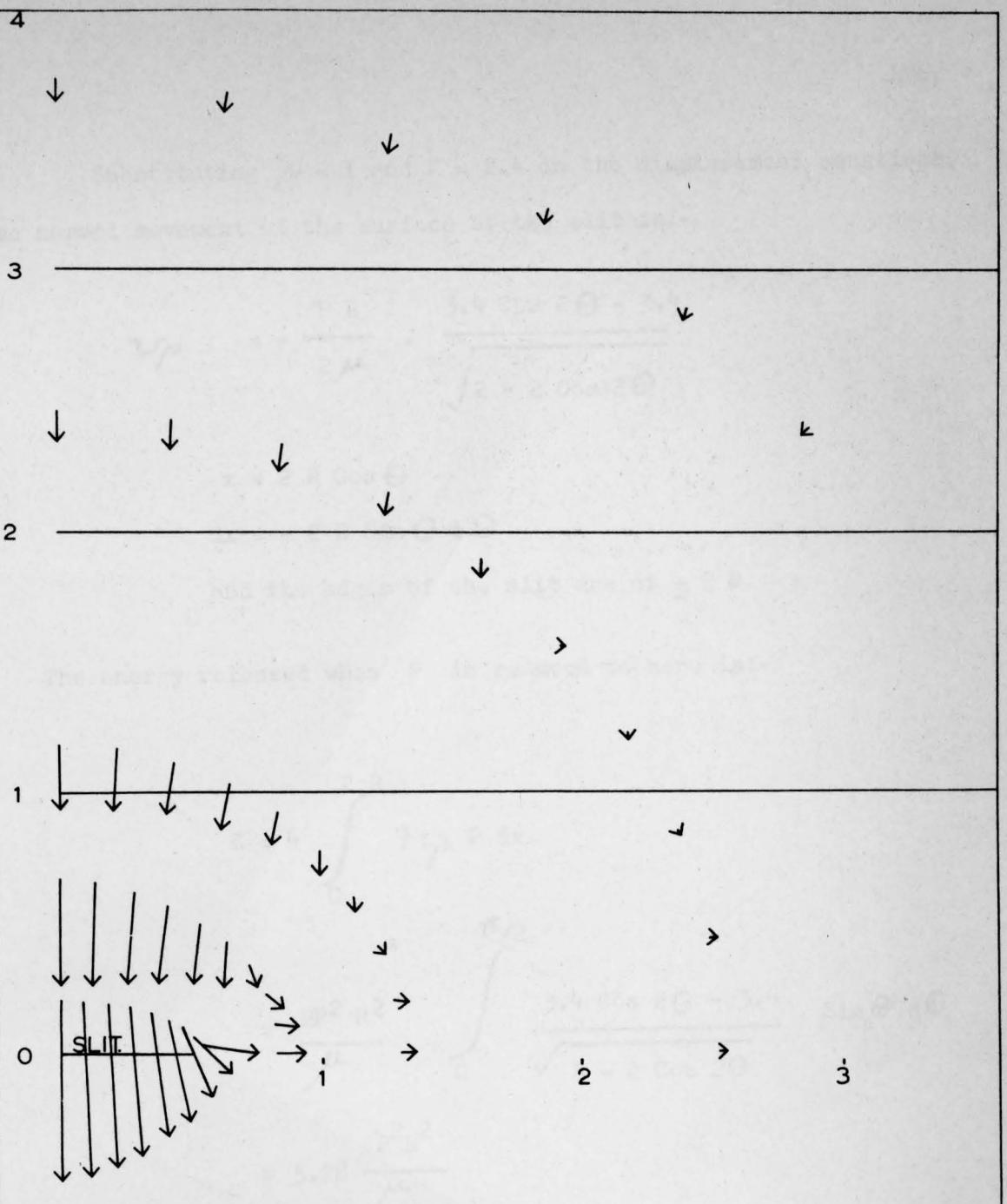
$$K = \frac{3 - \nu}{1 + \nu}$$

ν = Poisson's ratio, μ = Modulus of rigidity, and v_ρ, v_θ are the displacements along the ρ and θ directions defined previously.

These displacements are shown in Figure 3.2, where they are drawn relative to the plane through the centre of the stope which is itself depressed.

Using the displacement equations, it is possible to determine the total energy released by making a slit in an elastic solid subject to gravity. Let the material be maintained in an undisturbed state by a uniform pressure P applied to the surface of the slit, where P = the vertical stress due to gravity at the elevation of the slit. If the pressure P is reduced, the surfaces of the slit will converge, releasing energy.

/Substituting....



SCALES.

1 UNIT EQUALS THE SPAN OF THE SLIT.

MOVEMENTS ARE MAGNIFIED BY $2\mu/p$. WHERE:

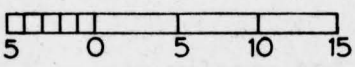
μ = MODULUS OF RIGIDITY.

p = VERTICAL STRESS AT THE ELEVATION OF SLIT DUE TO THE SUPERINCUMBENT WEIGHT

FOR A SLIT OF 2000' SPAN AND 8000' B.S. WHERE:

d = 169·5 lbs./cu.ft., AND $\mu = 6 \times 10^6$ p.s.i.

THE SCALE OF MOVEMENT IS:



DIRECTIONS AND MAGNITUDES OF THE MOVEMENT IN ONE QUADRANT CAUSED BY AN HORIZONTAL SLIT IN AN ELASTIC BODY SUBJECT TO GRAVITY.

Substituting $\rho = 1$ and $K = 2.4$ in the displacement equations, the normal movement of the surface of the slit is:-

$$v_p = -\frac{P\,R}{2\mu} \cdot \frac{3.4 \cos 2\theta - 3.4}{\sqrt{2 - 2\cos 2\theta}}$$

$$x = 2R \cos\theta$$

$$dx = -2R \sin\theta \, d\theta$$

and the edges of the slit are at $\pm 2R$.

The energy released when P is reduced to zero is:-

$$E = 4 \int_0^{2R} \tfrac{1}{2} v_p P \, dx$$

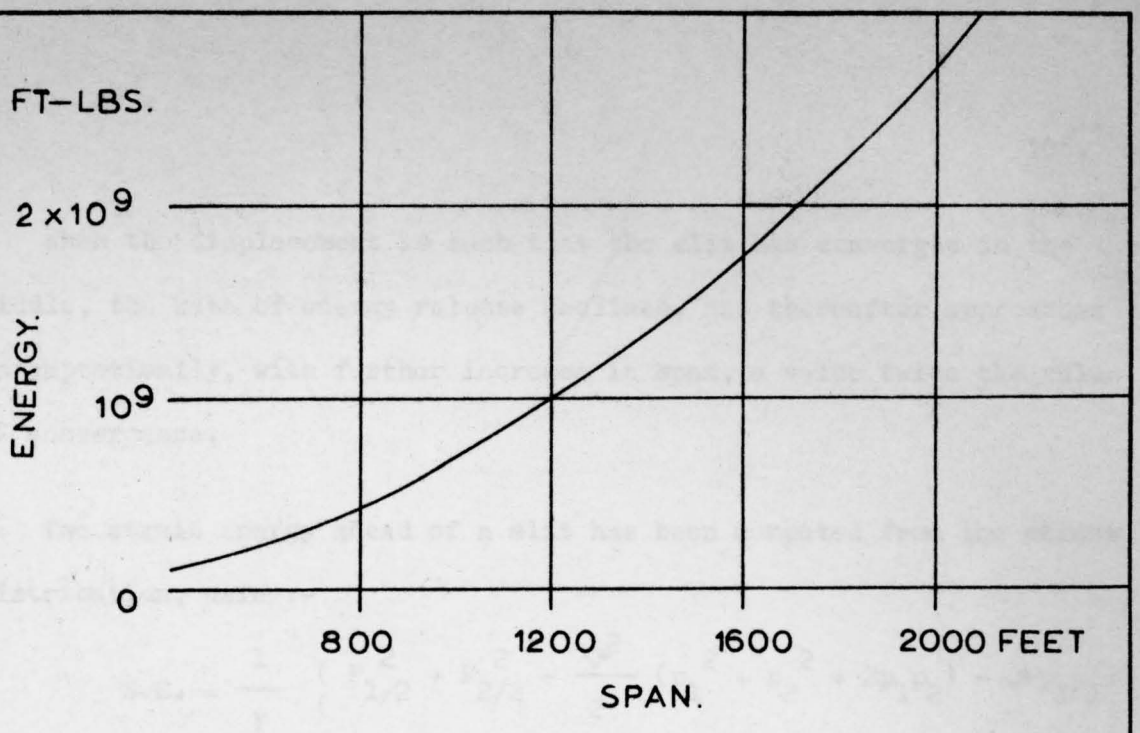
$$= \frac{2P^2R^2}{\mu} \int_0^{\pi/2} \frac{3.4 \cos 2\theta - 3.4}{\sqrt{2 - 2\cos 2\theta}} \sin\theta \, d\theta$$

$$= 5.28 \frac{P^2R^2}{\mu}$$

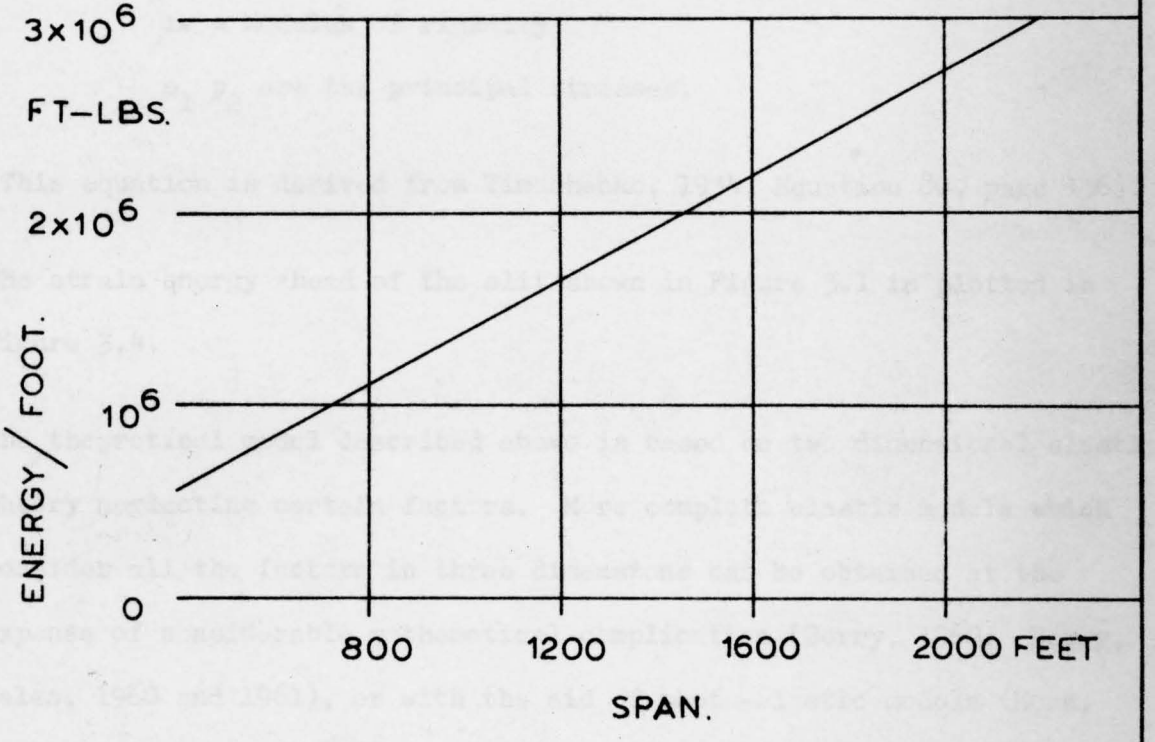
This is the energy released by making a slit in an elastic body subject to gravity. The energy release per unit increase in the span of the slit is:-

$$\frac{dE}{dR} = 10.56 \frac{P^2R}{\mu}$$

In Figure 3.3, the total energy release and the rate of energy release, for one foot of slit, computed from the above equations, are plotted.



TOTAL ENERGY RELEASED.



ENERGY RELEASED PER FOOT INCREASE IN SPAN.

$Y = 14 \times 10^6$ p.s.i. $\mu = 6{\cdot}1 \times 10^6$ p.s.i.

d. = 169·5 LBS / CU. FT. DEPTH = 8000 B.S.

ENERGY RELEASED WHEN AN HORIZONTAL SLIT IS MADE IN AN ELASTIC SOLID SUBJECT TO GRAVITY.

When the displacement is such that the slit has converged in the middle, the rate of energy release declines, and thereafter approaches assymptotically, with further increase in span, a value twice the value at convergence.

The strain energy ahead of a slit has been computed from the stress distribution, using:-

$$S.E. = \frac{1}{Y}\left(P_{1/2}^2 + P_{2/2}^2 - \frac{\nu^2}{2}(p_1^2 + p_2^2 + 2p_1p_2) - \nu p_1p_2 \right)$$

Where S.E. = strain energy per unit volume in plane strain.

Y. = Young's modulus

ν = Poisson's ratio

μ = Modulus of rigidity

p_1 p_2 are the principal stresses.

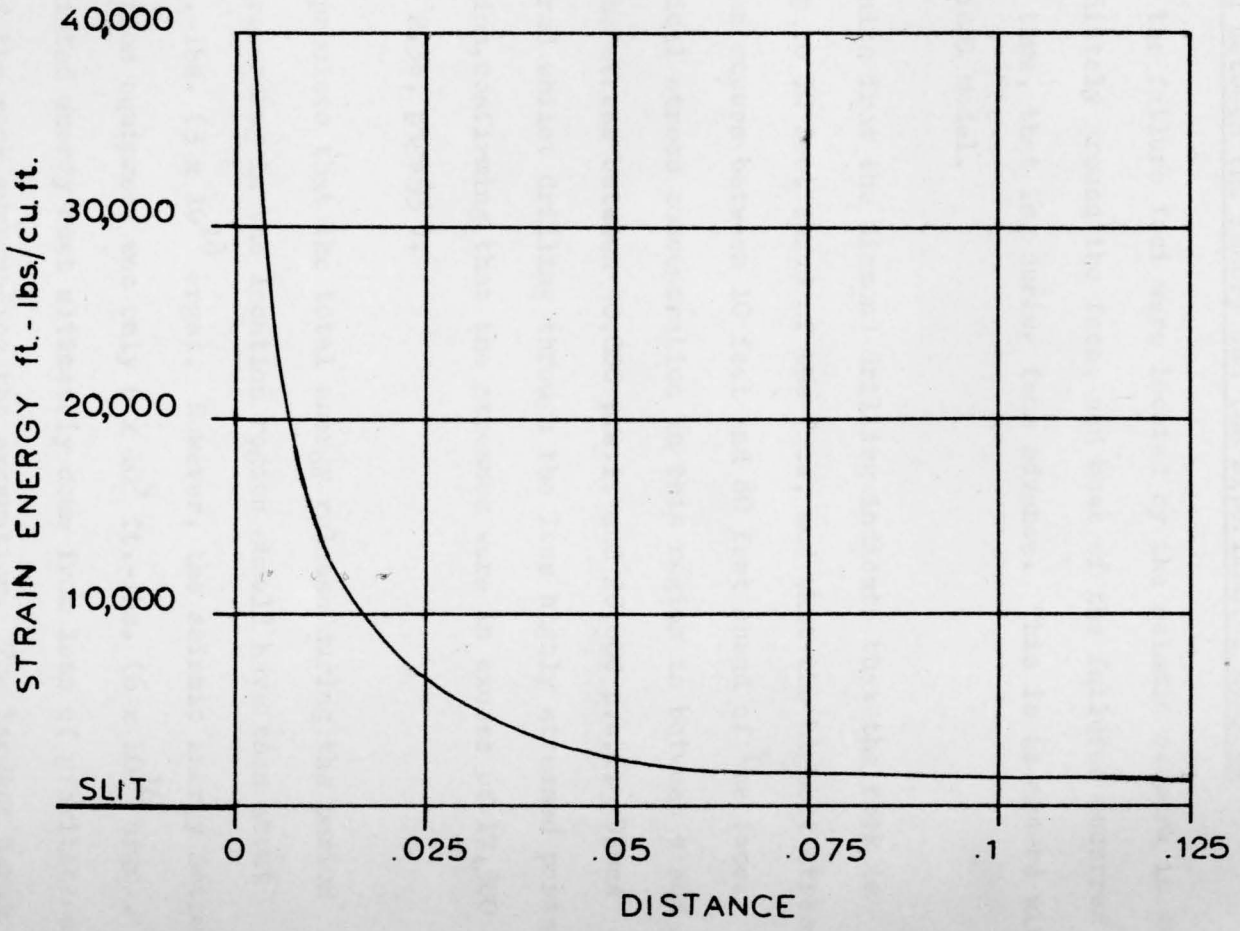
(This equation is derived from Timoshenko, 1934, Equation 80, page 136).

The strain energy ahead of the slit shown in Figure 3.1 is plotted in Figure 3.4.

The theoretical model described above is based on two dimensional elastic theory neglecting certain factors. More complete elastic models which consider all the factors in three dimensions can be obtained at the expense of considerable mathematical complication (Berry, 1960; Berry, Sales, 1960 and 1961), or with the aid of photo-elastic models (Hoek, 1961). Elastic models, however elaborate, only approximate the behaviour of the rock, particularly if failure takes place. For this reason it was felt that further elaboration would prove unrewarding.

It is felt that bearing in mind the approximations and changes in the stress caused by failure, the model provides a useful indication of the type of stress distribution and the magnitudes of the stresses around a longwall stope.

/



STRAIN ENERGY AHEAD OF AN HORIZONTAL SLIT IN AN ELASTIC BODY SUBJECT TO GRAVITY.

The slit is in the solid 8,000' below surface. At points removed from the opening the vertical stress is due to the weight of the super-incumbent solid = 9450 p.s.i.

Horizontal stress = .37 x Vertical Stress = 3500 p.s.i. Density of solid 169.5 lbs/cu. ft.

DISTANCE SCALE
1 UNIT = SPAN OF SLIT

Figure 3.4

The theoretical energy release in making such an excavation is based on an unfractured elastic model. This is the most rigid condition with minimum displacement and maximum strain energy. In practice, the energy release will be greater than the model indicates. The value of this calculation is that it indicates that a large amount of energy must be released in making such an excavation. The effect of the failure of a small region of solid rock ahead of the excavation is to extend the excavation, thereby releasing large amounts of energy and causing a downward motion of the ground surface.

3. 2 A Comparison between the Theory and the Experimental Results

Most of the failure foci were located by the seismic network in the region immediately around the face, and most of the failures occurred at blasting time, that is, during face advance. This is in accord with the theoretical model.

The results from the diamond drilling indicate that the rock is fractured up to 10 feet ahead of the face, and that the highest stress concentration occurs between 10 feet and 80 feet ahead of the face. The theoretical stress concentration in this region is between 4 and 2, making the stress between 40,000 p.s.i. and 20,000 p.s.i. Discs were recovered whilst drilling through the less highly stressed parts of this region, confirming that the stresses were in excess of 17,500 p.s.i. (See 2.3b, page 93).

Theory predicts that the total energy release during the period of seismic recording in the location region should have been about 3×10^{11} ft.-lbs. (3×10^{18} ergs). However, the seismic energy detected by the location equipment was only 6×10^{9} ft.-lbs. (6×10^{16} ergs). All the radiated energy must ultimately come from loss of gravitational potential of the rock surrounding the excavation. The largest burst radiated 10^{9} ft.-lbs. at frequencies between 15 c.p.s. and 160 c.p.s.,

/from....

from what appeared to be a relatively small volume of rock. Figure 3.4 indicates that the strain energy per cubic foot, about 15 feet ahead of the face, is 2×10^4 ft.-lbs. Therefore, the energy in the largest bursts is equal to the strain energy in 5×10^4 cu.ft. of rock, that is, a region with dimensions between 10 feet and 100 feet. However, the rock mass involved in the loss of gravitational potential is thousands of feet in extent, and disturbances travelling at seismic velocities take about half-a-second to propagate from the stope to surface. Therefore it is quite likely that only a small proportion of the total energy is radiated at frequencies between 15 c.p.s. and 160 c.p.s., and that the energy at these frequencies comes from the strain energy in the rock which fails. Other seismic records of tremors, obtained from surface seismometers of the Bernard Price Institute, indicate that the energy radiated below 15 c.p.s. may be ten times as great as that radiated above 15 c.p.s. Energy must also be dissipated in friction across the fractures in the rock surrounding a stope. The discrepancy between the theoretical and measured energy release is, therefore, not as great as it at first seems.

Tests on the strength of partially constrained specimens of quartzite showed that the strength of such specimens was markedly in excess of the uniaxial strength of the quartzite. Before ultimate failure of such specimens, extensive failure and spalling of the quartzite in the gap occurred. It seems that this is probably similar to the behaviour of the rock ahead of a stope face, and that the increase in strength may be due to the support of the fractured rock, as the theory suggests.

3.3 Questions arising from the Results

The seismic results were obtained in a region with a high incidence of rockbursts. The equipment has recently been installed in another part of the mine which has a low rockburst incidence. This part of the

/mine....

mine is less extensively developed and the quartzite is much more shaly. It is hoped that the results obtained in the new site will throw some light on the difference between regions of high and low incidence.

It is suggested that other 24-hour seismic networks be built and installed on other mines with markedly different geology and rock-burst incidence, to further investigate this problem. Such equipment seems to be necessary so that data from different times and places can be compared quantitatively.

A seismic network covering thousands of feet, and a continuous 24-hour recorder are necessarily limited in resolution and frequency response. For this reason it was not possible to obtain data concerning the rock displacement or the propagation of each failure.

Measurements of the movement of the rock around a stope have been made. The question arises whether these are discrete movements, each following a failure, or whether continuous flow occurs as well. A continuous recorder, which will be able to resolve movements of a hundredth-of-an-inch and times of several seconds, is being built. This is to be installed so as to measure the axial strain in a vertical borehole 150 feet long, in the rock ahead of the face, in the region of the seismic network. It will be possible to correlate the seismic records with these strain measurements, to resolve this question.

In order to detect smaller displacements occurring over periods of a second, the output of a 2 c.p.s. seismometer is going to be integrated and recorded by amplitude modulation on the seismic tape recorder.

The seismic data indicate that most of these failures occur during blasting. Seismic prospecting equipment has been obtained with which it will be possible to make detailed studies of the failures which occur during and immediately after blasting. Details of the propagation of the failures might be gained by examining high frequency

/seismic

seismic radiation from the failures. Low frequency seismic records should yield information about rock movements following blasting or a failure. It may be possible to integrate such records, to determine what displacement of the rock occurs. Simultaneous records of stress changes in the rock ahead of the face will enable the relationship between stress and failure to be established.

At depth, failures must occur in the rock around a stope as mining proceeds. Most of these failures occur during blasting, when the stopes are free of people. Only failures releasing energy in excess of 5×10^4 ft.-lbs. appear to cause noticeable damage to the workings. It is suggested that the most fruitful approach to the rockburst problem is to establish a mining technique which ensures the regular development of the failures in a series of small releases which occur during blasting. The most efficient way of generating these failures is to make use of the stress concentrations in the rock by adjusting the rate of face advance per blast, the blasting technique and the interval between blasts. It is hoped that the detailed seismic studies will enable the effect of different techniques to be established.

Of 187 bursts radiating energy in excess of 5×10^4 ft. -lbs., only 7 caused noticeable damage to the workings. There appear to be no differences in location or energy between bursts which are noticed and those which are not. In this respect, two major bursts which occurred in the seismometer network are interesting. Both of these bursts radiated about 10^9 ft.-lbs., were on the face and slightly in the footwall. The rockburst classification of the first burst was medium to slight intra-dorsal, and the classification of the second burst was severe extra-dorsal. It seems that this difference can be attributed only to the condition of the fractured rock immediately around the face. In this respect, it may be significant that the

/first....

first burst caused the least damage.

It is well known that the hanging immediately above a pack often remains in place after a rockburst, whilst the hanging between packs comes down. It is suggested that the stability of the hanging, footwall and support may have a major effect in determining the damage caused by a failure in a stope. No information about the stresses in the fractured rock, and how they change when a failure occurs, is available. Such information, and additional data concerning the properties of the joints, is necessary before the stability of the hanging and footwall can be analyzed.

Friction between surfaces of rock is obviously important in assessing the behaviour of fractured rock. It seems that friction between crack surfaces may be of equal importance in determining the strength (Brace, 1960) and attenuation of stress waves (Knopoff and MacDonald, 1958) in solid rock. Simple apparatus in which it is possible to measure friction and creep between rock surfaces, over a wide range of stresses and other conditions, has been devised. To date, only a few preliminary tests have been made, but they have indicated that the equipment will work.

APPENDICES

A.1 Seismic Wave Attenuation

Vibrations in solids are damped by internal energy losses. Birch (1942) has reduced measurements of this loss to a dimensionless quantity, $1/Q$. If d E is the energy loss per cycle, and E the total energy, then $1/Q$ = d E / 2πE. A solution for damped elsatic waves spreading from a focus is:-

$$u = \frac{A}{r} \; e^{-\alpha r} \; e^{2\pi i f(t - \frac{r}{v})}$$

where:

f = frequency

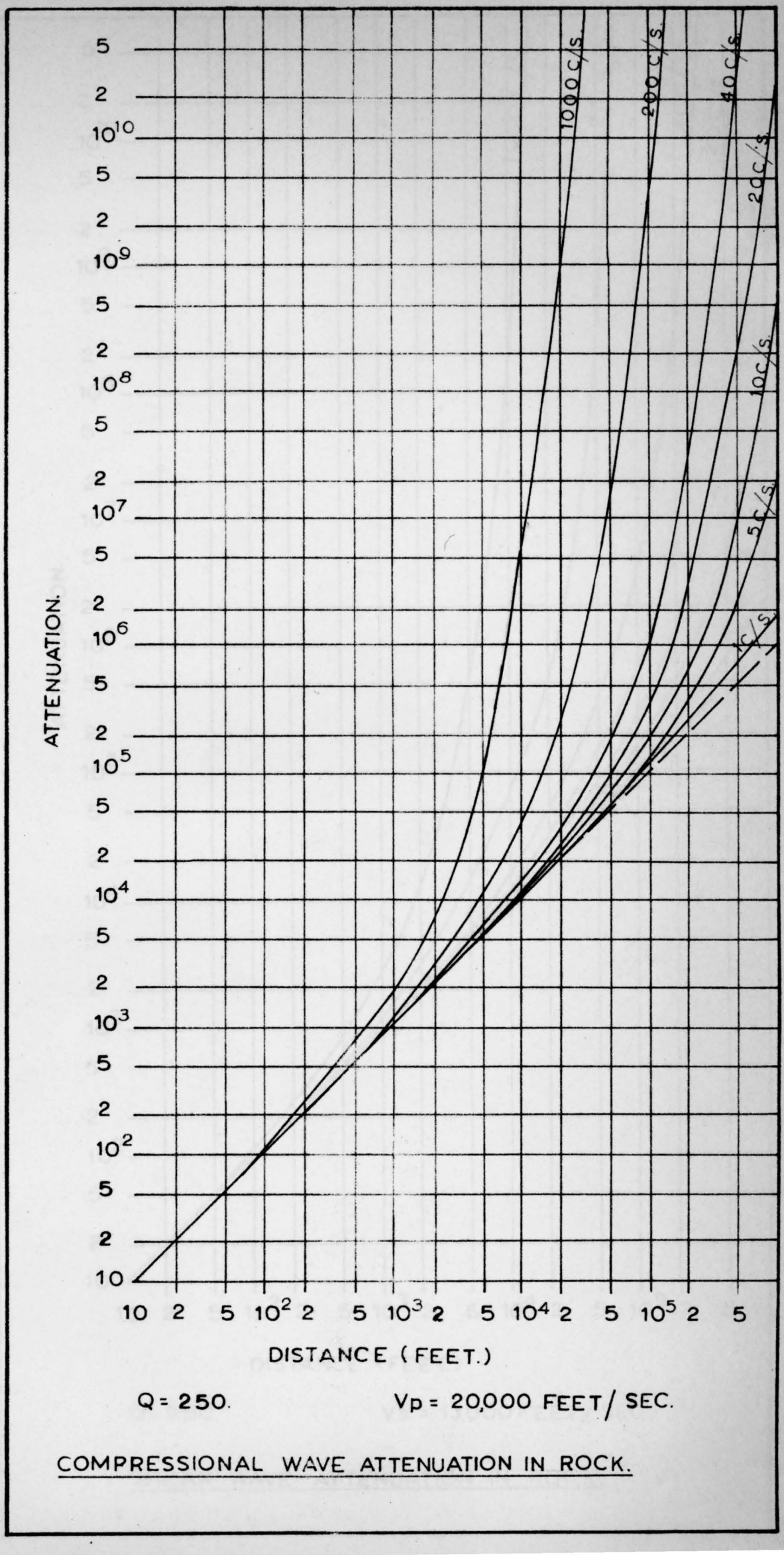
v = velocity

$\alpha = \pi f / Qv$

u = displacement

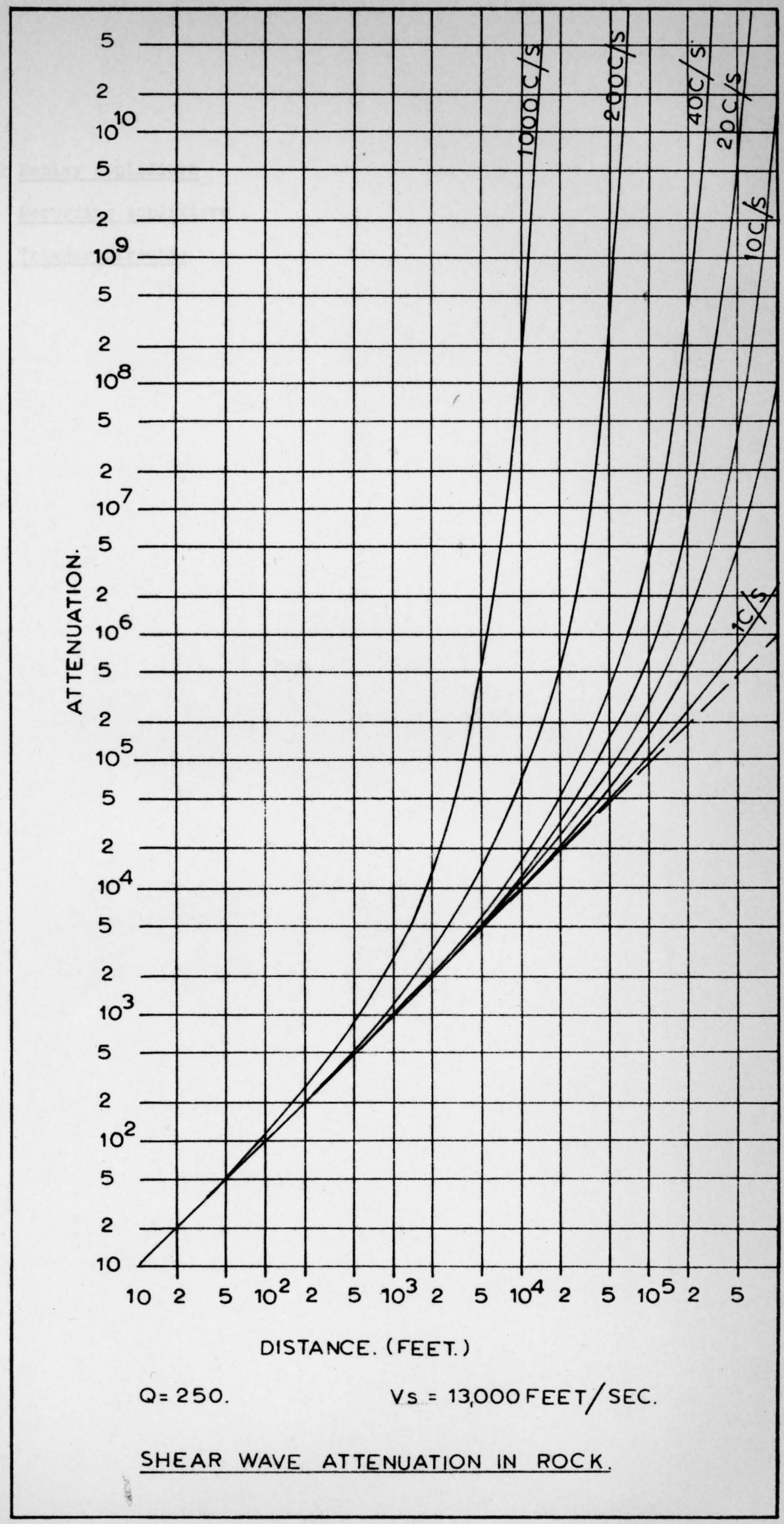
r = radius from the focus

The solution to this equation for different frequencies and velocities equal to the velocities of compressional and shear waves in quartzite are shown in Figure A.1 and Figure A.2. A conservative estimate of Q = 250 (Birch, 1942) has been used for both compressional and shear waves, though it is probable that Q is less for shear waves.



Q = 250. Vp = 20,000 FEET/SEC.

COMPRESSIONAL WAVE ATTENUATION IN ROCK.



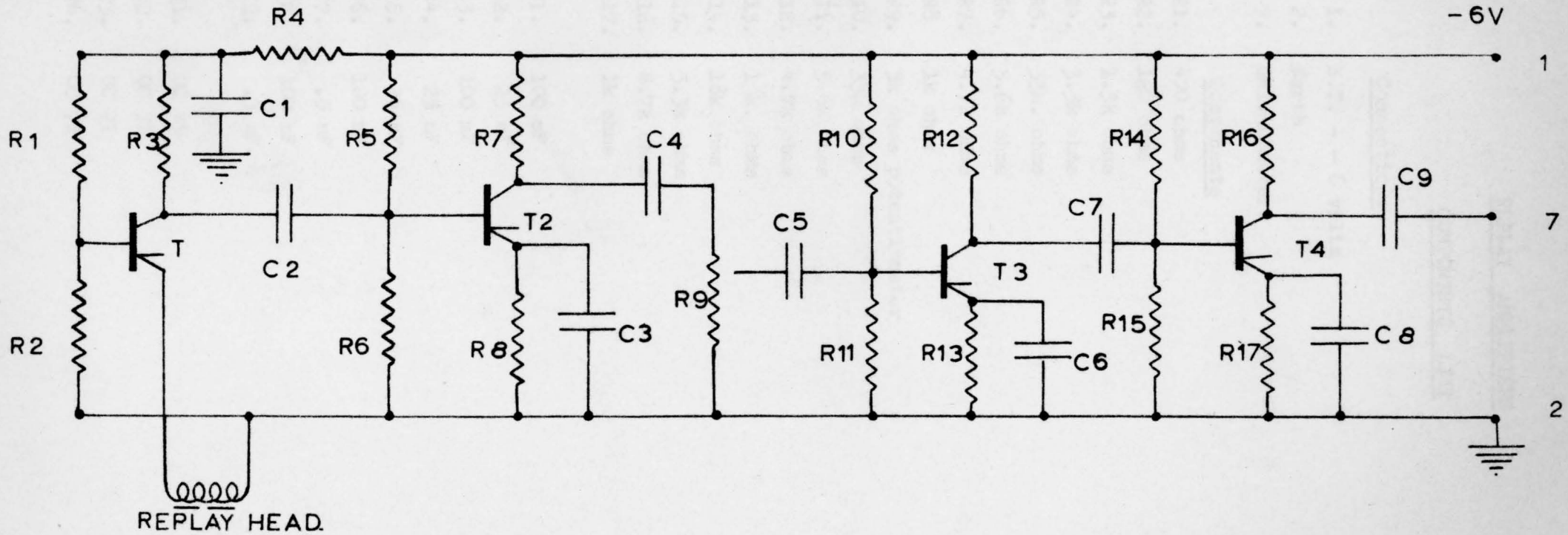
Q= 250. Vs = 13,000 FEET/SEC.

SHEAR WAVE ATTENUATION IN ROCK.

A. 2 Replay Amplifiers

Recording Amplifiers

Trigger Circuits



MAXIMUM VOLTAGE GAIN 5×10^4. NOISE 1 μV. PEAK TO PEAK.

REPLAY AMPLIFIER.

REPLAY AMPLIFIERS

COMPONENTS LIST

Connections

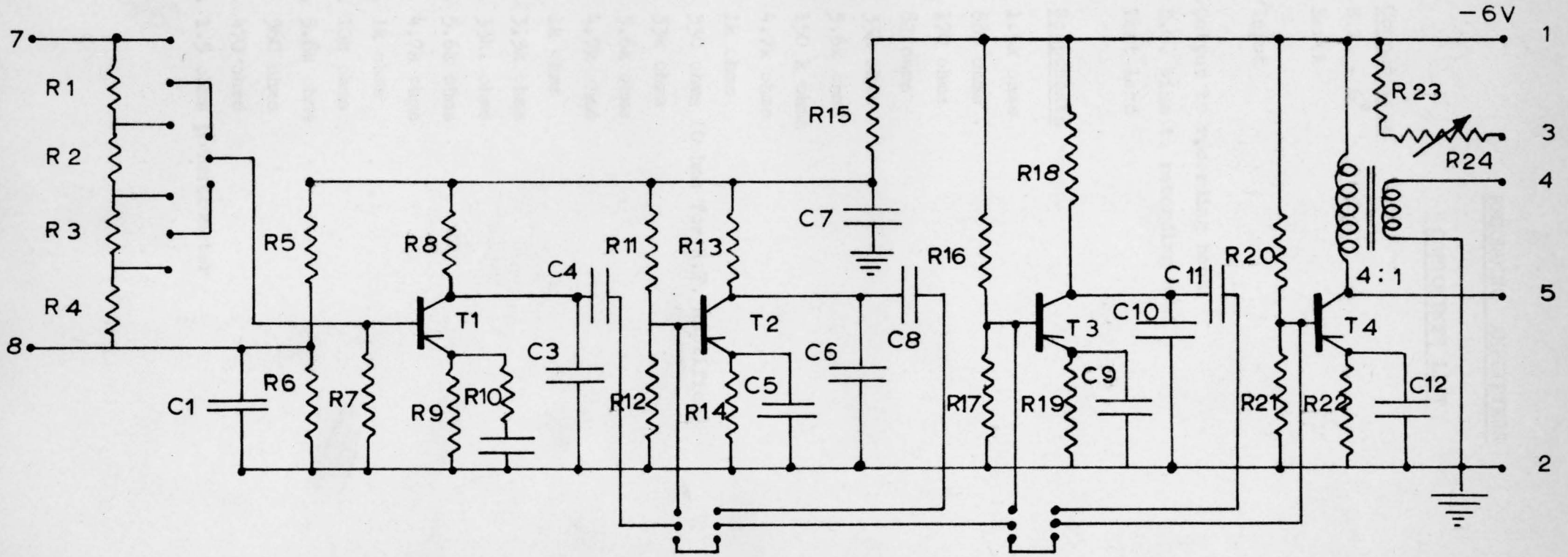
1. H.T. - - 6 volts
2. Earth
7. Galvanometer

Components

R1. 470 ohms
R2. 120 ohms
R3. 1.5k ohms
R4. 3.3k ohms
R5. 33k. ohms
R6. 5.6k ohms
R7. 4.7k ohms
R8 1k ohms
R9. 5k ohms potentiometer
R10. 33k ohms
R11. 5.6k ohms
R12. 4.7k ohms
R13. 1 k. ohms
R14. 18k ohms
R15. 3.3k ohms
R16. 4.7k ohms
R17. 1k ohms

C1. 100 mF
C2. 25 mF
C3. 100 mF
C4. 25 mF
C5. 25 mF
C6. 100 mF
C7. .5 mF
C8. 100 mF
C9. .5 mF

T1. OC 45
T2. OC 71
T3. OC 71
T4. OC 71



MAXIMUM VOLTAGE GAIN BETWEEN 7 AND 5 4×10^4. NOISE 2μV. PEAK TO PEAK.

RECORDING AMPLIFIER.

RECORDING AMPLIFIERS

COMPONENTS LIST

. Connections

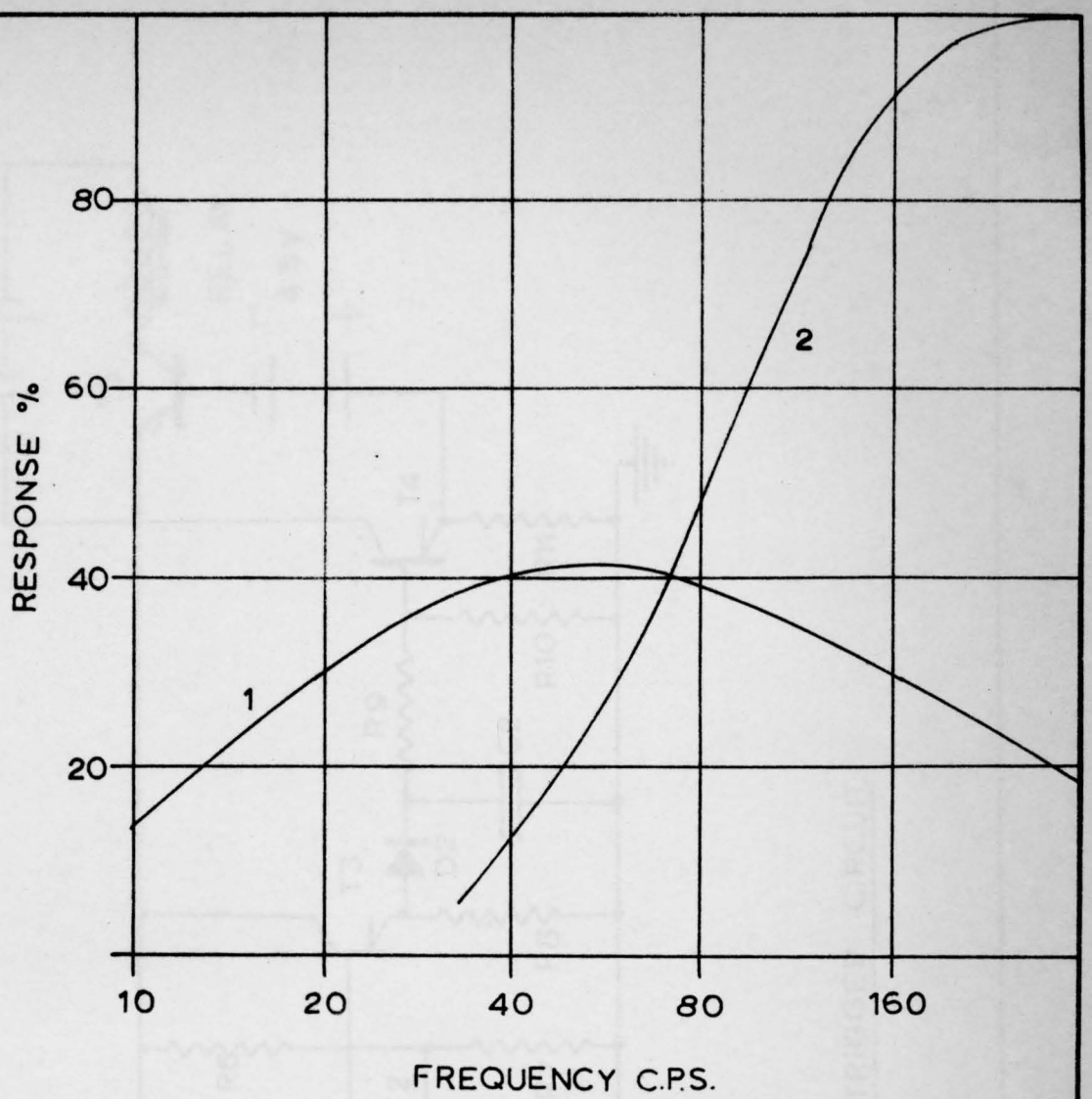
1. H.T. - 6^{v}
2. Earth
7. and/Input 8
4. Output to recording head
3. D.C. bias to recording head
5. Test lead

Components

R1. 1.5k ohms
R2. 680 ohms
R3. 170 ohms
R4. 82 ohms
R5. 33k ohms
R6. 5.6k ohms
R7. 150 k ohms
R8. 4.7k ohms
R9. 1k ohms
R10. 330 ohms (Oohms for H.F. amplifier)
R11. 33k ohms
R12. 5.6k ohms
R13. 4.7k ohms
R14. 1k ohms
R15. 3;3k ohms
R16. 33k. ohms
R17. 5.6k ohms
R18. 4.7k ohms
R19. 1k ohms
R20. 10k ohms
R21. 5.6k ohms
R22 560 ohms
R23. 470 ohms
R24. 1.5 ohms potentiometer

RECORDING AMPLIFIERS

	Ordinary Amplifiers	H.F. Amplifiers
C1.	250 mF	
C2.	50 mF	
C3.	.5 mF	.1 mF
C4.	50 mF	2 mF
C5.	250 mF	25 mF
C6.	.5 mF	.1 mF
C7.	250 mF	
C8.	50 mF	2 mF
C9.	250 mF	25 mF
C10.	.5 mF	.1 mF
C11.	50 mF	2 mF
C12.	250 mF	25 mF
T1.	OC 71	
T2.	OC 71	
T3.	OC 71	
T4.	OC 71	

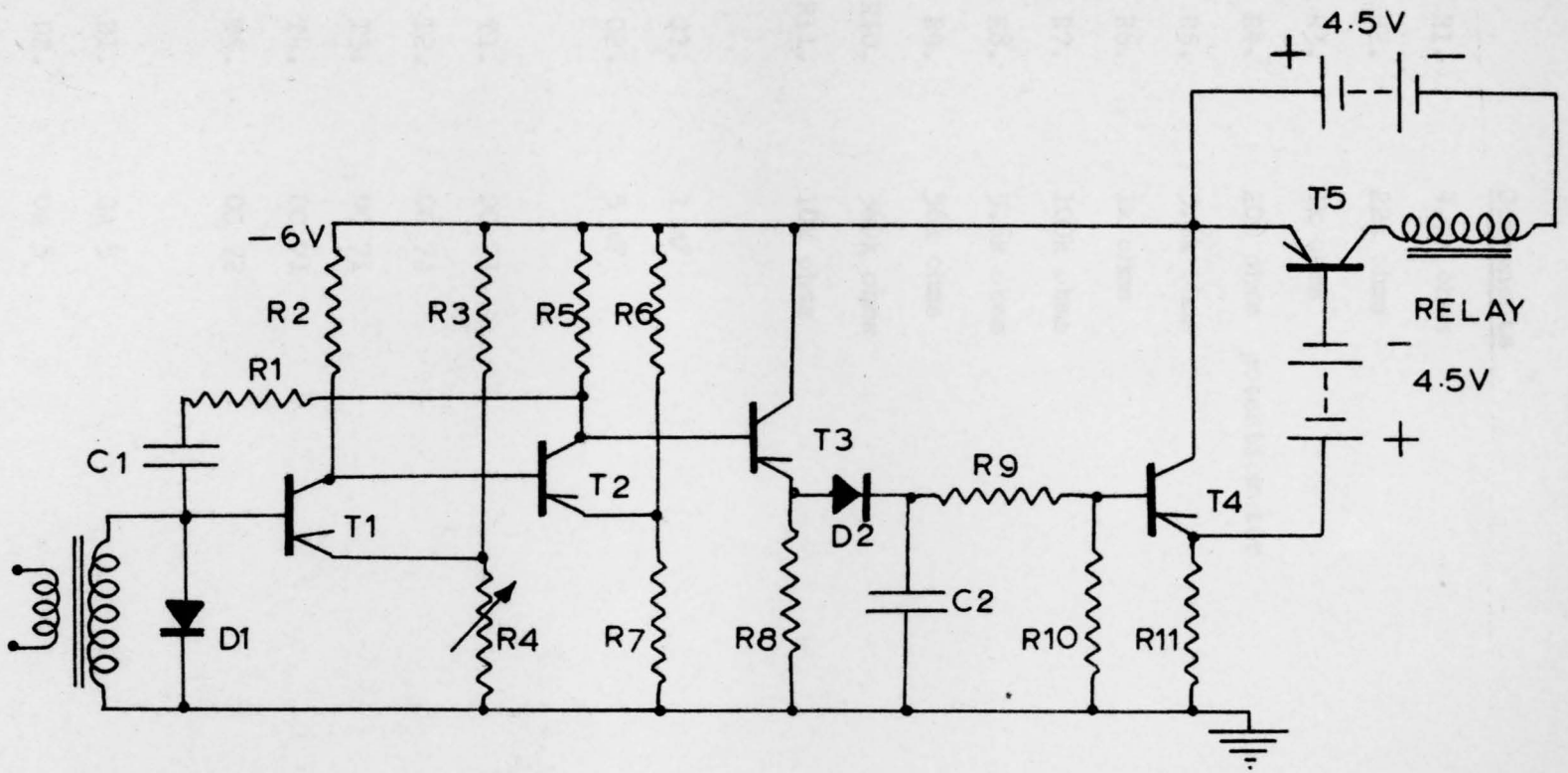


CURVE 1 IS THE STANDARD RECORDING AMPLIFIER.

CURVE 2 IS THE AMPLIFIER WITH HIGH FREQUENCY EMPHASIS.

FREQUENCY RESPONSE OF THE RECORDING AMPLIFIERS.

Figure A.5



TRIGGER CIRCUIT.

Figure A.6

TRIGGER CIRCUIT

COMPONENTS LIST

	Components
R1.	4.7k ohms
R2.	22k ohms
R3.	1k ohms
R4.	200 ohms potentiometer
R5.	5.6k ohms
R6.	1k ohms
R7.	100k ohms
R8.	5.6k ohms
R9.	56k ohms
R10.	360k ohms
R11.	10k ohms
C1.	1 mF
C2.	5 mF
T1.	OC 71
T2.	OC 71
T3.	OC 71
T4.	OC 71
T5.	OC 72
D1.	OA 5
D2.	OA 5

A. 3 Strain Gauges

Assuming temperature stability and stability of the bond between the strain gauge and the specimen, the accuracy obtainable with a strain gauge is determined by its output signal.

The output from a strain gauge is proportional to the voltage across the gauge, but the electrical power which a gauge can dissipate is limited. For a given power dissipation $2\sqrt{2}$ times the output voltage can be obtained from a strain gauge by using an alternating instead of a direct current supply for the gauge. This process can be carried further to obtain increases greater than 5 times in the output voltage by supplying the gauge with short duration positive and negative pulses separated by relatively long intervals. The interval between the pulses must be much less than the interval over which the strain measurement is significant.

A mechanical chopper providing ten pulses per second from a battery supply was used. This was connected to a strain gauge bridge and the output was amplified in a low noise silicon transistor D.C. pre-amplifier. The output from the pre-amplifier was fed to an oscilloscope. Using a chopped signal had the further advantage of avoiding trouble due to drift of the D.C. amplifier.

N O T A T I O N

a = Ratio

b = Frequency

c = Constant

d = Density

g = Gravity

h = Depth

l = Length

m = Number

n = Index

p = Normal Stress

q = Factor

r = Radius

s = Shear Stress

t = Time

u = Pitch

v = Velocity

w = Wire(subscript)

x)
)
y) Co-ordinates
)
z)

C = Velocity of Propagation

D = Diameter

E = Energy

H = Horizontal Component

J = Wire Diameter

K = Constant

L = Load

P = Compressional; Pressure

Q = Compressive Strength

R = Variable

S = Shear

T = Duration

V = Vertical Component

Y = Young's Modulus

λ, μ Lamé's Constants

μ = Modulus of Rigidity

ν = Poisson's ratio

$\rho\ \theta$ = Curvilinear Co-ordinates

$\xi\ \eta$ = Elliptic Co-ordinates

ω = Frequency

v_ρ Displacement along p-axis

v_θ Displacement along - axis

A C K N O W L E D G M E N T S

The research described in this Thesis was financed by the Transvaal and Orange Free State Chamber of Mines, on whose behalf the project was undertaken by the Bernard Price Institute of Geophysical Research.

Underground research is beset with multitudes of unpredictable difficulties. It is with great pleasure that I acknowledge the assistance of the many people who helped to overcome them.

I would like to thank Dr. A.L. Hales, Director of the Bernard Price Institute of Geophysical Research for his guidance and assistance.

I am indebted to Professor J.C. Jaeger for his valuable advice and for the time he spent assisting with tests on rock specimens and stress measurements.

I am indebted to members of the staff of the Bernard Price Institute, particularly to Dr. I.S. Sacks for assistance and helpful discussions; to Mr. J.A. Keller, who constructed most of the equipment and whose skill and experience contributed to its successful operation in underground conditions; to Mrs. J.D. Cook, for completing the enormous task of reading all the records and locating the bursts; to Mr. G.A. Wiebols for his cheerful assistance and to Mrs. N. Robb for tracing most of the figures in this Thesis.

I would like to thank the Technical Manager of Rand Mines, Mr. F.G. Hill, and Mr. M. Barcza, and Mr. W.D. Ortlepp of his Department, for their help.

I am indebted to the General Managers of East Rand Proprietary Mines, Limited, Mr. D. McNiven, Mr. E. Thiel and Mr. G.B. Hamilton, for their assistance and for so readily drawing on their vast experience to help me.

/I....

I am grateful to Mr. P.G.D. Pretorius, Mr. J.O. Kempe, Mr. N.M. McAlpine and Mr. W.O. Donnelly for their encouragement and assistance.

It is with pleasure that I acknowledge the assistance of Mr. A.J. White, of East Rand Propriatary Mines, Limited. He undertook a major part of the installation of the equipment underground, and took great trouble to ensure its continued operation. His experience and assistance, which he offered so freely to me, contributed in a large measure to this study.

I would like to thank the Banksmen on F. Shaft, East Mines Proprietary, Limited, who undertook the task of changing the recording tapes daily.

I would like to thank Mr. C. Reed and Mr. M. Roux, who helped me in Mr. White's absence, and many other employees of East Rand Proprietary Mines, Limited, for help and encouragement.

I would like to thank members of the Staff of the Department of Mechanical Engineering of the University of the Witwatersrand for allowing me such free use of their equipment.

I would like to thank the Cementation Company (Africa), Limited, who went to considerable trouble diamond-drilling under difficult conditions, and the Electronics Division of the Transvaal and Orange Free State Chamber of Mines for assembling some of the circuits.

REFERENCES

1. Barcza, M.; von Willich, G.P.R. 1958
Strata Movement Measurements at Harmony Gold Mine.
Ass. Min. Mngrs. S. Afr. Circ. 10.

2. Berry, D.S. 1960.
An Elastic Treatment of Ground Movement due to Mining - I
Isotropic Ground
J. Mech. Phys. Solids. Vol 8, 280-292.

3. Berry, D.S.; Sales, T.W. 1960.
An Elastic Treatment of Ground Movement due to Mining - II
Transversely Isotropic Ground.
J. Mech. Phys. Solids. Vol. 9, 52 - 62.

4. Berry, D.S.; Sales, T.W. 1961
An Elastic Treatment of Ground Movement due to Mining - III
Three Dimensional Problem, Transversely Isotropic Ground.
J. Mech. Phys. Solids. Vol. 10, 73 - 83.

5. Birch, F. 1942.
Handbook of Physical Constants.
Geol. Soc. Am. Special Papers No. 36, 88-92.

6. Brace W.F. 1960.
An Extension of the Griffith Theory of Fracture of Rocks.
Jour. of Geophysical Res. 65: 3477 - 3480.

7. Brown, A.N. 1959.
The Measurement and Analysis of Strata Movement Connected with the Extraction of a Shaft Pillar at Depth.
M.Sc. Thesis. Witwatersrand University.

8. Cumpsty, J.S. 1952.
The Direct Measurement of Rock Pressure.
Univ. School Min. Res. Publ. Durham. Vol. 2, 16 - 26.

9. Denkhaus, H.G.; Roux, A.J.A.; Grobbelaar. 1958
A Study into the Mechanical Properties of Rock, with Special Reference to their Bearing on the Occurrence of Rockbursts.
J.S. Afr. Instn. Mech. Engnrs. Vol. 8, 67 - 85.

10. Denkhaus, H.G. 1958
The Application of the Mathematical Theory of Elasticity to Problems of Stress in Hard Rock at Great Depth.
Ass. Min. Mngrs. S. Afr., Circ. 8.

11. F.K.O. Memorandum, No. 30. 1959
Rock Blasting. Conference in Stockholm.

12. Gane, P.G.; Hales, A.L; Oliver, H.O. 1946.
A Seismic Investigation of the Witwatersrand Earth Tremors.
Bull. Seis. Soc. Am. Vol. 36, 49 - 80.

13. Gane, P.G.; Seligman P.; Stephen, J.H. 1952.
Focal Depth of Witwatersrand Tremors.
Bull. Seis. Soc. Am. Vol. 43, 239 - 250.

/14. ....

14. Grobbelaar, C. 1958.
Some Properties of Rock from a Deep Level Mine on the Central Witwatersrand.
Ass. Min. Mngrs. S. Afr. Circ. 8.

15. Hamilton, G.N.G.: Cooke, H.B.S. 1954.
Geology for South African Students. Third Ed.
C.N.A. S. Africa.

16. Hast, N. 1958.
The Measurement of Rock Pressure in Mines.
Sveriges Geologiska Undersökning.
Årsbok. 54. No. 3.

17. Hoek, E. 1961.
The Application of Experimental Mechanics to the Study of Rock Stress Problems encountered in Deep Level Mining in South Africa.
International Cong. on Exp. Mech.

18. Jaeger, J.C. 1959.
The Frictional Properties of Joints in Rock.
Geofisica Pura e Applicata. Vol. 43, 148 - 158.

19. Knopoff, L.; MacDonald, G.J.F. 1958.
Attenuation of Small Amplitude Stress Waves in Solids.
Review of Modern Physics. Vol. 30 No. 4, 1178 - 1192.

20. Kundorf, W.; Rotter, D. 1961.
Eine Untersuchung über die Anwendung der Methode Natürlicher Hochfrequenter Seismischer Felder (Eigenimpulsmethode), im Steinkohlen - und Erzbergbau.
Freiberger Forschungshefte. C.120 Geophysik.

21. Leeman, E.R. 1958.
Some Underground Observations relating to the Extent of the Fracture Zone around Excavations in some Central Rand Mines.
Ass. Min. Mngrs. S. Afr. Circ. 10.

22. Leeman, E.R. 1960.
Measurements of Stress in Abutments at Depth.
International Conf. Strata Control. Paris.

23. Lutch, A. 1959.
The Experimental Determination of the Extent and Degree of Fracture of Rock Faces by Means of an Ultrasonic Pulse Reflection Method.
J.S. Afr. Inst. Min. Metall., Vol. 59, 412 - 429.

24. Lutch, A.; Szendrei, M.E. 1958.
The Experimental Determination of the Extent and Degree of Fracture of a Rock by means of Sonic and Ultrasonic Methods.
Ass. Min. Mngrs. S. Afr. Circ. 10.

25. Macelwane, J.B.; Sohon, F.W. 1936.
Theoretical Seismology, Part 1. Geodynamics.
John Wiley.

/26. ....

26. Mohr, F. 1956.
Measurement of Rock Pressure.
Min. Quarr. Engng. Vol. 22, 178 - 189.

27. Muskelishvili, N.I. 1953.
Some Basic Problems of the Mathematical Theory of Elasticity.
Noordhoff, Ltd. Holland.

28. Potts, E.L.J. 1955.
The Practical Application of Scientific Measurement to Problems in Strata Control.
Iron Coal Tr. Rev., 1169 - 1179.

29. Pretorius, P.G.D. 1958.
Some Observations on Rock Pressure at Depth on the East Rand Proprietary Mines, Ltd.
Ass. Min. Mngrs. S. Afr., Circ. 10.

30. Robertson, E.C. 1955.
Experimental Study of the Strength of Rocks.
Geo. Soc. Am. Bull. Vol. 66, 1275 - 1314.

31. Sacks, I.S. 1957.
A Low-Noise Transistorized Seismic Pre-Amplifier.
Jour. Geo. Res. Vol. 62, No. 2., 267 - 278.

32. Savin, G.N. 1951.
Kontsentratsiya Napryazhenii Okolo Otverstii
(Stress Concentrations around Openings).
Moscow/Leningrad, Gostekhteoretizdat.

33. Szendrei, M.E.; Lochner, J.P.A. 1958.
The Determination of the Extent of Fracture of Rock Faces by Sonic Means.
J.S. Afr. Inst. Min. Metall. Vol. 59, 202 - 214.

34. Terman, F.E. 1943.
Radio Engineers' Handbook.
McGraw - Hill.

35. Timoshenko, S. 1934.
Theory of Elasticity,
McGraw - Hill.